

UC Berkeley

UC Berkeley Previously Published Works

Title

High-Pressure Scanning Tunneling Microscopy

Permalink

<https://escholarship.org/uc/item/2ss600jg>

Journal

Chemical Reviews, 121(2)

ISSN

0009-2665

Authors

Salmeron, Miquel

Eren, Baran

Publication Date

2021-01-27

DOI

10.1021/acs.chemrev.0c00429

Peer reviewed

High Pressure Scanning Tunneling Microscopy

Miquel Salmeron,^{*, †, ‡} and Baran Eren,^{**, †, §}

[†]*Materials Sciences Division, Lawrence Berkeley National Laboratory, 1 Cyclotron Road, Berkeley, California 94720, United States, and*

[‡]*Department of Materials Science and Engineering, University of California, Berkeley, United States*

[§]*Department of Chemical and Biological Physics, Weizmann Institute of Science, 234 Herzl Street, 76100 Rehovot, Israel,*

* E-mail: mbsalmeron@lbl.gov

** E-mail: baran.eren@weizmann.ac.il

Abstract

This is a Review of recent studies on surface structures of crystalline materials in the presence of gases in the mTorr to atmospheric pressure range, which brings Surface Science into a brand new direction. Surface structure is not only a property of the material, but also depends on the environment surrounding it. This Review emphasizes that high/ambient pressure goes hand-in-hand with ambient temperature, because weakly interacting species can be densely covering surfaces at room temperature only when in equilibrium with a sufficiently high gas pressure. At the same time, ambient temperatures help overcome activation barriers that impede diffusion and reactions. Even species with weak binding energy can have residence lifetimes on the surface that allow them to trigger reconstructions of the atomic structure. The consequences of this are far from trivial, because under ambient conditions the structure of the surface dynamically adapts to its environment and as a result completely new structures are often formed. This new era of surface science emerged and spread rapidly after the re-tooling of characterization techniques that happened in the last two decades. This Review is focused on the new surface structures enabled particularly by one of the new tools: High pressure scanning tunneling microscopy. We will cover several important surfaces that have been intensely scrutinized, including transition metals, oxides, and alloys.

Table of Contents

1. Introduction
 - 1.1 Why High (Ambient) Pressure?
 - 1.2 Why STM?
2. Instrumentation
3. Carbon Monoxide Adsorption Studies on Low Miller-Index Surfaces
4. Adsorption Studies of other Molecules on Low Miller-Index Surfaces
5. Adsorption on Low Miller-Index Surfaces of '*Soft*' Metals (Copper and Gold)
 - 5.1 CO on Low Miller-Index Cu Surfaces
 - 5.2 CO on Low Miller-Index Au Surfaces
 - 5.3 Other Gases on Low Miller-Index Cu Surfaces
6. Reaction Studies on Low Miller-Index Surfaces
 - 6.1 CO Oxidation
 - 6.1.1 CO Oxidation on Pt Surfaces
 - 6.1.2 CO Oxidation on Pd Surfaces
 - 6.1.3 CO Oxidation on Rh Surfaces
 - 6.1.4 CO Oxidation on Cu Surfaces
 - 6.2 Ethylene Oxidation on Ag(111)
 - 6.3 NO Reduction
7. Non-reactive Co-adsorption Studies on Low Miller-Index Surfaces
8. Adsorption and Reactions on Vicinal Surfaces
9. Fischer-Tropsch Synthesis on Co Surfaces
10. Metal/Oxide Surfaces
11. Bimetallic Surfaces
12. Conclusions and Outlook

1. Introduction

1.1 Why High (Ambient) Pressure?

Surface Science is the field of elucidating the fundamental aspects of chemistry and physics occurring on the surfaces of materials, with the goal of providing fundamental information to industrially important fields of heterogeneous catalysis, electrochemistry, corrosion, lubrication, and others. Traditional Surface Science is carried out in rarefied conditions of ultra-high vacuum (UHV) where the pressure is usually below 10^{-9} Torr/mbar, which make it possible to control the sample composition and cleanliness to within 0.1% of a monolayer (ML) or better. Surface Science, as practiced until the end of the 20th century, has provided much of our present understanding of solid surfaces.¹⁻² This is because an extensive array of surface-sensitive microscopy and spectroscopy techniques exists that operate in UHV, and these techniques have revealed the atomic, electronic, and chemical structure of many crystal surfaces in their ideally pristine state at pressures below 10^{-6} Torr, and mostly at a sample temperature of room temperature or below. While these low pressure–low temperature studies have helped us to understand the structural aspects, thermodynamics, and kinetics of certain model reactions, practical catalytic reactions typically take place in the presence of gases (or liquids) at much higher pressures and at room temperature or above.

Our knowledge of surfaces under such realistic conditions is far less extensive than in UHV, because a few surface-sensitive techniques exist outside the optical domain that can probe surfaces in the presence of gases at ambient pressure conditions. This lack of knowledge is referred to as the “pressure gap”. However, it is more accurate to think of this lack of knowledge as made up of three different gaps, determined by pressure, temperature, and complexity of the system. The pressure gap is due to two reasons: The first reason is that most surface-sensitive techniques require high vacuum for operation because probe particles (electrons, ions, etc.), whether incoming or outgoing, have mean free paths below 1 mm at pressures above a few mTorr. A high coverage of adsorbed atoms or molecules on surfaces is the norm in operating or storage conditions, but in UHV conditions high densities of adsorbed atoms or molecules can often be obtained only by keeping the surface at low temperatures (typically at liquid nitrogen temperature (77 K) and below). This requirement for controlling the adsorbed layer is the second reason for the pressure gap. However, at low temperature, the kinetics of surface processes can be too slow compared to timescales of an experiment, which is mostly of minutes to hours. The “temperature gap” therefore is more important because temperature affects kinetics in an exponential way, while pressure affects the kinetics in a slow power law (e.g., linear for first order processes, quadratic for second order, etc.). In short, a pressure–temperature gap occurs as a consequence of kinetic hindrances that might not allow for the thermodynamically favorable structure to form. In addition, entropic effects also play a role at higher temperatures. Both the pressure–temperature effects and the entropic

contributions are difficult to fully take into account when extrapolating experimental results obtained in UHV to the relevant reaction conditions. Finally there is also a “complexity gap”, related to the fact that most practical materials are not single-crystals, but are in the form of powders, nanoparticles, porous media, etc., that add additional barriers to molecular and atomic level characterization.

The approach in Surface Science that we call ‘Ambient Pressure Surface Science’, stems from an effort to bridge these three gaps between science and technology. The vast majority of studies in this new research field are conducted within the context of heterogeneous catalysis. This is because catalysts are the work horses in the refinery, chemical production, and energy conversion processes, and there is a significant demand for improvements in their activity (the rate at which the reactants are converted to products) and selectivity (the fraction of the products which are the desired chemical). Furthermore, chemical process costs can be reduced significantly by replacing precious metal catalysts with others based on low-cost materials, like transition metals with 3d-valence electrons and their alloys. A condition for the rational design of improved catalysts is a thorough understanding of the underlying mechanisms by which the catalyst functions. In particular, the atomic and chemical structure of a catalyst surface plays a crucial role in its performance in terms of its activity and selectivity towards sought-after products, and this can change dramatically with reaction conditions. For example, as we will show with examples in this Review, model single-crystal catalyst surfaces have been observed to restructure dramatically as the pressure is increased from UHV to the Torr/mbar pressure regime and above, a phenomenon indirectly predicted more than a century ago by Irving Langmuir, the Founding Father of Surface Science. He stated:³

“The atoms in the surface of a crystal must tend to arrange themselves so that the total energy will be a minimum. In general, this will involve a shifting of the positions of the atoms with respect to each other.”

The amount of experimental observations of this long-anticipated atomic scale phenomenon increased very significantly with the advent of Scanning Tunneling Microscopy (STM), an imaging technique capable of resolving single atoms.⁴ The results presented in this Review were all obtained by STM, usually in a separate smaller volume chamber connected to the main UHV chamber, at ambient/high pressure, broadly defined as 1 mTorr and above, hence the name high pressure STM or simply HPSTM. The scope of HPSTM is limited to bridging the pressure-temperature gap, as atomically flat single-crystal samples are necessary for imaging with atomic resolution. This trade-off between atomic-level information and bridging the complexity gap was suggested by Irving Langmuir about a century ago. In his own words, Langmuir suggested using “checkerboard surfaces” (single-crystals) as model systems for more complex “porous bodies” (real catalysts like nanoparticles or foils).⁵

There are several surface-sensitive spectroscopy techniques that can also operate under ambient conditions which provide invaluable information to help to interpret the HPSTM images. One is ambient pressure x-ray photoelectron spectroscopy (APXPS). XPS relies on the short inelastic mean-free paths (IMPF) of electrons, and can provide powerful information on chemical composition, but has traditionally been limited to UHV conditions to minimize gas-phase scattering prior to collection of the photoelectrons and to prevent deterioration of its electron optics and electron detector components. During the last decades, APXPS has been developed, extending the operating pressure into the Torr/mbar pressure regime.⁶ The current generation of APXPS analyzers utilizes electron optics to focus photoelectrons through several apertures as part of a multistage, differentially pumped lens system, increasing the photoelectron collection efficiency and extending the measurement range up Torr/mbar pressure regime. Another important technique is infrared reflection absorption spectroscopy (IRRAS), which has been used extensively since the beginning of surface and catalysis science.⁷ Compared to APXPS, this technique is superior in determining the chemical state of adsorbates and their adsorption sites, but it is not element specific and less quantitative than APXPS. An important advantage of IRRAS over APXPS is the pressure range; by modulating the linear polarization of the infrared light in real-time, it is possible to investigate surfaces even in the presence of 1 bar of reactant gases. This is because gas-phase species are randomly dispersed in space and have no polarization dependence, whilst adsorbed species are oriented.

1.2 Why STM?

STM is an atomic-resolution imaging technique (lateral resolution ~100 pm and vertical resolution ~1-3 pm at room temperature) which is best suited for atomically-flat surfaces, due to the finite tip apex size. STM can operate in ambient gases and air, so there is no limitation on its operation under controlled gas pressures.

Among the surface characterization tools that are applicable in the presence of gases, STM has one great advantage: the measurement itself is not invasive, i.e., it does not affect or modify the surface structure significantly, in contrast to microscopy or spectroscopy techniques that either employ or produce a high energy and high flux of electrons (e.g., environmental transmission electron microscopy (e-TEM), APXPS, etc.). The high energy particles ionize the gas phase molecules and they also produce secondary electrons that are very effective in dissociating the adsorbed molecules. This is called 'beam-induced chemistry' or 'beam damage', and it is highly undesirable.⁸ These problems can be circumvented, but this is an important topic worthy of a separate review. Another practical advantage of HPSTM instruments is that it can be used by individual research groups, without the need for large and often remotely located user facilities.

The downside of operating under ambient gas pressures is the possible contamination of the inner

walls of the chambers that house the analysis instruments when reactive species are used. Base pressures of 10^{-10} Torr/mbar can be restored in several ways, including the conventional baking at over 110 °C for two days, and by performing a 'plasma cleaning' of the chamber prior to measurements at ambient pressures. The latter is an efficient way to remove hydrocarbons, water, and other contaminants desorbing from the chamber walls as they can be displaced by the reactant gases introduced in the chambers. Another source of potential contamination is the crystal itself, even after the conventional cleaning procedure of sputtering and annealing cycles. Similar to STM studies in UHV, most research groups performing HPSTM measurements check the cleanliness of their samples with Auger-Meitner electron spectroscopy (AES), or with XPS, prior to STM measurements, to confirm that the contaminant level is below the detection limit of these techniques (<1% of a monolayer). However, even an initially clean surface may become contaminated again when contaminant species dissolved in the bulk diffuse to the surface and, in the presence of gases, react and become anchored there.

In traditional Surface Science studies, combination of STM with low energy electron diffraction (LEED) has proven to be very effective in determining the atomic structure of surfaces. At ambient pressures, it is not possible to use LEED as it employs low energy electrons as the probe particles. Instead, various forms of x-ray scattering can be used, including grazing x-ray diffraction, and others that will not be reviewed here. In addition to the experiment tools, theoretical methods have been developed that continuously improve, chiefly among them is density functional theory (DFT) for structural and chemical analysis. In some recent studies, the gas phase chemical potential is included in the calculations, making them comparable to experimental studies at ambient pressures and temperatures.

This Review article will be devoted solely to HPSTM as the main structural analysis tool, supported as needed with spectroscopy and theory results for interpretation of the images. Readers may refer to the original papers for full details of the theoretical and experimental techniques used in determining the surface structures.

Leading groups in HPSTM are based in Berkeley, Aarhus, Leiden, Berlin, Munich, and increasingly in many other institutes. Thanks to efforts by research groups in Aarhus University in Denmark,⁹ and the University of Leiden in the Netherlands,¹⁰ different HPSTM setups that can operate in the presence of gases are now commercially available. The Leiden HPSTM, for example, quotes that it can operate at 6 bar and ~300°C, reaching the industrial reaction conditions of many important catalytic reactions.

All the transition metals discussed in this Review have a face-centered cubic (fcc) structure, with the exception of Co which has a hexagonal close-packed (hcp) structure at room temperature.

A final remark is that we use both mbar and Torr throughout this Review, depending on the pressure unit used in the original paper.

2. Instrumentation

Traditional Surface Science experiments are conducted in UHV conditions and it is rather straightforward today to obtain atomic resolution on crystal surfaces with commercial or custom-built UHV-STM instruments. There are two ways to adapt any type of Surface Science experiment from UHV conditions to ambient/high pressures. The first and simpler one is backfilling the UHV chamber with gases up to 1 bar pressure. STM can work in air, so there are no technical constraints in operating it in the mbar-bar pressure range. The only consideration should be the possibility of igniting a low-temperature plasma in the 10^{-2} - 10^{-3} Torr pressure range triggered by the high voltage applied to the piezoelectric material of the STM scanners. This problem can easily be dealt with by mixing the reactant gas with argon and keeping the total pressure higher. The maximum pressure is limited by the viewports of the UHV setup that cannot sustain higher pressure differences between ambient air and the pressure inside the vacuum vessel. Therefore, for a safe operation, this approach is limited to 1 bar pressure. The main advantage of this approach is that it is easy to build and maintain a very robust scanning head, and therefore it is easier to get atomically resolved images. It is also very easy to exchange tips between measurements. The main disadvantage is controlling the temperature, as this approach is only applicable near room temperature because convective heat transfer could also warm the materials in the scanning head and sample support, causing temperature gradients and thereby thermal drift.

The second way of performing HPSTM experiments is to use a small high-pressure cell inside the UHV chamber. This approach is technically more difficult, but it has several advantages over the backfilling approach. First of all, since only a small volume is pressurized, a lot of gas is saved and it is easier to reach atmospheric pressures. More importantly, it is possible to heat the entire cell and reach moderate temperatures. Finally, the gas cell will reduce the surface area of the surrounding walls. For instance, typical contamination at ambient pressure experiments is water molecules emanating from chamber walls; using a reactor cell with an inert Au-coating might reduce its partial pressure. The Berkeley HPSTMs and the Aarhus HPSTMs work on this principle.¹¹⁻¹³ We show the original designs of these two HPSTMs in Figures 1 and 2.

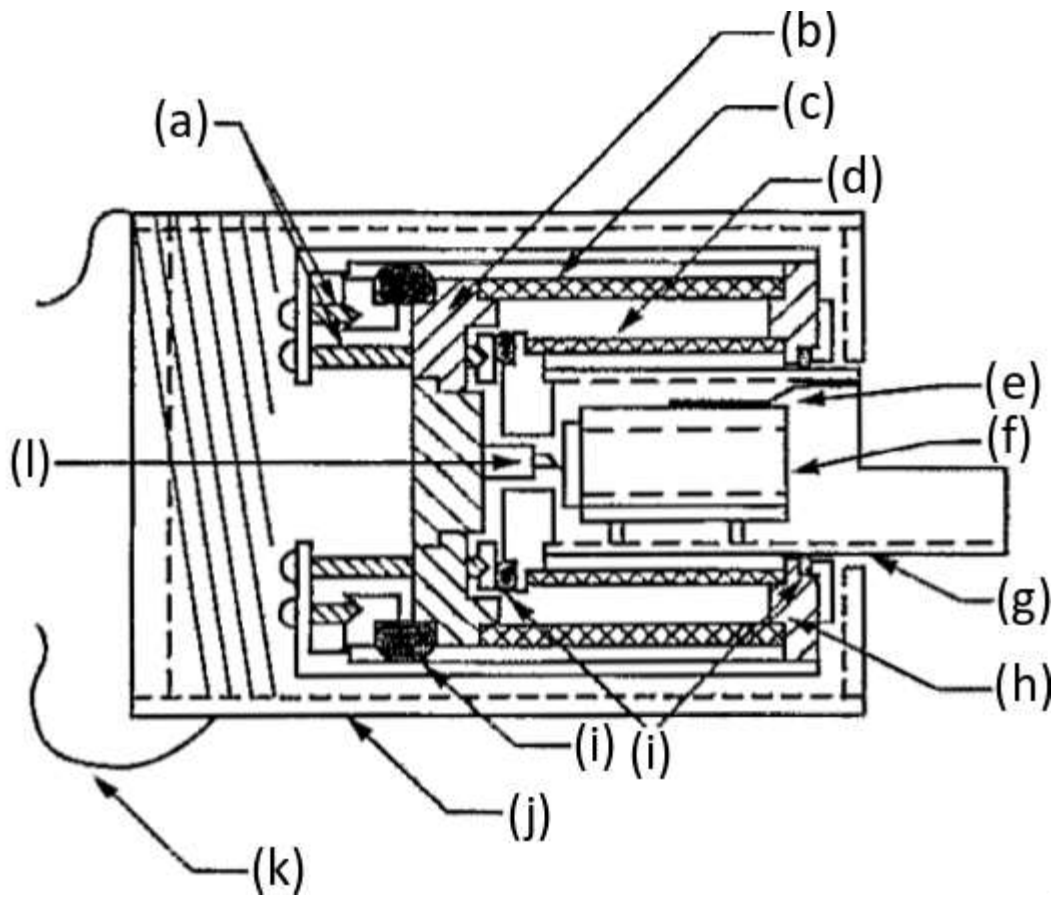


Figure 1: The first design of the Berkeley HPSTM. Labeled parts are: (a) machine screws; (b) scan plate and tip assembly; (c) outer piezo (scan); (d) inner piezo (offset); (e) gold foil; (f) sample holder; (g) anodized aluminum tube; (h) base plate; (i) Viton cord; (j) anodized aluminum heating shroud; (k) Kapton insulating copper heating wire; (l) tip. Reprinted with the permission from Ref.¹¹. Copyright 1993 American Institute of Physics.

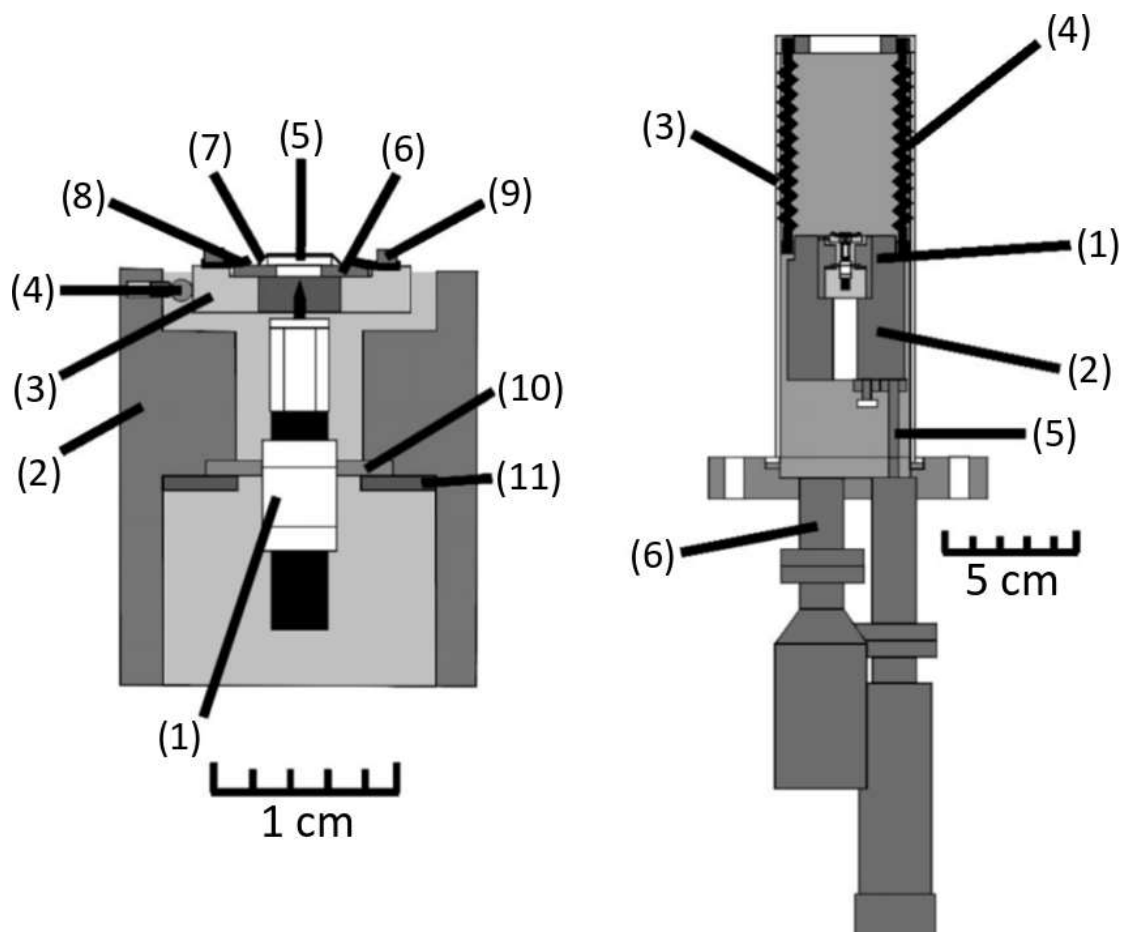


Figure 2: The first design of the Aarhus HPSTM. Labeled parts in (a) are: (1) Inchworm-scanner-tip assembly; (2) Invar housing; (3) sample holder; (4) quartz balls; (5) sample; (6) Ta support; (7) Ta foil; (8) leaf springs; (9) screws; (10) Macor ring; and (11) support ring. Labeled parts in (b) are: (1) STM assembly; (2) mounting block; (3) outer steel tube; (4) suspension springs; (5) linear translator; and (6) electrical feedthroughs. Reprinted with the permission from Ref.¹³. Copyright 2001 American Institute of Physics.

Another design uses a small reactor cell with a small orifice for the STM tip to protrude into the cell. The advantage of this approach is that there is only limited gas flow outside of the reactor cell, in a separate compartment where the piezoelectric scanner is located. This results in smaller thermal drift even at gas pressures of a few bar. The Leiden HPSTM works according to this principle,¹⁴⁻¹⁵ and its design is shown in Figure 3.

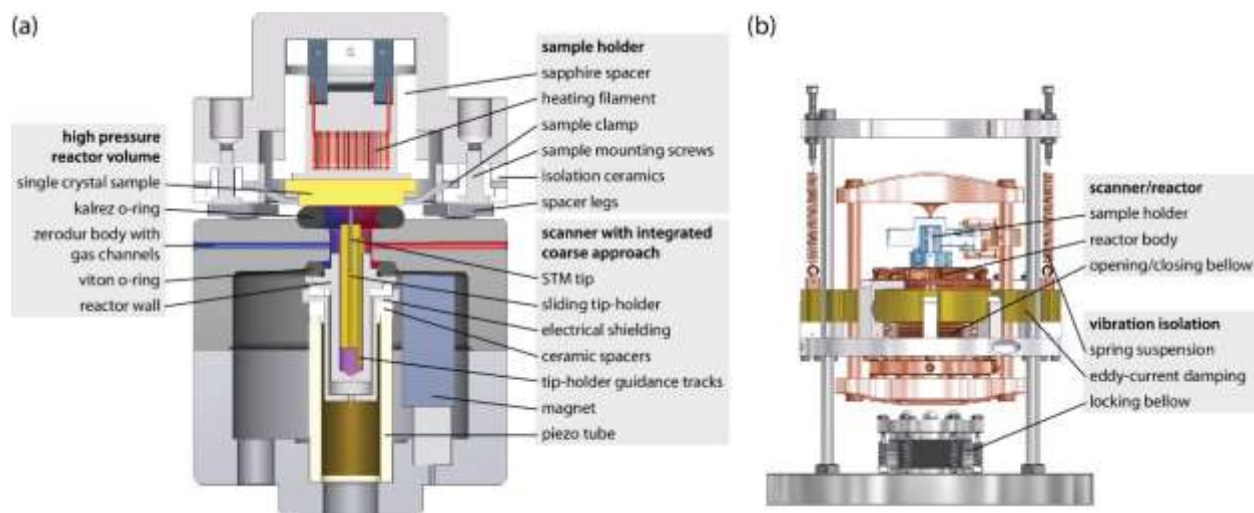


Figure 3: The design of the state-of-the-art 'Reactor STM'. Reprinted with the permission from Ref.¹⁵. Copyright 2014 American Institute of Physics.

An advantage of using reactor cells is that the gas leaking into the UHV chamber housing the reactor cell can be analyzed with a mass spectrometer to measure the reaction products. In this way, changes in the surface structure can be correlated with reactivity.

3. Carbon Monoxide Adsorption Studies on Low Miller-Index Surfaces

Carbon monoxide is an important molecule involved in many chemical catalytic reactions: CO oxidation, Fischer-Tropsch synthesis, water gas shift, and many more. It is also special because of its σ -donation and π^* -back-bonding adsorption mechanism on transition metal surfaces.¹⁶ CO is also used in STM and in non-contact atomic force microscopy (NC-AFM) while chemically bound to the tip apex. In this configuration it solves a problem that has been plaguing STM and AFM since their inception; standard tips have a termination of uncontrolled shape and chemical identity. By decorating the scanning tip with a CO molecule the problem is resolved in an easy and elegant manner. Today this widely used method has facilitated obtaining images with very high resolution in a routine way.¹⁷ We should mention here that more than half of the HPSTM studies are with gas mixtures containing CO, and therefore, CO will also be adsorbed on the metallic tip, which explains many of the highly resolved images obtained in these studies. Because of its historically important role in the understanding of the structure of surfaces at ambient pressures, we start this Review with CO adsorption studies performed with HPSTM. In this Section, we will focus on some transition metals on which CO adsorbs to strongly.

CO on Pt(111): The adsorption system CO on Pt(111) was named the “*Drosophila*” of Surface Science,¹⁸ referring to this system as being the most studied. We owe a considerable amount of our

present understanding of the surface-adsorbate interaction, thermodynamics, and kinetics of adsorption to this specific system. In addition, one of the most impressive structures identified with HPSTM forms when gas phase CO is in equilibrium with the adsorbed CO molecules on the Pt(111) surface. The specific binding configurations of adsorbed CO molecules depend on the type of transition metal. In the case of Pt(111), adsorbed CO takes nonspecific binding positions when the CO pressure is higher than 10^{-6} Torr,¹⁹ i.e., the steric repulsion between adjacent chemisorbed CO molecules at a high coverage plays a very important role in determining the binding structure of CO on the Pt(111) surface. In these high coverage structures formed in equilibrium with the surrounding CO gas, each adsorbed CO molecule is surrounded by six neighboring CO molecules forming a two-dimensional hexagonal structure with lattice periodicity different from that of the Pt(111) surface. As a result the CO adlayer overlapping with the hexagonal pattern of Pt(111) forms a moiré pattern (Figure 4a and 4b). In Figure 4a and 4b, both the individual chemisorbed CO molecules and the moiré pattern is resolved since they both appear brighter than the rest of the surface.

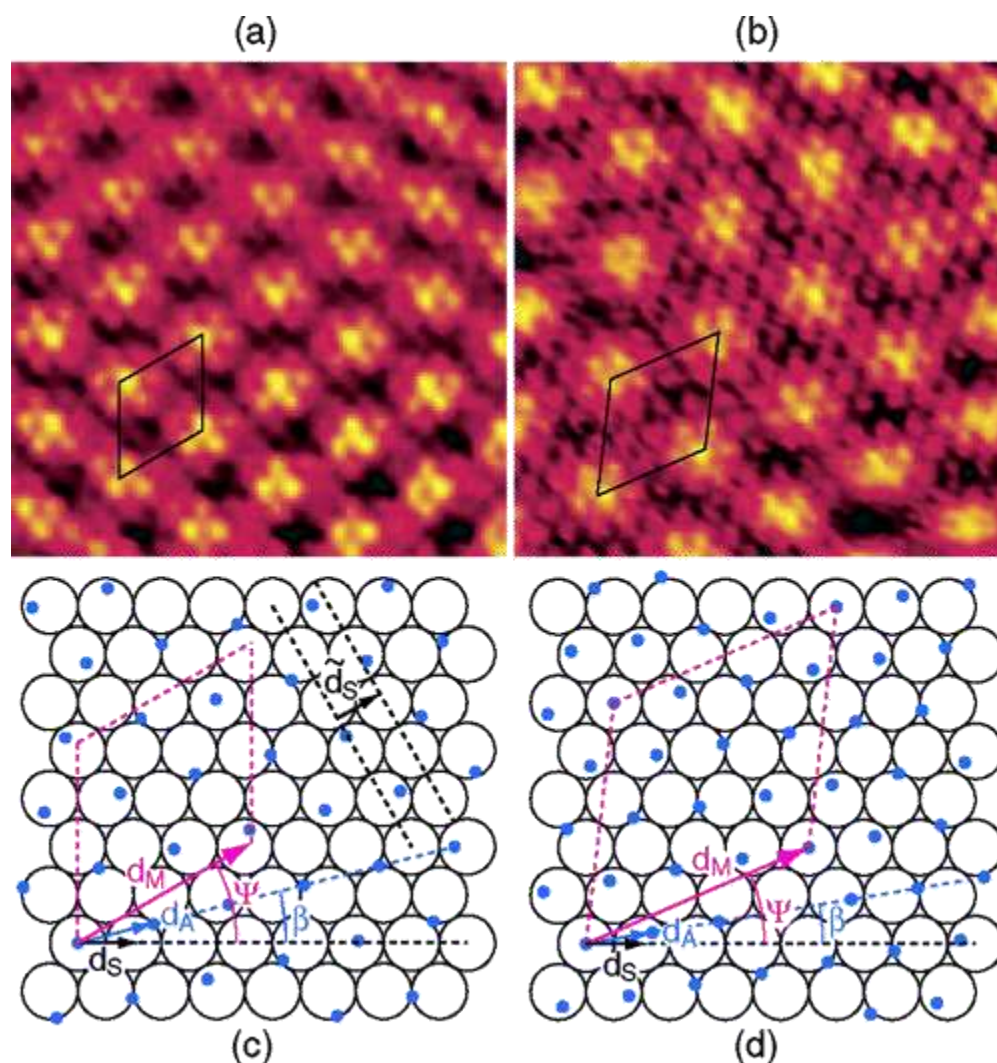


Figure 4: (a) and (b) HPSTM images of the Pt(111) surface in the presence of 0.01 Torr and 720 Torr CO at room temperature, respectively. The images in (a) and (b) are aligned so that the $[1\bar{1}0]$ direction is oriented along the x axis. (c) and (d) show the structural model of the Pt(111) surface with adsorbed CO molecules in the presence of CO at 0.01 Torr and 720 Torr of CO at RT, respectively. In the ball-models in (c) and (d), the open circles represent Pt atoms and the blue dots CO molecules. \vec{d}_m and \vec{d}_s form angles Ψ (rotational angle between substrate and moiré lattice), and β (rotational angle between the substrate and the adsorbate lattices), respectively, relative to the $[1\bar{1}0]$ direction of the substrate. (c) incommensurate structure with $\Psi = 30^\circ$, $\beta = 10.4^\circ$, $d_M/d_S = 3.6$. (d) commensurate ($\sqrt{19} \times \sqrt{19}$) R23.4°-13CO structure with $\Psi = 23.4^\circ$, $\beta = 9.5^\circ$, $d_M/d_S = 4.4$. Unit cells are shown both in the HPSTM images and in the ball-models. Reproduced with permission from Ref.¹⁹. Copyright 2004 American Chemical Society.

We should mention that the structures observed in Figure 4a and 4b are different from the various non-hexagonal and commensurate adlayer structures (all related to $c(2 \times 4)$ periodicity) observed in adsorption experiments at low temperatures performed in UHV.²⁰⁻²² Figures 4c and 4d show ball-models of two adlayer structures adsorbed on the surface at different pressures. The CO adlayer is continuously compressed with increasing pressure, resulting in a continuous coverage variation from 0.5 to 0.7. The orientation of the moiré pattern, whose formation is due to the superposition of the hexagonal adsorbate layer with the hexagonal substrate, is also pressure dependent. At coverages between ~ 0.5 and 0.6, the moiré pattern is rotated by 30° with respect to the $[1\bar{1}0]$ direction, but at a coverage of 0.6, the system undergoes a rotational phase transition that does not change anymore by further increasing the pressure. According to Ref.¹⁹, this behavior is due to increasing importance of the repulsive lateral molecular interaction, which starts to dominate over the corrugation of the substrate interaction potential.

According to the models in Figure 4, CO adsorbs both on the top sites and near the bridge sites. This was later confirmed with both APXPS and IRRAS studies.²³⁻²⁴ The adsorption system CO on Pt(111) is unique in the sense that a moiré pattern through adsorption was not observed on any other system studied with HPSTM.

CO on Pt(110): Bare Pt(110) surface is reconstructed into a (1×2) missing-row reconstruction in the absence of adsorbates.²⁵ Figure 5a shows a model of the surface with missing-row reconstruction, on which the coordination number of each atom is labeled. Figure 5b shows the atomically resolved STM image of the Pt(110)- (1×2) surface. Interestingly, except for Pt(111), all the low Miller-index surfaces of Pt and Au are readily reconstructed. The reconstructed surfaces differ in energy only slightly from that of the (1×1) surface structure; for instance the energy per atom of the Pt(110)- (1×2) surface structure was calculated to be only 27 meV lower than the Pt(110)- (1×1) .²⁶ Without exception all surfaces that are readily reconstructed in their clean state undergo transformation upon chemisorption even under low CO

gas pressure. In the case of Pt(110)-(1×2), under CO pressures in the 10^{-9} - 10^{-7} mbar the coverage of CO is sufficient to lift the reconstruction and form a Pt(110)-(1×1) surface.²⁷ This (1×1) surface, however, is not a perfectly flat surface, but contains still many monatomic step edges.²⁷⁻²⁸ Faster kinetics at 373 K facilitates diffusion and results in a smaller number of step edges, and channels along the [001] direction formed by displaced Pt atoms,²⁸ as shown in Figure 5c. Figure 5c-h shows the evolution of the surface at 373 K as a function of CO partial pressure. At low CO partial pressures (10^{-5} mbar and lower), the monatomic channels along the [001] direction remain, whereas the transition of the step edges from low to high kink-density start to become observable within minutes at CO partial pressures of 10^{-3} mbar.²⁸ Further increase in CO partial pressure to 1 bar eventually leads to replacement of the monoatomic channel structure by islands elongated in the $[1\bar{1}0]$ direction. Figure 5h shows a high-resolution image acquired in the presence of 1 bar CO, which shows a zigzag structure.²⁸ This zigzag structure is not due to the atomic structure of the Pt surface, which remains (1×1), but is due to tilted CO molecules as a result of steric repulsion.²⁸ Such zigzag pattern has also been observed in high CO coverage studies in UHV on Pt(110) surface,²⁸ as well as on Ni(110) surface with 19° tilt angle, and on Cu(110) with 2.5° tilting in the $\langle 001 \rangle$ directions.²⁹ The crystallographic notation of this zigzag pattern is $(2\times 1)\text{-}p2mg\text{-}2\text{CO}$ layer.

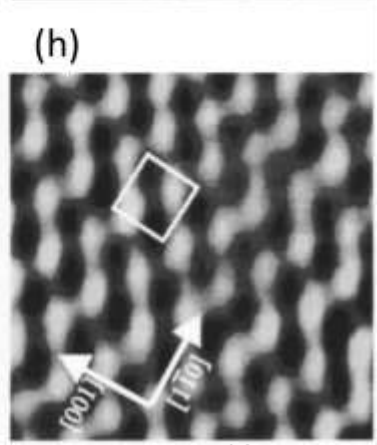
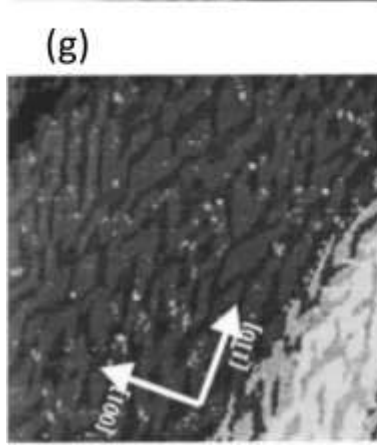
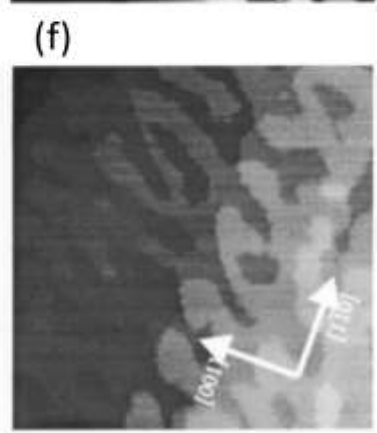
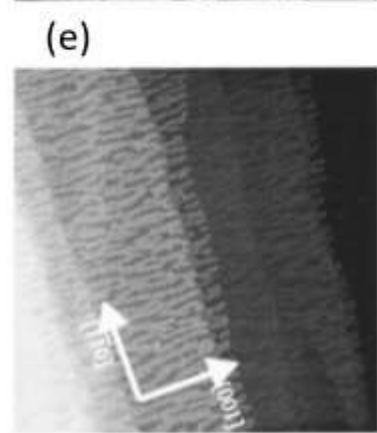
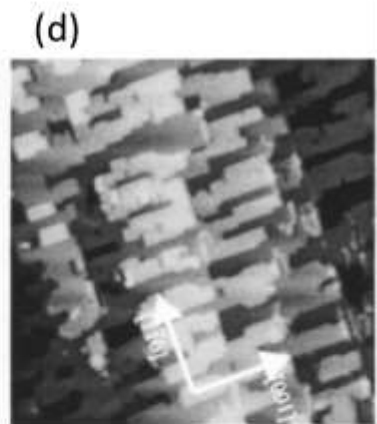
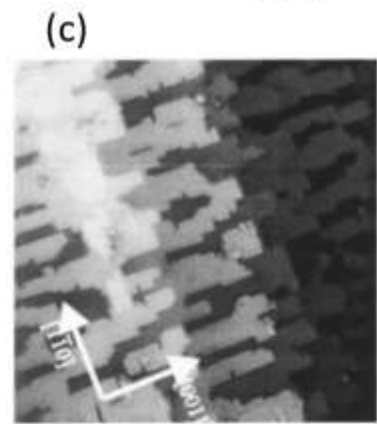
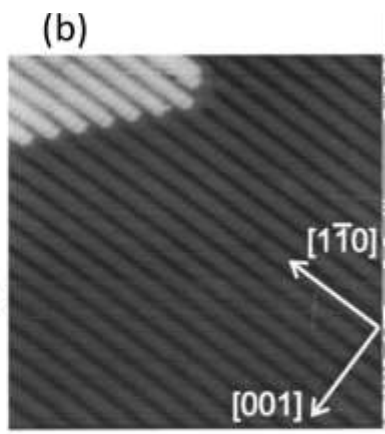
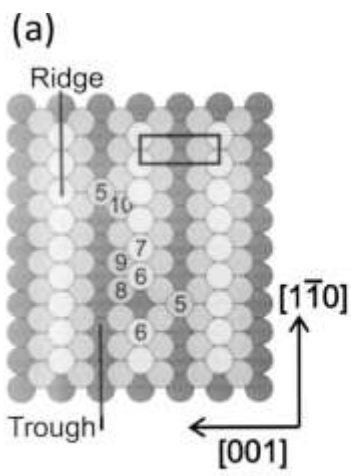


Figure 5: (a) The atomic model of the Pt(110)-(2×1) surface. (b) STM image of the Pt(110)-(2×1) surface in UHV at room temperature (14.1×15.5 nm²). HPSTM images of Pt(110) at different CO pressures: (c) 10⁻⁷ mbar CO, (30×30 nm²); (d) 10⁻⁶ mbar CO, (30×30 nm²); (e) 10⁻⁵ mbar CO, (100×100 nm²); (f) 10⁻² mbar, (70×70 nm²); (g) 1000 mbar CO (90×90 nm²); and (h) 1000 mbar CO (2.8×2.8 nm²). The contrast in (c-g) originates from the monatomic height differences, whereas the contrast in (h) originates from the tilted CO molecules on the surface. The images (c)-(h) were obtained at 373 K. Reproduced with permission from Ref.²⁸. Copyright 2004 American Institute of Physics.

The authors of Ref.²⁸ explain the structural changes on the surface using DFT calculations, which suggest that the gain in CO binding energy on a low-coordinated step edge site relative to the high coordination terrace sites is similar to the formation energy of step edges. Thus, at finite temperatures step edges will form due to the higher entropy of a stepped surface. At low CO coverage, kink formation is not energetically favorable, while at a CO coverage close to saturation, CO starts to adsorb also on high-coordinated Pt atoms in the second-layer, and the energy gained in the kink-free channel structure vanishes. Entropic effects are then manifested as kinked step edges.

This work on CO/Pt(110) is the first in the literature where roughening of the surface was observed with atomic-resolution real-space images,²⁸ and therefore carries a significant importance in terms of our present understanding of the equilibrium structure of surfaces in the presence of gases. The roughening geometry in this case proceeds via monoatomic channel formation. In the next case, we will see roughening of the surface by the break-up of the surface layer into two-dimensional nanoclusters.

CO on Pt(100): Similar to the Pt(110) surface, Pt(100) surface is also readily reconstructed in UHV: Instead of a square (1×1) structure, the surface overlayer forms a quasi-hexagonal structure with 6 Pt atoms residing on top of 5 Pt atoms of the subsurface layers. In fact, the existence of such a special surface structure was already suggested more than half a century ago in one of the earliest Surface Science studies in UHV.³⁰ Figure 6a shows a model of the quasi-hex-Pt(100) surface, and Figure 6b shows a sample STM image acquired in UHV at room temperature. It is well established that chemisorption of CO lifts this reconstruction so that the topmost Pt atoms form a square lattice structure.³¹⁻³⁶ Some of these studies were performed using LEED in UHV,^{32,34-36} which provides crystallographic information of the ordered part of the surface when the domain dimensions are larger than the coherence length of the electron beam. Smaller domains, however, would give rise to broadened diffraction spots, which would make crystallographic analysis of the structure more difficult. Additionally, in most cases, the surfaces were examined after pumping away the CO gas, which results in desorption of the more weakly bound CO molecules.

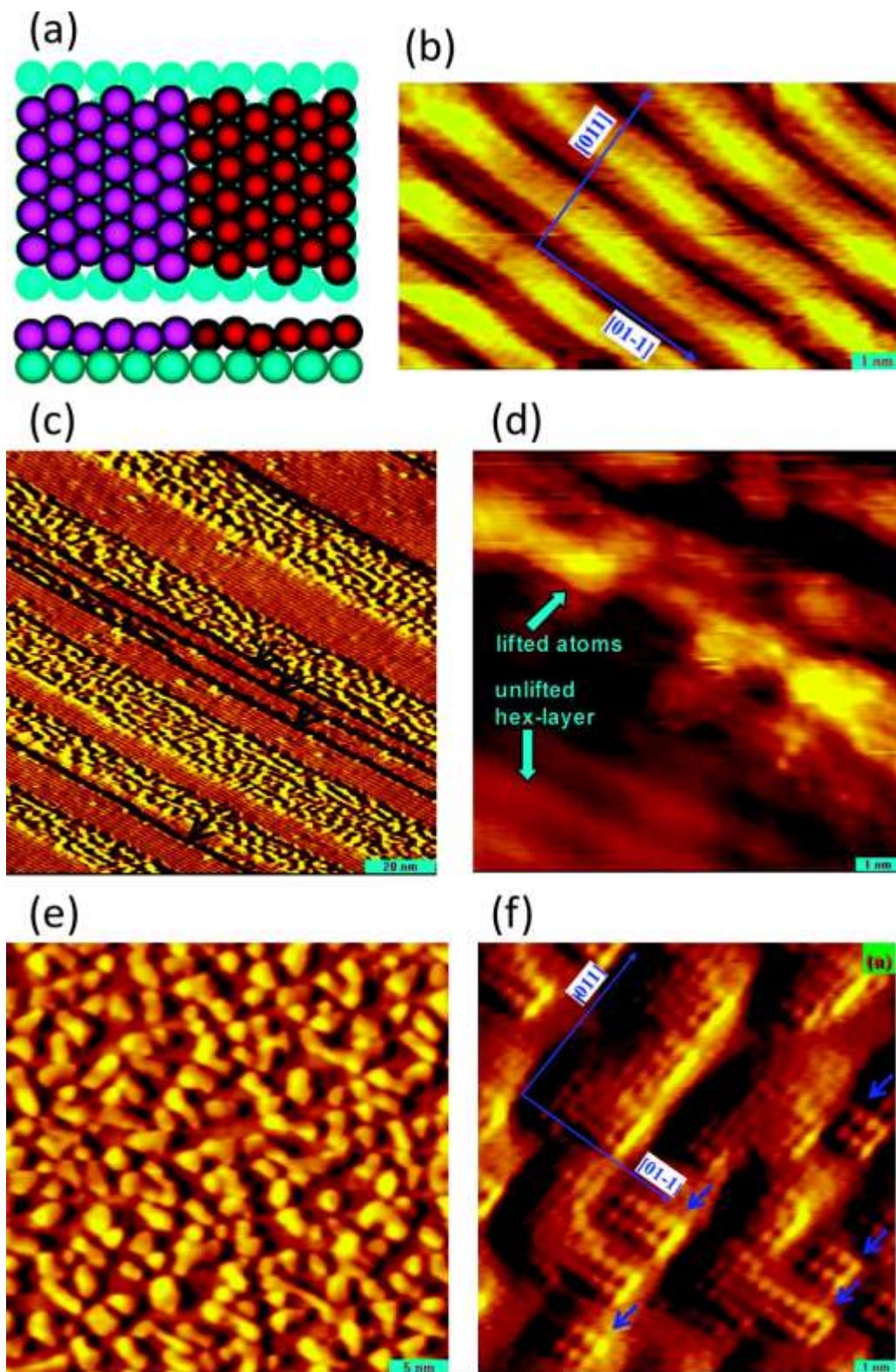


Figure 6: (a) Top and side view of the atomic model of the quasi-hexagonal reconstructed surface of Pt(100). (b) STM image of the reconstructed Pt(100) surface in UHV at room temperature. HPSTM images of Pt(100) at different CO pressures: (c-d) 2×10^{-9} - 10^{-8} mbar CO; (e-f) 10^{-6} to few mbar CO,

(38×36 nm²) and (10×10 nm²). Images were obtained at room temperature. While (c) and (d) show the lifting of the reconstruction, (e) and (f) show formation of Pt clusters on the surface. Reproduced with permission from Ref.³⁷. Copyright 2009 American Chemical Society.

An earlier STM study of the quasi-hex-Pt(100) after dosing a few Langmuir (one Langmuir is equal to 10⁻⁶ Torr·s of exposure) of CO suggested clusters of CO to form on patches of Pt(100)-(1×1).³³ The authors of Ref.³³ suggested adsorbed CO to be trapped on the (1×1) patches due to the difference in stability of CO on Pt(100)-(1×1) and quasi-hex-Pt(100) surfaces. A more recent HPSTM study agrees that CO lifts the quasi-hex-reconstruction (Figures 6c and 6d), but the authors propose another mechanism where the 20% extra Pt atoms on the surface diffuse and form rectangular clusters on the surface covered by CO molecules (Figures 6e and 6f).³⁷ In other words, whilst Ref.³³ suggests purely CO clusters, Ref.³⁷ suggests CO covered Pt-clusters on the surface. In the latter model, chemisorbed CO molecules at the edge of the clusters fan out away from the cluster due to steric hindrance between neighboring CO molecules. The total number of bright spots in Figure 6f corresponds to 23% of the area, close to the expected 20% in the model. The total area of the two-dimensional Pt-cluster coverage is 45%, but the clusters appear larger than they are due to the tilt of the CO molecules on the step edges. More examples of decoration of cluster edges with tilted CO molecules are seen in other studies discussed later in this Review.

There is a discrepancy between the proposed model based on HPSTM images, and the (2×2) structure observed by LEED after exposing the Pt(100) to CO.^{32,34-36} The structure revealed by LEED refers to the large coherent domains between the small islands, whereas STM detects the top of the two-dimensional clusters. These clusters, because of their small size, should contribute mostly to the background in the diffraction pattern.³⁷

To summarize the CO adsorption experiments on low Miller-index Pt surfaces: on both Pt(100) and Pt(110), the initially reconstructed surfaces undergo large structural changes in the presence of CO, both at low and at high pressures (1 mbar and above). The Pt(110) and Pt(100) are readily-reconstructed surfaces, and one should expect that such reconstructions would be lifted thanks to the energy provided by the exothermic adsorption of CO molecules on the surface. In fact, no roughening was observed on the unreconstructed Pt(111) surface consisting of large and flat (111) domains. Instead, a dense adlayer of adsorbed CO molecules covered the surface. These observations bring into question whether there are other transition metal surfaces where an unreconstructed and compact (1×1) surface can also undergo massive transformations in the presence of gases. The answer is yes, as explained in a later section of this Review.

CO on Rh(111): One of the earliest atomically-resolved HPSTM study was on CO adsorption on the Rh(111) surface.³⁸ Similar to Pt(111), Rh(111) is not readily-reconstructed in UHV and no rearrangement of the surface Rh atoms were observed in the presence of up to almost 1 bar CO. Instead, similar to the CO/Pt(111) case discussed above, CO forms dense adsorbate layers with various structures depending on the pressure (Figure 7). The dense adsorbate layers of CO form a (2×1) pattern at 5×10^{-8} Torr (Figure 7a), a $(\sqrt{7} \times \sqrt{7})R19^\circ$ pattern between 10^{-6} Torr and 10^{-5} Torr (Figure 7b), and a (2×2) pattern between 5 Torr and 700 Torr.³⁸ The (2×1) structure has one CO molecule on a top site in the unit cell, which appears as a protrusion in the STM image.³⁸ Ref.³⁸ also mentions that LEED patterns obtained at this pressure have either (2×2) symmetry or consist of three domains of (2×1) symmetry. STM, however, shows three domains of (2×1) symmetry rotated by 120° from each other. Structures formed above the pressure regime which LEED can access could therefore not be observed. Particularly interesting is the $(\sqrt{7} \times \sqrt{7})R19^\circ$ structure, which gives two different patterns: The first one is a trimer structure (ball-model is shown in Figure 7b-left), where 3 CO molecules adsorb on the hollow sites. The second one is similar, but with an additional CO sitting on a top site which gives a higher CO contrast than the CO on the hollow sites (ball-model is shown in Figure 7b-right). The transition from the (2×1) structure to $(\sqrt{7} \times \sqrt{7})R19^\circ$ -3CO structure requires only a small increase in coverage from 0.5 ML to a mixture of 3/7 ML and 4/7 ML. At higher pressures, a very clear (2×2) structure can be observed in Figure 7c. The contrast here originates from the CO on the top sites, which has higher contrast, i.e., higher tunneling probability, than CO on the hollow sites. The suggested model in Ref.³⁸ includes two additional CO molecules adsorbed on the hollow sites (ball-model is shown in Figure 7c), hence it is a (2×2)-3CO structure.

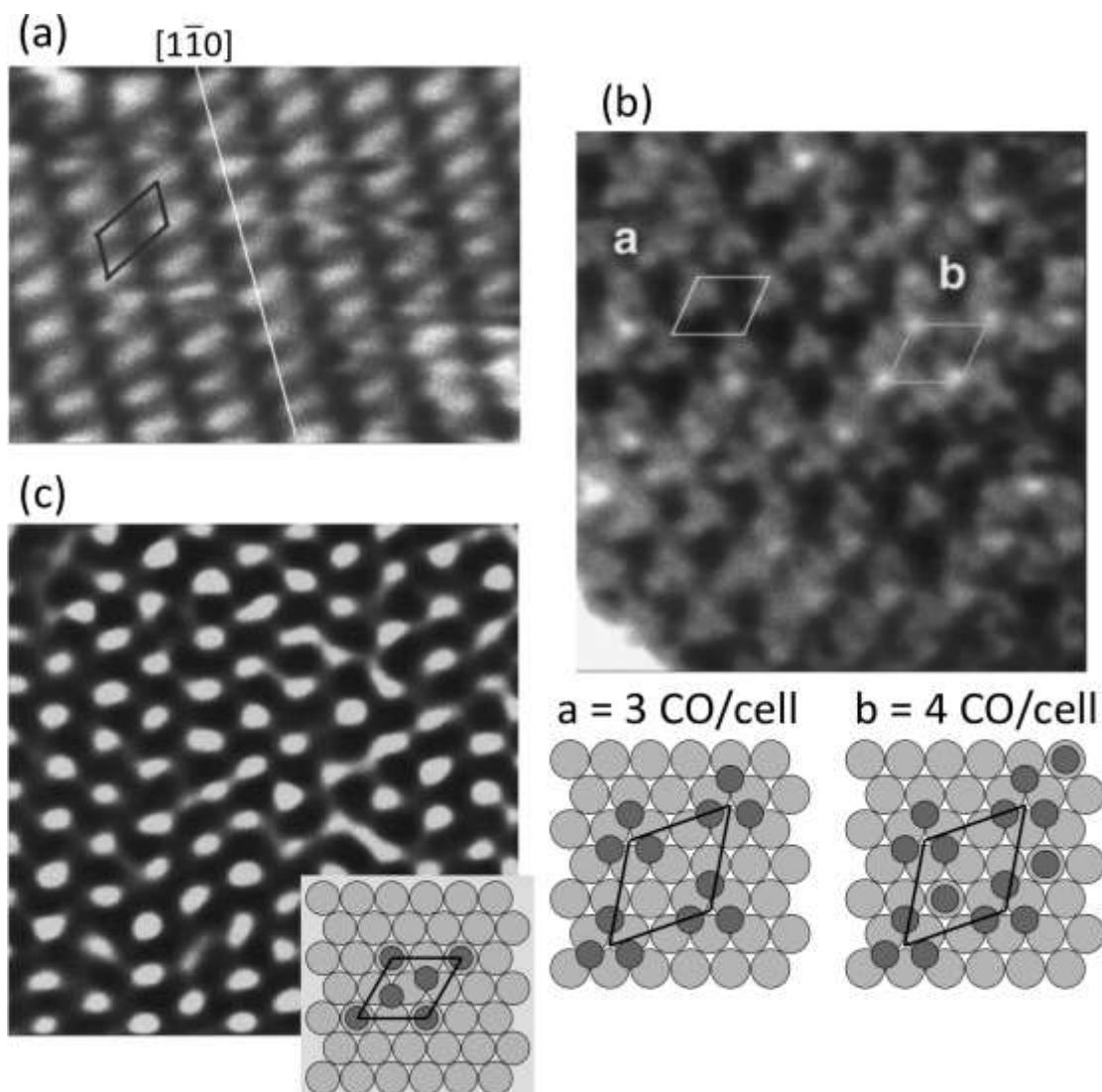


Figure 7: HPSTM images of the Rh(111) surface at room temperature in the presence of (a) 5×10^{-8} Torr, (b) between 10^{-6} and 10^{-5} Torr, and (c) between 5 Torr and 700 Torr CO. The white line in (a) shows the $[1\bar{1}0]$ direction. In (a), the adsorbed CO molecules form a (2×1) unit cell. Ball models underneath the images in (b) and (c) show the unit cells and the structures of the CO layers formed on the unreconstructed (1×1) surface. Light grey: Rh atoms, dark gray: CO molecules. Images were obtained at room temperature. Reproduced with permission from Ref.³⁸. Copyright 2000 Elsevier.

In summary, Rh(111) surface does not undergo structural reconstructions involving displacement of Rh metal atoms at room temperature in the presence of up to almost 1 bar CO. The condensed CO forms the following structures: (2×1) unit cell with 1 CO on a top site at 5×10^{-8} Torr, $(\sqrt{7} \times \sqrt{7})R19^\circ$ -3CO unit cell with 3 CO on hollow sites or $(\sqrt{7} \times \sqrt{7})R19^\circ$ -4CO unit cell with 3 CO on hollow sites and 1 CO on a

top site at 10^{-5} Torr- 10^{-6} Torr, and (2×2) -3CO unit cell with 2 CO on hollow sites and 1 CO on a top site at 5 Torr and above.³⁸

4. Adsorption Studies of other Molecules on Low Miller-Index Surfaces

NO on Pd(111): In this system the adsorbate structure formed at high pressure and room temperature is the same as that observed at the low pressure – low temperature experiments.³⁹⁻⁴² This structure has a (2×2) -3NO unit cell, with 0.75 ML coverage (Figure 8d). Figure 8a shows the STM image of the uncovered Pd(111)-(1 \times 1) surface, whereas Figure 8b shows the STM image of the 0.75 ML NO-covered Pd(111) surface.⁴³ Both images were obtained at room temperature, but the former in UHV and the latter in the presence of almost 1 bar of NO gas. Figure 8c shows the line profile across the surface, which shows that the NO molecule adsorbed on the top site has a higher STM contrast than that of the two other NO molecules on the hollow sites.

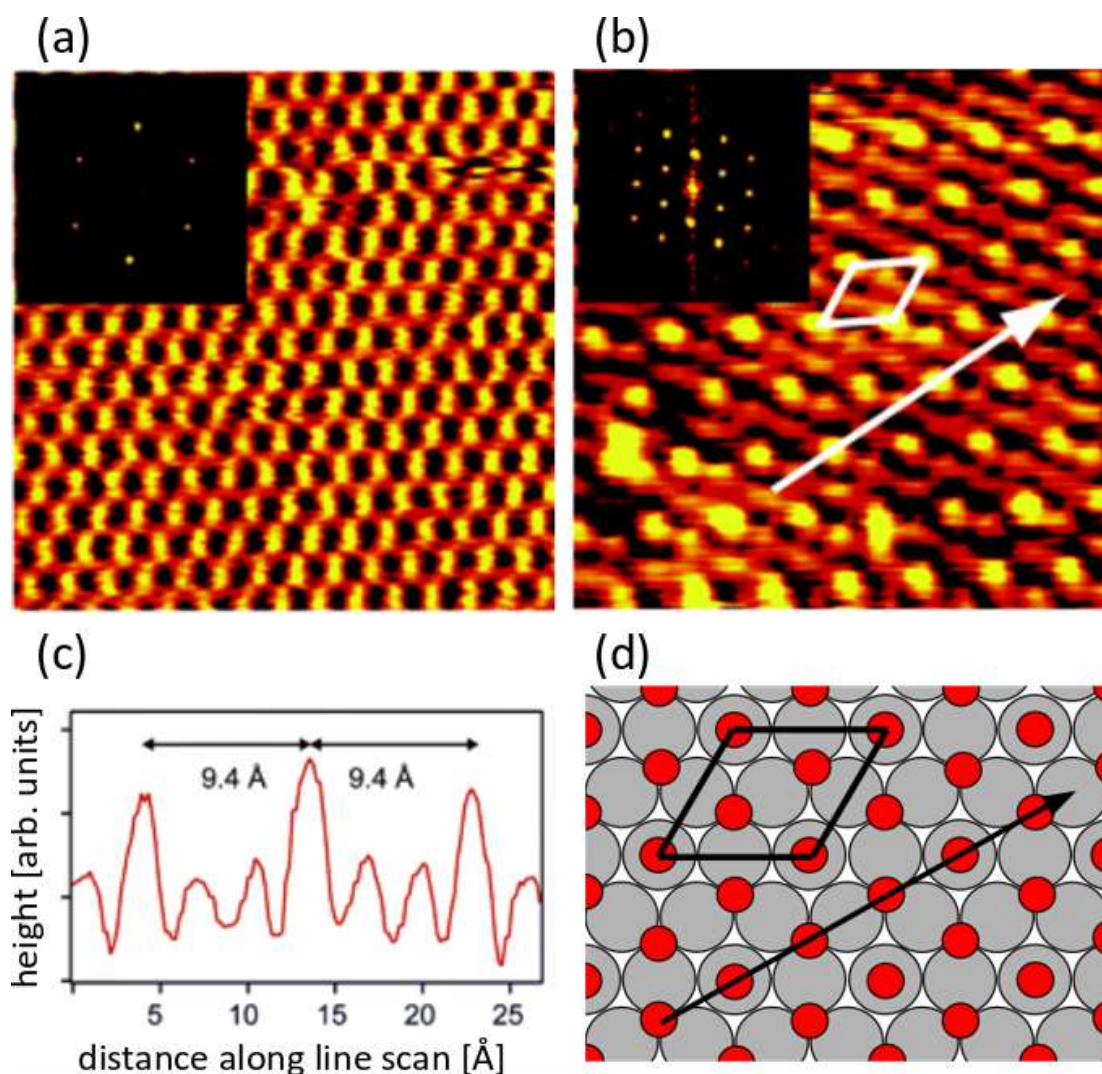


Figure 8: (a) STM image of the bare Pd(111) surface. (b) HPSTM image of the Pd(111) surface in the presence of 720 Torr NO. Both images are acquired at room temperature. The surface in (b) exhibits a (2×2) symmetry originating from the CO molecules attached to the surface, as shown in the ball-model (Pd: grey, NO: red) in (d). 3 NO molecules reside inside the (2×2) unit cell, 2 of them on the hollow sites and 1 of them on the top site. Top site NO molecules have a higher tunneling contrast than the NO molecules in the hollow sites, as shown in (c). Reproduced with permission from Ref.⁴³. Copyright 2005 American Chemical Society.

NO on Rh(111): Traditional Surface Science studies on NO adsorption on Rh(111) revealed a (2×2) adlayer structure at a coverage of 0.75 ML. This unit cell contains 3 adsorbed NO molecules, one on top and two in threefold hollow sites, with the on-top molecule showing an apparent height 0.4 Å higher than that of the molecules on hollow sites.⁴⁴⁻⁴⁵ In the presence of NO in the range of 10⁻⁸ to 0.01 Torr at room temperature, the images show a (2×2)-3NO periodicity, with only one maximum per unit cell,⁴⁶ which is similar to that formed by CO on Rh(111) discussed before, where STM images also show one maximum per unit cell.³⁸ Figure 9a-c shows the evolution of the structure of the adsorbed NO layer with time in the presence of 0.03 Torr NO.⁴⁶ The series of HPSTM images in Figure 9a-c were acquired at 55 s intervals. Initially, the majority of the surface is covered with the (2×2) pattern although one corner of the images shows a small area with a (3×3) pattern. The boundary between the two zones (white line) propagates at a rate of about 2 nm/min from the upper-right corner towards the lower-left corner. In Figures 9a and 9b, an immobile defect has been marked for reference. Figure 9d shows an isolated (3×3) region (inside the dotted line) surrounded by the (2×2) structure. The cursor profile along A-B line in Figure 9d reveals two differences between the (2×2) and (3×3) structures: (i) The corrugation of the (3×3) is higher, and (ii) the apparent height is higher in the (3×3) regions. The (2×2) structure observed at ambient pressures is probably the same as that was observed in UHV studies (Figure 9d), but the (3×3) structure is new and exists only at ambient pressures. Figure 9d shows two potential model structures: The first (left) consists of one top-site NO molecule and six molecules near hollow sites, whereas the near hollow-site molecules are relaxed in the second model (right), so that they occupy threefold hollow sites.⁴⁶ In both models, the coverage is 0.778 ML, which is only slightly higher than 0.75 ML (the highest coverage obtained in UHV studies thus far), but consistent with the higher pressure.⁴⁶

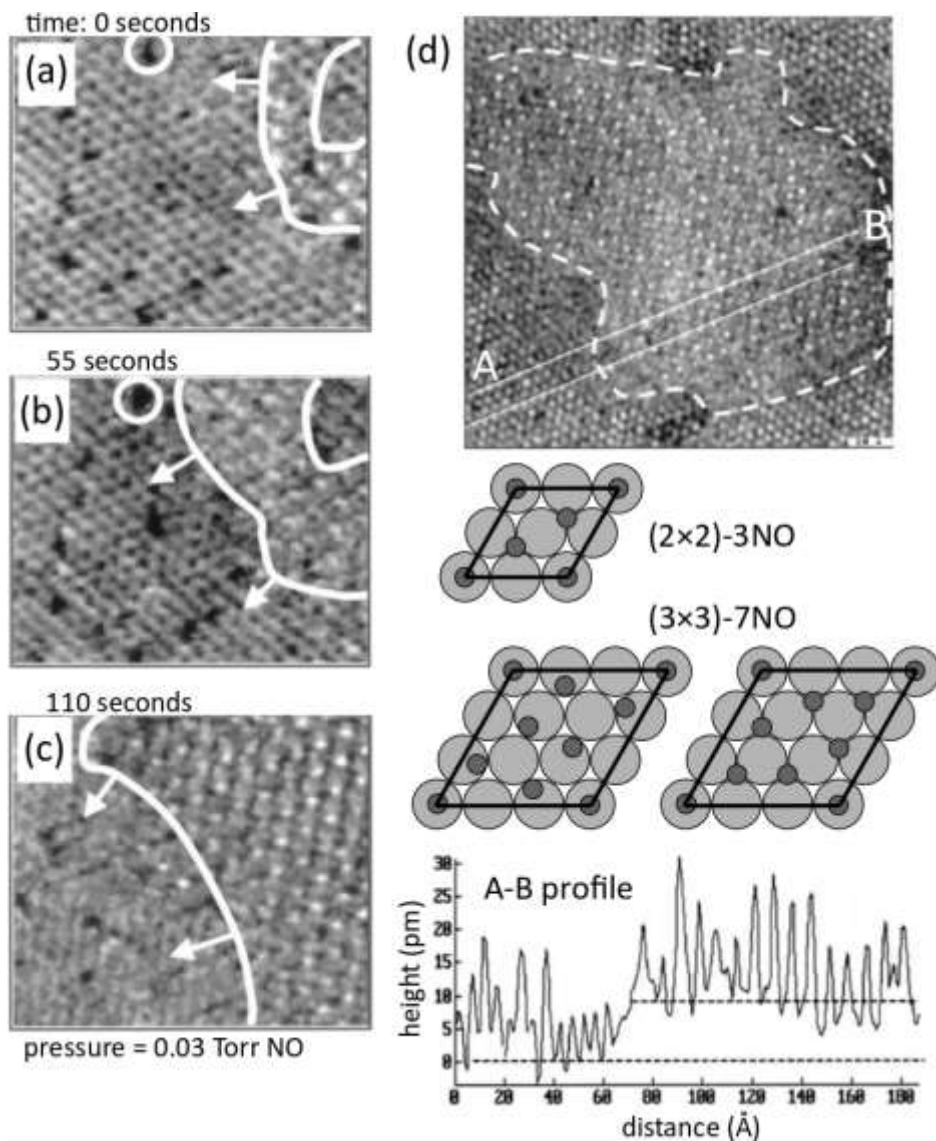


Figure 9: HPSTM images of the Rh(111) surface in the presence of 0.3 Torr NO at room temperature. (a-c) shows the evolution of the surface covered initially with a (2x2)-3NO layer, which is replaced by the (3x3)-7NO. (d) shows an island of the (3x3)-7NO structure inside the (2x2)-3NO zone. The line profile along the A and B points are also shown, with the (3x3)-7NO zone having a higher corrugation and higher apparent height compared to the (2x2)-3NO zone. There are two potential arrangements of the NO molecules on the surface that can result in the observed (3x3) pattern, which are shown in the ball-models. Light grey: Rh atoms, dark gray: NO molecules. Both in (2x2) and (3x3) patterns, the STM contrast originates from the NO molecules on the top sites. Reproduced with permission from Ref.⁴⁶. Copyright 2001 American Institute of Physics.

Ethylene on Pt(100): Ethylene hydrogenation is a model reaction for alkene to alkane conversion studies. On Pt catalysts, this reaction is considered as structure insensitive as the turnover rate is found to be independent of the Pt catalyst structure.⁴⁷⁻⁴⁸ We will deal with the ethylene and hydrogen co-adsorption on Pt surfaces in a later section, and here we only focus on the ethylene adsorption. UHV studies of ethylene adsorption on the quasi-hexagonal Pt(100) surface suggest that at 120 K, C₂H₄ adsorbs molecularly as a di- σ -bonded complex, favoring the 3-fold hollow sites at the surface.⁴⁹ At 350 K, all the di- σ -bonded ethylene rearranges to ethylidyne that also resides at the 3-fold hollow sites. Vibrational spectroscopy studies in the presence of 35 Torr ethylene have shown that both ethylidyne and di- σ -bonded ethylene are present on the Pt(100) surface.⁵⁰ At catalytically active temperatures and pressures, the pathway for ethylene hydrogenation involves the π -bonded ethylene species, whereas the hydrogenation of ethylidyne and di- σ -bonded ethylene occurs relatively slowly.⁵⁰ Structural studies in UHV suggest that ethylene adsorption lifts the quasi-hexagonal reconstruction,⁵¹⁻⁵³ just as in the previously discussed case of CO adsorption lifting this reconstruction both in UHV and at ambient pressures.²⁸ The HPSTM studies, however, question this interpretation.⁵⁴ Figure 10a shows the STM image of the Pt(100) surface in the presence of 5×10^{-6} Torr ethylene where the surface appears broken up into clusters of (1 \times 1) domains, as previous studies predicted. Once the ethylene pressure is increased to 1 Torr, the surface structure remains similar (Figure 10b).⁵⁴ Interestingly, however, if 1 Torr ethylene is dosed directly (i.e., without keeping with the sample in the 5×10^{-6} Torr ethylene environment), the quasi-hexagonal structure remains unchanged to a large extent (Figure 10c).⁵⁴ The discrepancy between the two observations is attributed to contamination with CO, which as we previously mentioned can lift the quasi-hexagonal reconstruction of the surface even at very low pressure.²⁸ In the present case, the increase in the partial pressure of background CO in the UHV chamber after dosing ethylene, is very low but still sufficient to cause structural changes. However, once a complete layer of ethylidyne and di- σ -bonded ethylene covers the surface (measured with APXPS spectra in Ref.⁵⁴), it prevents the subsequent adsorption of background CO, thereby preserving the quasi-hexagonal structure.⁵⁴

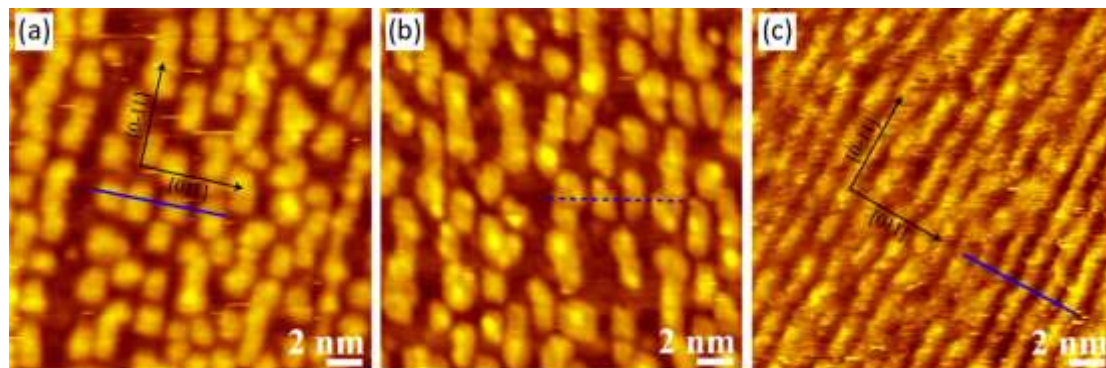


Figure 10: HPSTM images of the Pt(100) surface at room temperature in the presence of (a) 5×10^{-6} Torr ethylene, (b) after ethylene pressure was increased up to 1 Torr, (c) after directly dosing 1 Torr ethylene. Whilst the quasi-hexagonal overlayer structure of the surface Pt atoms is retained in (c), low pressure dosing resulted in clustering in (a), most likely due to co-adsorption of the background CO molecules. Reproduced with permission from Ref.⁵⁴. Copyright 2013 American Chemical Society.

5. Adsorption on Low Miller-Index Surfaces of 'Soft' Metals (Copper and Gold)

5.1 CO on Low Miller-Index Cu Surfaces

CO on Cu(111): Unlike CO adsorption on Pt and Rh mentioned in Section 3, the CO adsorption on Cu is much weaker. Therefore, CO can stay on Cu surfaces at UHV-compatible pressures only at cryogenic temperatures. At room temperature however, a high coverage can be obtained in equilibrium with a sufficiently high pressure (e.g., 0.1 Torr and above). On Cu(111), the most common structure of adsorbed CO at low temperature is the $(\sqrt{3} \times \sqrt{3})R30^\circ$,⁵⁵ and there is a plethora of different condensed and dilute CO adlayer structures on the Cu(111) surface depending on the dose and sample temperature.⁵⁵⁻⁵⁶

The Cu(111) surface behaves very differently when it is exposed to CO gas at ambient pressures than in UHV, as Figure 11 illustrates.⁵⁷ Figure 11a shows an image of the clean Cu(111)-(1 \times 1) surface in UHV, together with an atomically resolved image of the terrace in the inset. After introduction of 0.1 Torr CO in the chamber a new structure was observed along the step edges, while the rest of the terrace remained atomically flat (Figure 11b).⁵⁷ At 0.2 Torr the terraces became covered with clusters (Figure 11c), which increased in number with CO pressure. Above 10 Torr the clusters filled nearly completely the surface as shown in Figure 11d. Figure 11e shows a magnified image of the surface in the presence of 0.2 Torr CO at room temperature. The surface consists of small metal clusters formed by Cu atoms detached from the kink and step sites.⁵⁷ A roughly bimodal size distribution is apparent, with larger hexagonal-like shaped clusters with ~ 1.5 nm diameter and smaller poorly resolved triangular shaped clusters with ~ 0.5 nm diameter. The larger clusters are assigned to 19-Cu-atom clusters forming hexagonal closed shell structures (typically with an apparent height corresponding to a monatomic step). Adsorption of CO molecules to each Cu atom at the periphery results in net energy gain, as predicted by DFT calculations. The driving force is the gain in energy by adsorbing CO to the newly formed under-coordinated sites, which provides the energy to detach the Cu atoms from the steps and form the clusters. The fact that only six bright spots are observed at the periphery of the hexagon is related to the electronic structure and tunneling probability of the different CO molecules, as explained in detail in Ref.⁵⁷. The 19-atom closed shell structures are known in the literature to be the building blocks for the homo-epitaxial Cu growth on Cu(111).⁵⁸ The smaller clusters could not be resolved by the STM tip but their size indicates that they probably contain 3-Cu atoms. Their apparent height is about half that of a monatomic

step, as found also in other UHV studies.⁵⁹ The clusters are not static with time, but fluctuate by coalescing with other clusters or by adding atoms and also splitting in two in time scales of minutes, as evidenced with time-lapse HPSTM images that could be captured thanks to the slow kinetics of the process at room temperature. As mentioned above at pressures in the 10–100 Torr range, the Cu(111) surface was found to be completely covered with clusters that are larger and closer to each other. Figure 11d shows an example of the topography of the surface under 10 Torr CO with clusters densely covering adjacent terraces separated by monatomic steps. The clusters are densely covered by CO molecules, imaged as bright spots, separated by distances of $\sqrt{3}$ and 2 times the atomic periodicity, and aligned in directions forming 60 and 90 degrees between them, which can be interpreted as arising from atop CO molecules in local $(2\times 2)\text{-}3\text{CO}$ and $c(4\times 2)$ geometries and coverages of 0.75 and 0.5 ML, respectively.

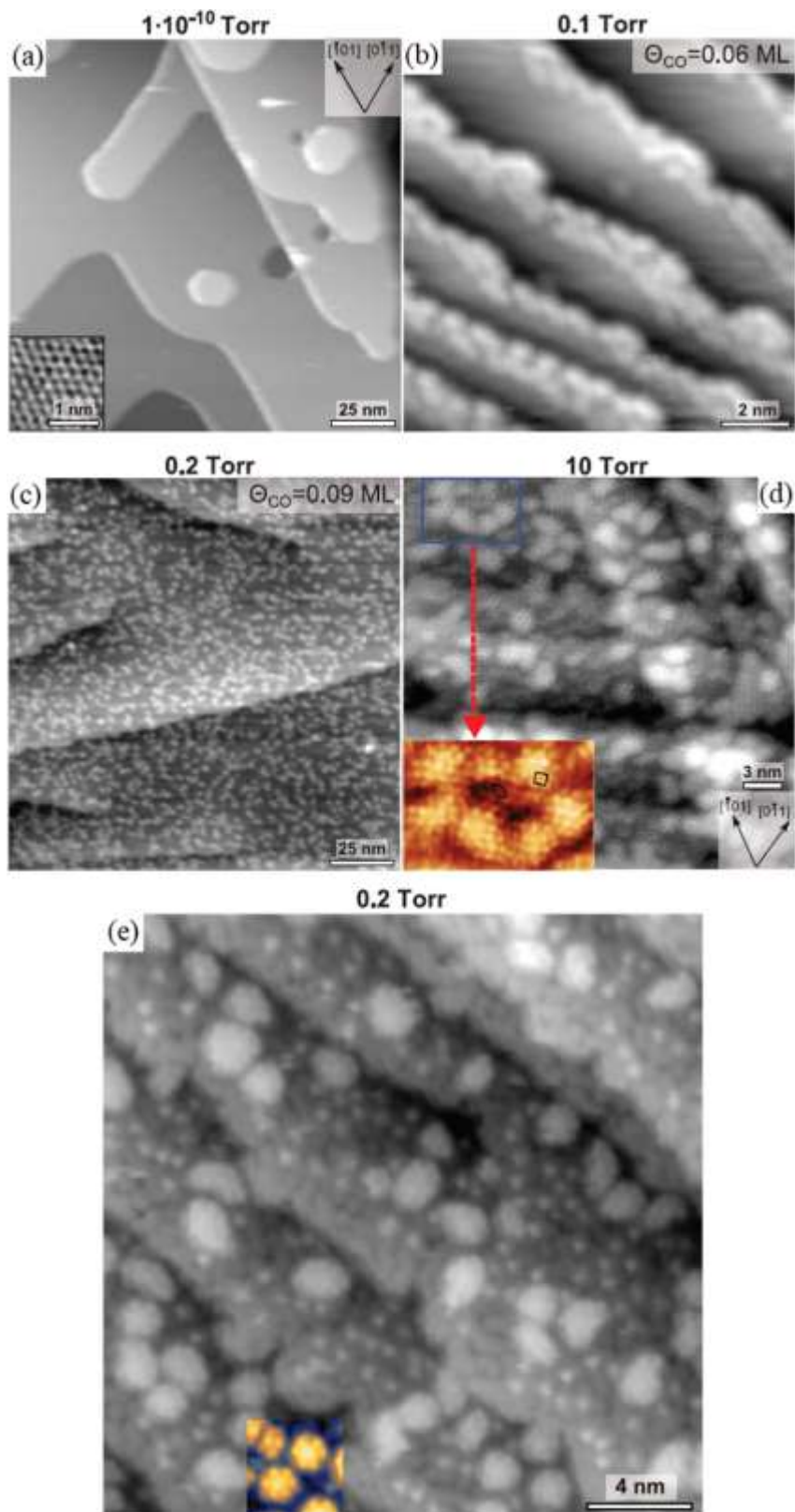


Figure 11: (a) STM image of the bare Cu(111) surface. HPSTM image of the Cu(111) surface in the presence of (b) 0.1 Torr CO, (c) and (e) in the presence of 0.2 Torr CO, and (d) in the presence of 10 Torr

CO. All images were acquired at room temperature. The HPSTM images show the breaking up of the Cu(111) surface into clusters as a function of CO pressure. The hexagonal 19-atom clusters can be seen in (e), and they are visually clearer in the two-color contrast used in the inset. DFT calculations can generate similar images of the clusters, with their periphery covered with adsorbed CO molecules. Reproduced with permission from Ref.⁵⁷. Copyright 2016 American Association for the Advancement of Science.

CO on Cu(100): The Cu(100) surface behaves very similar to the Cu(111) surface in the presence of CO gas at room temperature. Whilst adsorption studies in UHV and at cryogenic temperatures show a dense ($\sqrt{2}\times\sqrt{2}$) adsorbate layer at the highest coverage,⁶⁰ the surface breaks up into clusters at room temperature in the mbar pressure range.⁶¹ Figure 12a-i shows STM images of the Cu(100) surface in the presence of 0.25 mbar CO, which appears broken up into rectangular nanoclusters with edges oriented along $\langle 001 \rangle$ directions. The smallest of these clusters consist of 5 atoms, as shown in Figure 12a-ii. Away from the edges, several terrace regions are seen with the (1×1) periodicity (Figure 12a-iii), whereas the step edge atoms of nanoclusters and terraces are spaced by $\sqrt{2}$ times the Cu–Cu distance. As the pressure is increased to 20 mbar, the clusters increase in size and number (Figure 12b-i). Two structures can be observed: Some regions on the surface have a local ($\sqrt{2}\times\sqrt{2}$) arrangement of adsorbed CO molecules, similar to that formed at saturation coverage in UHV at cryogenic temperatures.⁶¹ The second and more dominant structure consists of elongated 3-atom wide nanoclusters (Figure 12b-ii) oriented along the $\langle 001 \rangle$ directions. As the pressure is increased to 115 mbar (Figure 12c-i), the elongated nanoclusters appear more numerous than at 20 mbar. Both in Figure 12b-ii and in Figure 12c-ii, the bright spots due to CO form a zigzag pattern along the $\langle 001 \rangle$ directions, with the central line of molecules showing higher contrast than those in adjacent lines. The zigzag originates from CO molecules repelling each other so that they tilt in opposite directions in neighboring molecules along the chain. This was also previously found in UHV at high CO coverage²⁹ for CO on Pt(110).²⁸ The higher contrast of the central line is due to CO molecules pointing upward, whereas CO molecules adsorbed to the adjacent rows are tilted due to repulsion between neighboring molecules. Most of the one-dimensional nanoclusters are separated by roughly 1 nm from each other, dictated by steric repulsion. DFT calculations confirm the formation of the 3-atom wide one-dimensional clusters, and simulated STM images also show both the higher STM contrast and the zigzagging of the middle row (Figure 12b-iii).

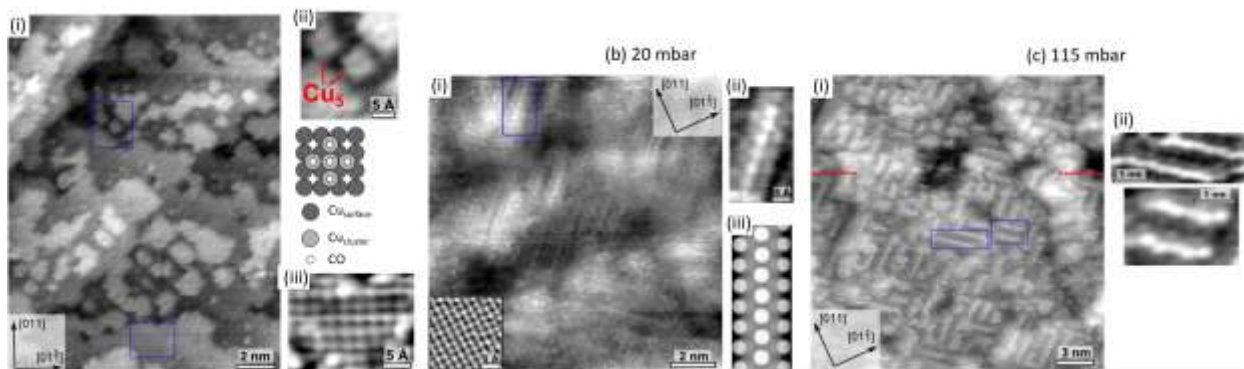


Figure 12: HPSTM images of the Cu(100) surface in the presence of (a) 0.25 mbar, (b) 20 mbar, and (c) 115 mbar CO, measured at room temperature. In (a-i), the surface appears broken up into two-dimensional nanoclusters, with edge of the clusters oriented along the $\langle 001 \rangle$ directions. The smallest clusters consist of 5 atoms, shown schematically in (a-ii). Some terraces still exhibit the (1×1) periodicity as shown in (a-iii). In (b-i) and (c-i), the surface consists of the linear clusters elongated along the $\langle 001 \rangle$ directions. These linear clusters have a width of 3 atoms, with CO occupying all the top sites on the clusters. The middle row appears higher in STM as the CO is pointing upwards (b-ii and c-ii), and shows zigzag features. Simulated images generated using DFT calculations (b-iii) also show this higher tunneling probability and the zigzagging of the middle row. The rectangular box marked in (b-i) shows the atomically resolved image of the surface in UHV, measured prior to the other images shown in (b) and (c). Dashed red line in (c-i) shows a change in the tip, which changes the STM contrast obtained from the linear clusters but the aforementioned general trends still hold. Reproduced with permission from Ref.⁶¹. Copyright 2016 Elsevier.

CO on Cu(110): The Cu(110) surface also breaks up into clusters, but rather mildly compared to Cu(111) and Cu(100) surfaces. This is likely because the coordination number of the Cu(110) surface is lower than that in the other two surfaces, hence CO adsorbs stronger on the Cu surface atoms and there is less energy gain in creating more low coordinated Cu atoms. The adsorption energies were measured as 0.49 eV, 0.53 eV and 0.56 eV respectively for Cu(111), Cu(100) and Cu(110) with thermal desorption spectroscopy.⁶² As shown in Figure 13, the initially flat Cu(110) surface (Figure 13a) restructures into short (1–3 nm) linear clusters along the $[110]$ direction separated by two lattice distances along the $[001]$ direction, as shown in Figures 13b and 13c, acquired at room temperature in the presence of 1 Torr CO. This is due to missing rows of atoms. A few rows can also be seen in the images spaced by three lattice distances,⁶³ due to either double or triple missing rows. The latter, with two missing rows in the first layer and one missing row in the second layer, are difficult to distinguish from double missing rows in the images. Figure 13d shows proposed models of the surface forming linear nanoclusters. The terminating

Cu atoms of these short clusters have a coordination number of 6, while the rest of Cu atoms are coordinated with 7 other Cu atoms similar to a bare Cu(110) surface.

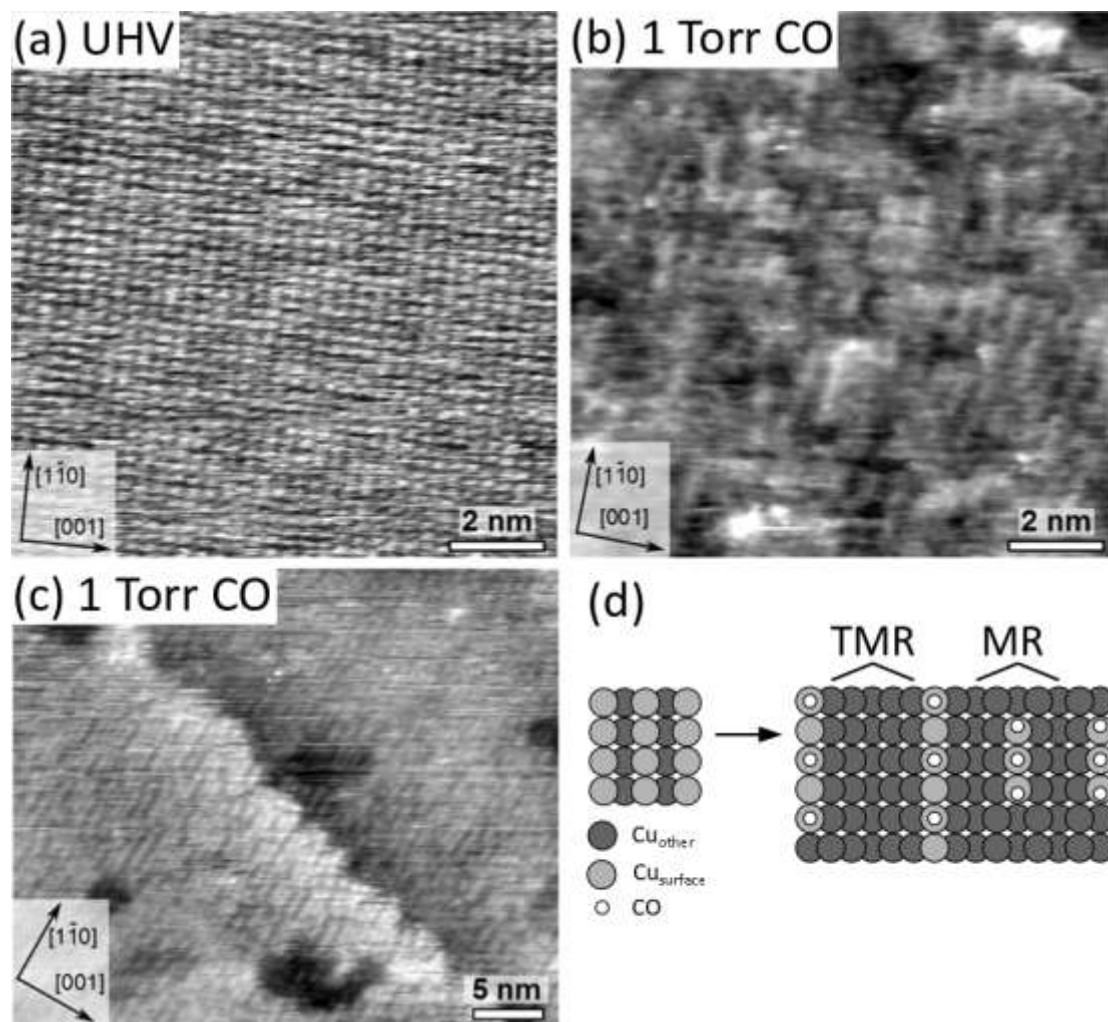


Figure 13: Cu(110) surface imaged with STM at room temperature (a) in UHV and (b-c) in the presence of 1 Torr CO. (d) Ball model of CO adsorbed on linear clusters in the form of missing rows and triple missing rows, denoted with MR and TMR, respectively. Reproduced with permission from Ref.⁶³. Copyright 2016 American Chemical Society.

Infrared spectroscopy: In STM and other microscopies, the results can sometimes be difficult to interpret, and to some degree subjected to “viewer selectivity”. For this reason it is important when studying new phenomena, such as the clustering induced by CO, to use other techniques to support the models inferred from the images. IRRAS is an excellent technique for this purpose because the CO stretching frequency shifts depending on the coordination number of the adsorption site. There are many factors affecting the frequency of a vibrational state of an adsorbed species compared to that of a gas

phase species: renormalization due to the formation of the M-CO bond (i.e., change in effective mass of C), interaction of the vibrating dipole with its image in the metal, and chemical effects such as back-donation which change the C-O bond strength, etc.⁷ Fortunately, there are many reference works on CO adsorption on Cu surfaces. They all indicate that the CO stretching frequency increases with decreasing coordination number of the adsorption site,⁶⁴ implying that as the surface breaks up into clusters in the presence of CO, new CO adsorption peaks should appear in the IRRAS spectrum, due to the generation of lower coordination sites.

Figure 14 shows IRRAS spectra obtained in three different studies of CO adsorption at ambient pressures. Figure 14a shows results from CO on Cu(100), where the adsorbed CO stretch features appear as two peaks at low pressures at 265 K.⁶⁵ As the pressure increases, the two peaks collapse into one peak, positioned at 2086 cm^{-1} , which is a higher wavenumber compared to CO on Cu(100) obtained at low temperature. There were no HPSTM studies at the time, but now we can attribute this change to the clustering of the surface, which shows that at 265 K CO could be present both on 8-coordinated metal sites and on the edges of the newly formed clusters, although there should be fewer clusters at this temperature compared to room temperature. With fewer clusters the two peaks should collapse into one as the pressure increases, due to intensity borrowing of the high wavenumber feature from the low wavenumber feature due to coupling between two vibrational modes. Another example of intensity borrowing is observed in the CO adsorption on the Pt(533) surface at cryogenic temperatures.⁶⁶

A more recent study performed on the Cu(110) surface shows that at cryogenic temperatures only a peak at 2086 cm^{-1} is visible (reference spectrum at the top), due to CO adsorbing on Cu(110)-(1×1), but two peaks arise when CO is adsorbed at ambient pressures at around 2084 and 2099 cm^{-1} , which are attributed to CO bound to top site Cu atoms with coordination numbers of 7 and 6, respectively (Figure 14b).⁶³ This is in line with the HPSTM observations: The surface breaks up into clusters in the form of missing rows, with the edge of the clusters having a coordination number of 6. A more recent study was conducted on Cu(100) in the presence of 0.1 mbar CO, with the temperature increasing from 200 K to 300 K.⁶⁷ While at 200 K CO adsorbs on 8-coordinated surface Cu atoms of Cu(100)-(1×1), as evidenced by a single absorption peak at 2082 cm^{-1} , another peak appears at 2112 cm^{-1} when the surface temperature is increased to 225 K (Figure 15c). This new peak is due to ad-atom formation on the surface, facilitated through CO adsorption which weakens the Cu-Cu bonds and thus facilitates detachment of step and kink sites atoms.⁵⁷ Finally, at room temperature, two intense peaks are present at 2093 cm^{-1} and 2103 cm^{-1} , due to CO adsorbed on 5-atom clusters and on single adatoms,⁶⁷ in accordance with HPSTM experiments discussed above. A third peak, with much weaker intensity, is present at 2074 cm^{-1} , which is assigned to small amounts of CO on the on the 8-coordinated surface Cu atoms.

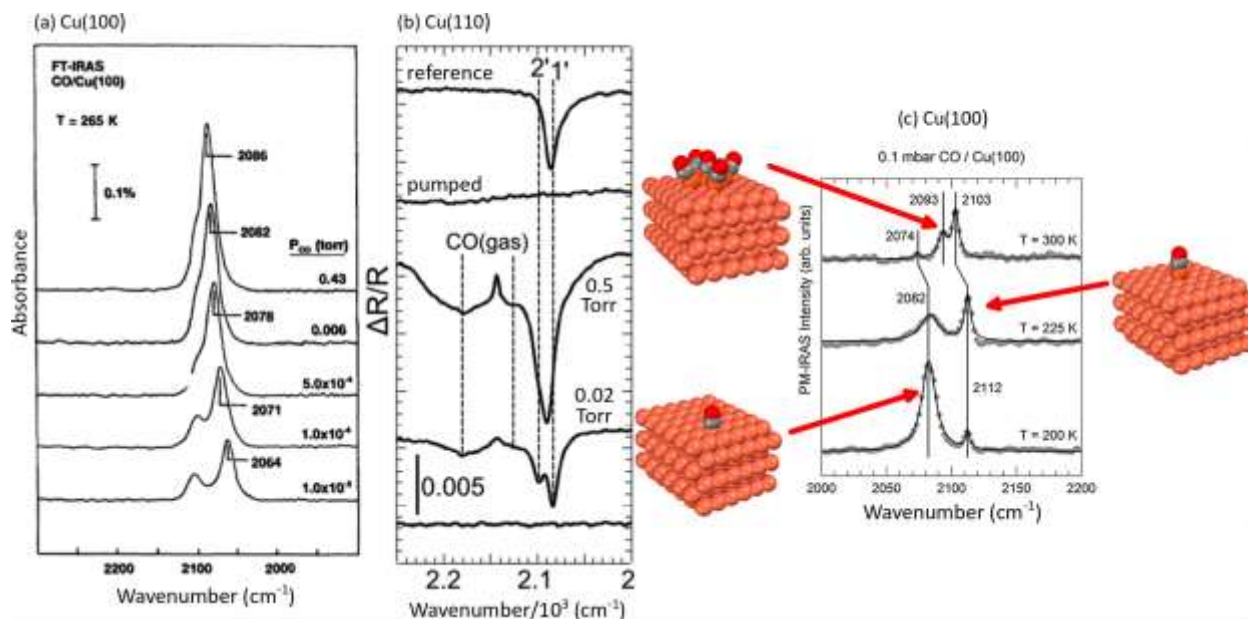


Figure 14: IRRAS spectra of CO adsorption at ambient pressures on (a) Cu(100), (b) Cu(110), and (c) one more time on Cu(100) surface. The spectra show additional features when CO is adsorbed at ambient pressures compared to CO adsorption at low pressure – low temperature studies, associated with the formation of newly formed low-coordinated sites on the surface. For instance, in (b), the reference spectrum shows an adsorption experiment at cryogenic temperature, which only shows 1' peak. At ambient pressures, an additional 2' peak appears. Adapted with permission from Ref.⁶⁵, Ref.⁶³, and Ref.⁶⁷. Copyright 1992 Elsevier, 2016 American Chemical Society, and 2019 American Chemical Society.

In summary, the IRRAS experiments support the HPSTM observations regarding the break-up of the Cu surfaces in the presence of CO in the Torr/mbar pressure regime at room temperature.

5.2 CO on Low Miller-Index Au Surfaces

Au and Cu have similar cohesive energies (3.81 eV/atom for Au and 3.49 eV/atom for Cu), so we can expect similar behavior between Au and Cu surfaces in the presence of gases. However, on Au CO adsorbs very weakly. Therefore, to produce enough CO coverage to drive reconstructions higher pressures may be needed. Another difference is that all three low Miller-index surfaces of Au are reconstructed, two of them forming denser top layer structures with more atoms than the bulk terminated (1×1). Such reconstructions are easily lifted and the surface becomes covered with clusters formed by the extra atoms of the initial surface.

CO on Au(110): In vacuum, the Au(110) surface has a reconstructed (1×2) structure. Figure 15a-c show the STM images of this structure before and after 20 Torr CO was introduced, which lifts the reconstruction to form large two-dimensional clusters on the surface.⁶⁸ The authors interpreted the result

as the surface structure becoming (1×1). Complementary IRRAS analysis shows the adsorbed CO peak on the Au(110), with an intensity increasing as expected with increasing pressure (Figure 15e). Interestingly, the spectra acquired in the presence of 20 Torr CO show a decrease of the intensity of peak at $\sim 2110\text{ cm}^{-1}$ with time (Figure 15f). The authors attribute this to the hydrocarbon contamination building up on the surface (base pressure of 10^{-9} Torr), which they measured with XPS after the CO dosing experiments.

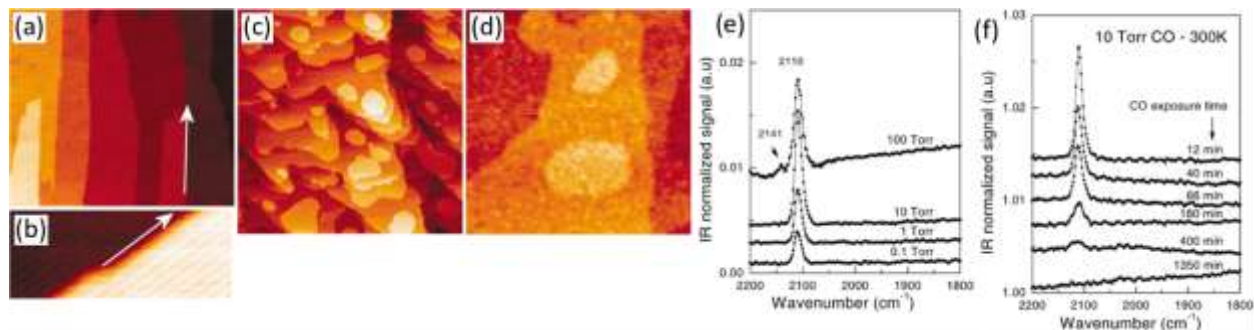


Figure 15: HPSTM images of the Au(110) surface acquired at room temperature (a-b) in UHV, (c) in the presence of 20 Torr CO, and (d) after the chamber is evacuated to vacuum. The arrows indicate the $\langle 1\bar{1}0 \rangle$ directions. (a) and (c) are $350 \times 350\text{ nm}^2$, whereas (d) is a $150 \times 150\text{ nm}^2$ image. The surface appears different in (c) from that in (a). The original (1×2) reconstruction is partially recovered in (d). (e) The IRRAS spectra at various CO pressures, and (f) time-lapse IRRAS spectra in the presence of 10 Torr CO. The chemisorbed CO peak disappears with time, which was attributed to hydrocarbon contamination building up. Reproduced with permission from Ref.⁶⁸. Copyright 2002 Elsevier.

CO on step edges of Au(111) #1: Although the experiments were not done at ambient pressures, we included Ref.⁶⁹ here, as the results in this study are relevant to adsorbate-driven clustering. Figure 16 shows images of the Au(111) surface before and after CO adsorption experiments at 110 K. The hexagonal islands in the images were formed by Ar^+ sputtering. After CO adsorption small nanoparticles were formed attached to the edges of the islands, which in addition lose their hexagonal shape. These changes were attributed to the weakening of Au-Au bonds by CO adsorption on the step and kink sites, and thereby facilitating the movement of the Au adatoms on surface.⁶⁹ Similar arguments were used to explain the restructuring of Cu(111) in Ref.⁵⁷.

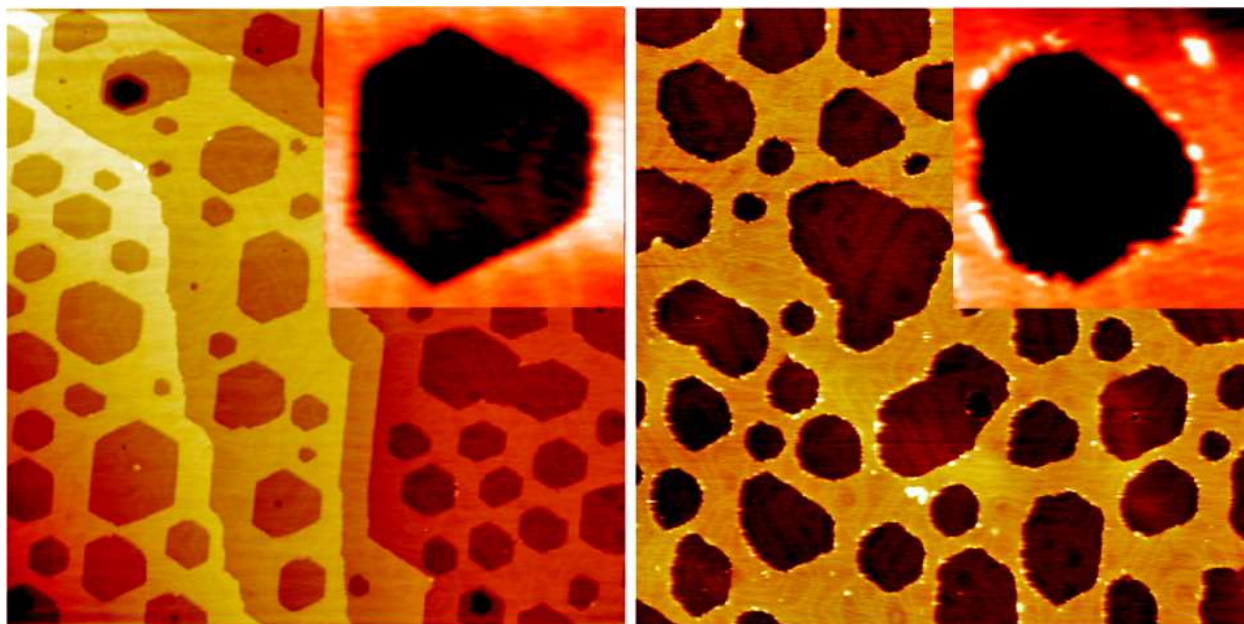


Figure 16: STM images of a Au(111) surface with hexagonal pits formed by Ar⁺ sputtering, before (left) and after (right) CO adsorption at 110 K. Reproduced with permission from Ref.⁶⁹. Image sizes are 200×200 nm², and 27×27 nm² for the insets. Copyright 2008 American Chemical Society.

CO on step edges of Au(111) #2: A study similar to that of Ref.⁶⁹ was performed in Ref.⁷⁰ The STM measurements were performed in UHV at room temperature after long exposure of the surface to CO gas. After $\sim 10^4$ Langmuir exposure the hexagonal shape of the pits was found to have deformed and some small clusters appeared both at the edge of the pits and on some of the terrace sites.⁷⁰ After increasing the dose to 10^5 and then to 10^6 Langmuir, the clusters on the terraces increased in density and the herringbone reconstruction (Au(111)-(22×√3)) was lifted.⁷⁰

CO on Au(111): CO adsorption at ambient pressures was also shown to lift the herringbone reconstruction of the Au(111) surface.⁷¹ Figures 17a and 17c show the STM images of the Au(111)-(22×√3) surface in UHV and Figures 17b and 17d show the HPSTM images of the Au(111)-(1×1) surface in the presence of 100-250 Torr CO. The surface reconstruction is lifted by CO, and the surface in Figure 17d shows steps decorated with clusters, likely originated from the extra atoms of the herringbone reconstruction, which represent $\sim 4.4\%$ of the surface atoms, and therefore not many clusters are apparent. IRRAS spectra shows a clear adsorbed CO peak on the Au(111) surface, with stretching frequency at ~ 2060 cm⁻¹, with an intensity increasing with pressure.⁷¹ This means CO adsorbs as a two-dimensional gas, which is not visible in the HPSTM image in Figure 17b.

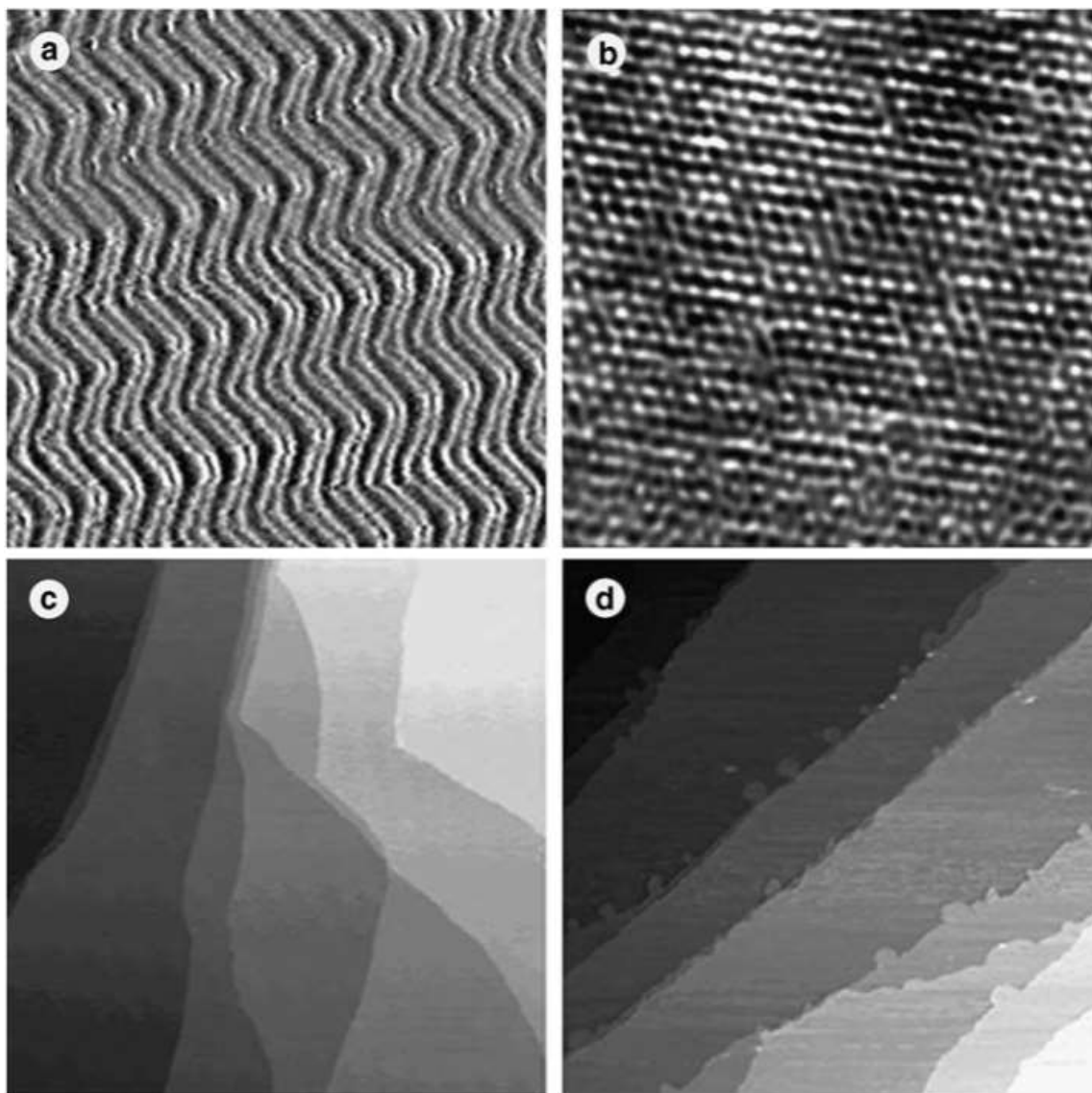


Figure 17: STM images of the Au(111) surface at RT (a) under 10^{-9} Torr, image size is $108 \times 108 \text{ nm}^2$; (b) under 250 Torr CO pressure, image size is $7.5 \times 7.5 \text{ nm}^2$; (c) under 10^{-9} Torr, image size is $490 \times 490 \text{ nm}^2$; (d) under 100 Torr CO pressure, image size is $950 \times 950 \text{ nm}^2$. Reproduced with permission from Ref.⁷¹. Copyright 2004 Elsevier.

We can conclude that the Au surfaces have a tendency to form clusters in the presence of CO, which originate from the extra atoms of the surface reconstructions, and from atoms detached from the steps. However, the density of clusters is less than those observed on Cu surfaces in the presence of CO gas.

5.3 Other Gases on Low Millex-Index Cu Surfaces

In Subsection 5.1, we have seen that in the presence of CO gas the low Miller-index Cu surfaces break up into clusters. As we will show now, this is not the general case. It is important to establish why clustering happens with certain gases and why it does not with others. We will investigate two other gases on Cu(100): One is CO₂ where the surface breaks up into clusters, the other CH₃OH vapor where it remains intact. We will also review H₂ on Cu(111), which also does not induce cluster formation on the surface.

H₂ on Cu(110): The H/Cu(110) system has been the subject of a few studies in UHV. They all show the formation of a hydrogen-induced (1×2) missing-row reconstruction, with every second close-packed [1 $\bar{1}$ 0] Cu row is removed.⁷²⁻⁷⁴ HPSTM studies of the Cu(110) surface in the presence of 1 bar of hydrogen gas shows the periodicity changing from (1×1) to (1×2), as shown in Figures 18a and 18d.⁷⁵ The latter structure originates from the missing-row construction caused by atomic hydrogen, similar to the surface structure observed in UHV. The atomic hydrogen is produced by the activation and breaking of the H-H bond on the Cu(110) surface. The high activation energy of H-H bond breaking, however, makes the process kinetics very low.⁷⁵ In high vacuum, this step can be skipped using atomic H produced by cracking H₂ molecules with a hot filament near the sample surface.⁷⁶ The thermal desorption peak of atomic hydrogen on Cu(110) surface appears at 340 K, which means hydrogen already starts desorbing from the surface at room temperature, but at slow rates.⁷⁵ As a result of desorption, 25 min after the evacuation of 1 bar H₂, the STM images revealed the (1×1) structure of the bare surface (Figure 8e).⁷⁵

Figures 18b and 18c show the surface structure at intermediate H₂ pressures of 2 mbar and 20 mbar, respectively. At 2 mbar, the surface still appears as (1×1) due to low coverage of atomic hydrogen (Figure 18b).⁷⁵ At 20 mbar, however, the surface has three different structures: (1×1) due to bare Cu(110) with locally low atomic hydrogen coverage, (1×2) missing-row reconstruction with locally high atomic hydrogen coverage, and a disordered structure which is a transient state between the two ordered (1×1) and (1×2) surface structures (Figure 18c).⁷⁵ Figure 18f shows the room temperature Langmuir isotherm of the atomic hydrogen coverage from 0 ML to 0.5 ML.

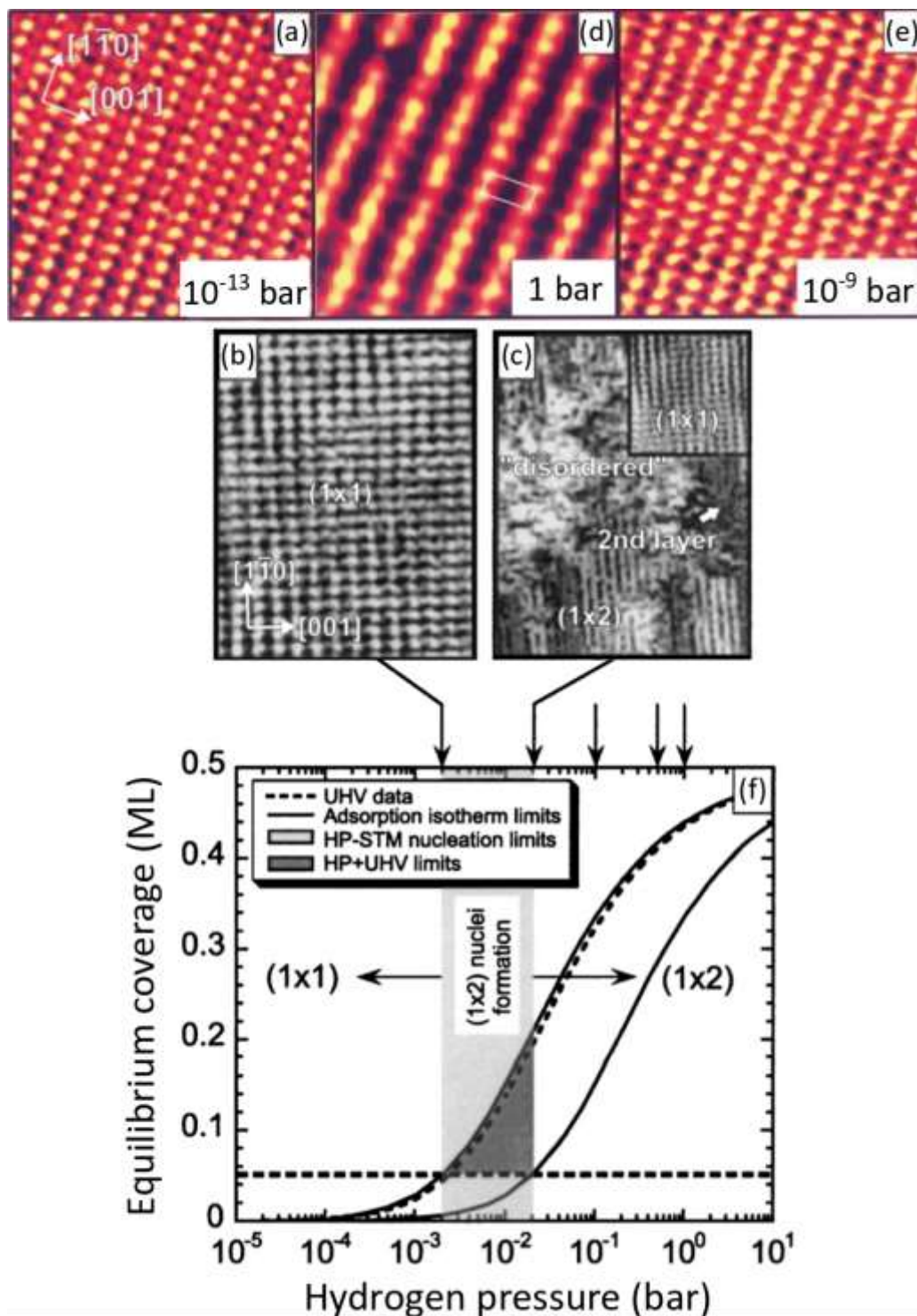


Figure 18: HPSTM images of the Cu(110) surface at room temperature (a) in UHV, and in the presence of (b) 2 mbar H_2 , (c) 20 mbar H_2 , (d) 1 bar H_2 , and (e) after 1 bar H_2 is pumped away. A transition from the (1×1) structure of the bare Cu(110) surface to the (1×2) corresponding to the missing-row construction with increasing H_2 pressure is apparent in the images. (f) shows the Langmuir isotherm

of atomic hydrogen coverage. Reproduced with permission from Ref.⁷⁵. Copyright 2001 American Institute of Physics

CO₂ on Cu(100): In the presence of 1 Torr CO₂, Cu(100) surface becomes covered with a fraction of a ML of atomic oxygen. The atomic oxygen originates from the dissociation of CO₂ on the surface, as evidence from the APXPS spectra and from the appearance of dark spots formed by O atoms in the HPSTM images.⁷⁷ A recent study proposes that the step edges are the active sites in the dissociation of CO₂ on a Cu(100) surface.⁷⁸ Once the CO₂ pressure is increased to 20 Torr, the terraces become covered with clusters, with roughly half of their edges oriented along the <011> orientations and the other half showing no preferential orientation (Figure 19).⁷⁷ This is different from the clusters formed in the presence of pure CO where all the edges of clusters and steps align along the <001> orientations.⁶¹ The formation of clusters in the presence of CO₂ is likely driven by the energy gain from the binding of oxygen atoms from the dissociated CO₂, and from the CO adsorbed on step edges and favoring the detachment of Cu atoms. However, CO does not remain attached to the clusters at room temperature due to its low binding energy so that only the atomic oxygen remains on the surface. The surface in Figure 19 is covered with atomic oxygen that originated from CO₂ dissociation, as evidenced from the APXPS results.

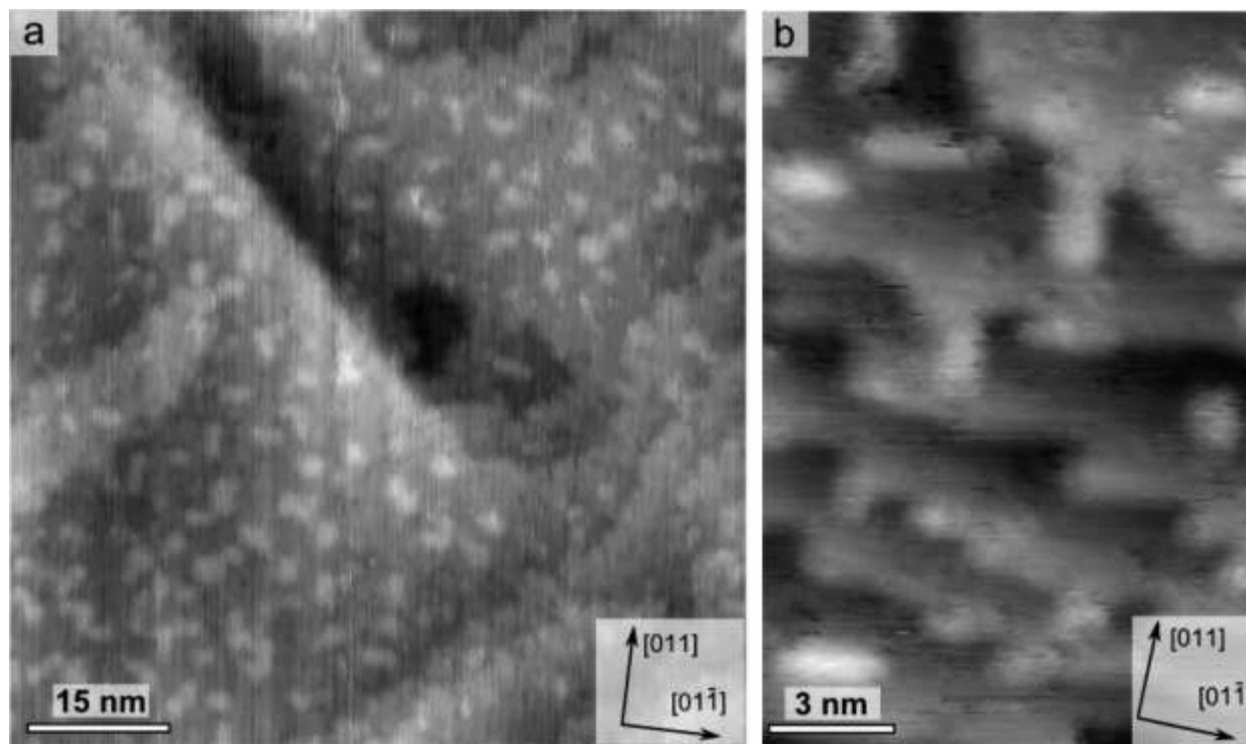


Figure 19: (a) Large-view and (b) close-up HPSTM images of the Cu(100) surface in the presence of 20

Torr CO₂ at room temperature. The surface breaks up into clusters, roughly half of them with edges oriented along the <011> directions. The step edges of the clusters were oriented along the <001> directions in the presence of CO (Figure 12). Reproduced with permission from Ref.⁷⁷. Copyright (2016) American Chemical Society.

Methanol on Cu(100): Unlike the case of CO and CO₂, no clustering of the Cu(100) surface was observed in the presence of methanol vapor.⁷⁹ HPSTM images taken in the presence of 0.01–0.2 Torr CH₃OH at room temperature show a ($\sqrt{2}\times\sqrt{2}$)R45° adlayer structure (Figure 20), which is due to a methoxy saturated surface, as shown by APXPS.⁷⁹ Sum frequency generation studies in Ref.⁸⁰ also suggests polycrystalline Cu foils to be covered with methoxy in the presence of methanol vapor. The absence of cluster formation could be understood by the small difference in the adsorption energy of methoxy on cluster edges compared to terraces, which is not sufficient to compensate the energy cost of detachment of Cu atoms to form clusters. Methoxy adsorption energies calculated by DFT in the literature varies widely,^{81–84} but a study comparing the adsorption energies on terraces and step edges predicts very similar energies,⁸⁴ which supports the lack of cluster formation in the presence of methanol.

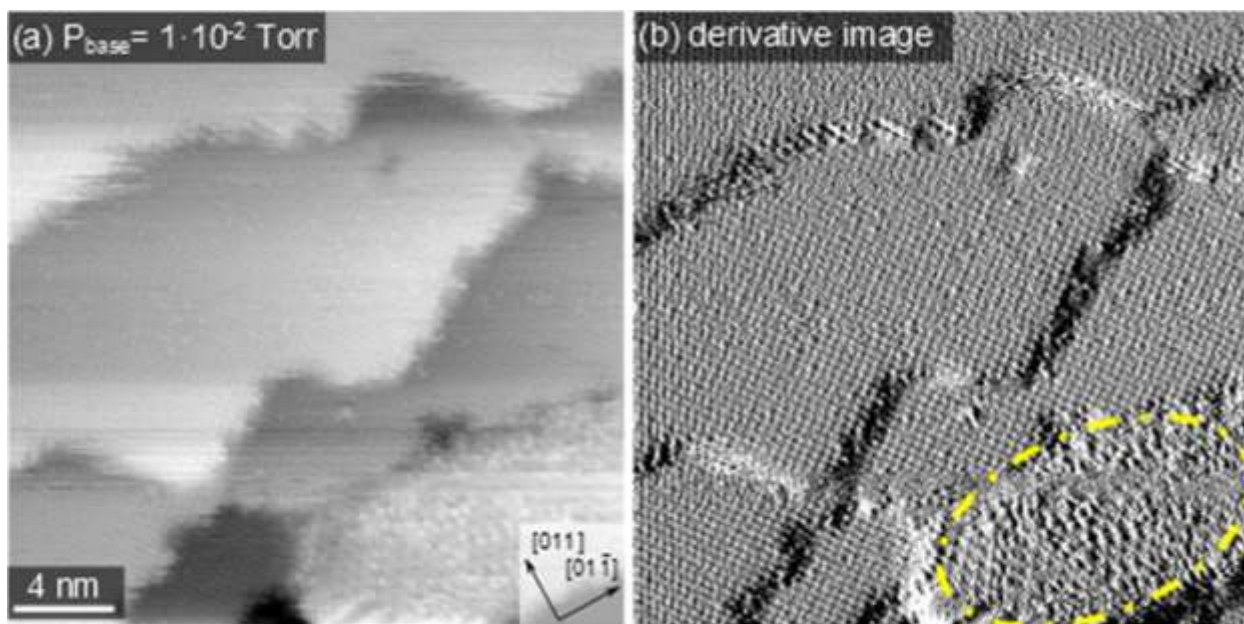


Figure 20: (a) HPSTM image of the Cu(100) surface in the presence of 0.01 Torr methanol vapor at room temperature. (b) Derivative image of (a) to enhance the contrast on the terraces. While most of the surface exhibits a ($\sqrt{2}\times\sqrt{2}$)R45° structure due to adsorbed methoxy, the area inside the ellipse has a different structure. Reproduced with permission from Ref.⁷⁹. Copyright (2018) American Chemical Society.

6. Reaction Studies on Low Miller-Index Surfaces

6.1 CO Oxidation

CO oxidation reaction is important for the mitigation of the pollutants generated by vehicles, and it can also be considered prototypical for more complicated oxidation reactions.⁸⁵ It is also the most studied reaction with HPSTM, because it involves only two reactant adsorbates and one product, which does not remain adsorbed on the surface, thus simplifying interpretation of the images.

6.1.1 CO Oxidation on Pt Surfaces

According to Ref.⁸⁶, there is a steady increase in the number of papers that deal with CO oxidation on Pt surfaces between 1975 and 2015, reaching almost 80 papers in 2015, showing that this topic continues to attract a great deal of interest. We also note that CO oxidation on Pt was one of the topics discussed in the Nobel Prize in Chemistry Lecture in 2007.² We can thus consider CO oxidation on Pt the “*Drosophila*” of surface chemistry reactions.

CO oxidation on Pt(111): Although not performed at ambient pressures, one of the most important studies on CO oxidation was performed on the Pt(111) surface more than two decades before this Review. Even at pressures in the $\sim 10^{-8}$ mbar range, CO was found to remove oxygen adsorbed on the Pt(111) surface in the scale of minutes at 247 K.⁸⁷ Whilst oxygen was pre-adsorbed in the form of a (2×2) structure with islands covering the surface, CO gradually formed islands of c(4×2) structure by removing the oxygen at the boundaries (Figure 21).⁸⁷ A kinetics analysis showed that the reaction rate scaled with the boundary length instead of the product of the total coverage of each adsorbate (mean-field approximation), which assumes a random distribution of the reactants.

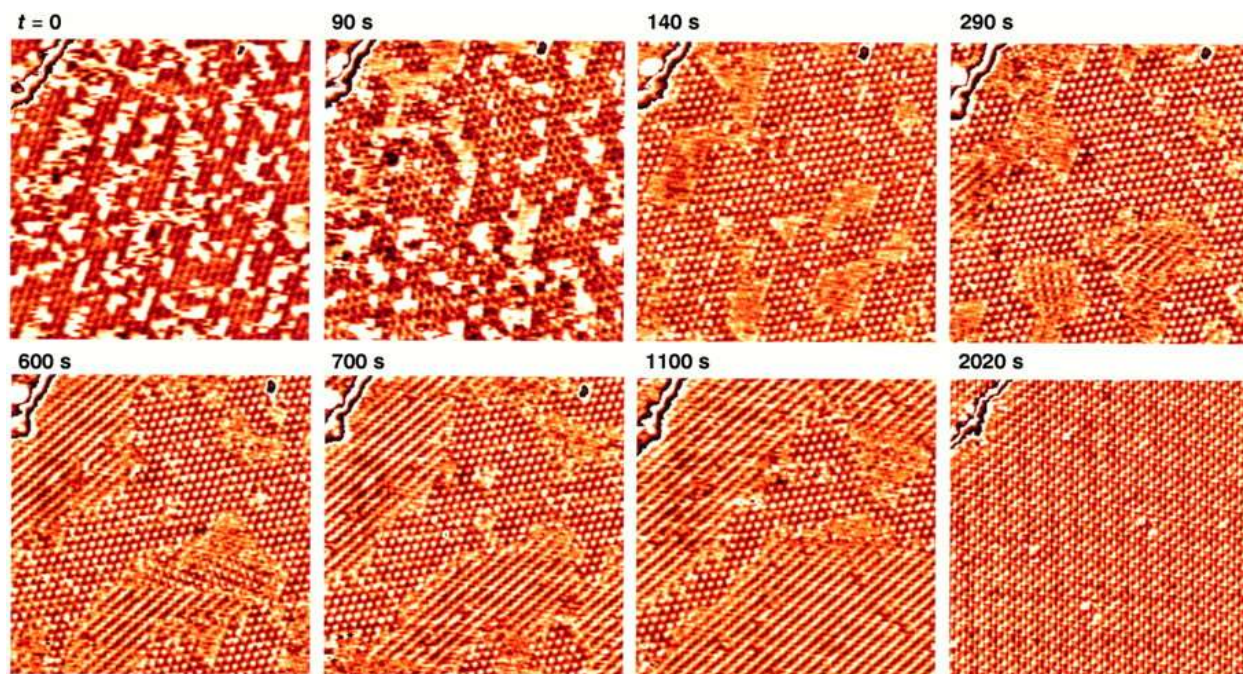


Figure 21: Time-lapse STM images of Pt(111) acquired during the reaction of pre-adsorbed oxygen atoms with co-adsorbed CO molecules at 247 K. The surface was initially partially covered with a (2×2)-O adlayer structure, which is gradually replaced by a c(4×2)-CO structure in the presence of 5×10^{-8} mbar CO. Times on the images are referring to the start of the CO exposure. Image sizes are 18×17 nm². The $O_{ad} + CO_{ad} \rightarrow CO_2$ reaction takes place at the frontiers between the O- and CO-covered regions. Reproduced with permission from Ref.⁸⁷. Copyright 1997 American Association for the Advancement of Science.

CO oxidation on Pt(110) #1: CO oxidation on various Pt surfaces is well-known to exhibit an oscillatory behavior, i.e., the CO₂ production oscillates with time in a wide pressure range.⁸⁸⁻⁸⁹ On the Pt(110) surface, at low pressures this was associated with the transformation from a CO-covered (1×1) surface to atomic oxygen covered (1×2) surface.² Note that the bare Pt(110) surface also exhibits a (1×2) reconstructed surface (so-called 'missing row'), but the oxygen covered (1×2) structure might be different from this bare structure, as we will discuss shortly. One of the earliest catalytic reaction studies with HPSTM was performed on the Pt(110) surface,⁹⁰ and suggested an alternative explanation to the oscillatory behavior. Simultaneously acquired STM images of the Pt(110) surface and mass spectra of the leaked gas outside of the STM-reactor cell is shown in Figure 22.⁹⁰ The total pressure was fixed to 0.5 bar and the surface temperature was kept at 425 K. The top HPSTM images in Figure 22 show the first cycle, whereas the bottom images show the second cycle, which show similar results, therefore we will only use the first cycle to discuss the results. The analysis starts with a flat, CO-covered surface in the presence of CO gas (Figure 22a). After the CO gas influx was shut off and O₂ introduced the surface remained initially flat (Figure 22b), but after certain time it became rough (Figure 22c) with protrusions of 0.2-0.4

nm height and 4-7 nm width.⁹⁰ A very significant increase in the CO₂ production starts at about the time when the surface becomes rough. It is argued in Ref.⁹⁰ that the rough surface is due to formation of an oxide. Once the O₂ gas influx into the reactor cell is stopped and CO is introduced again, the surface structure changed back to being flat (Figure 22e).

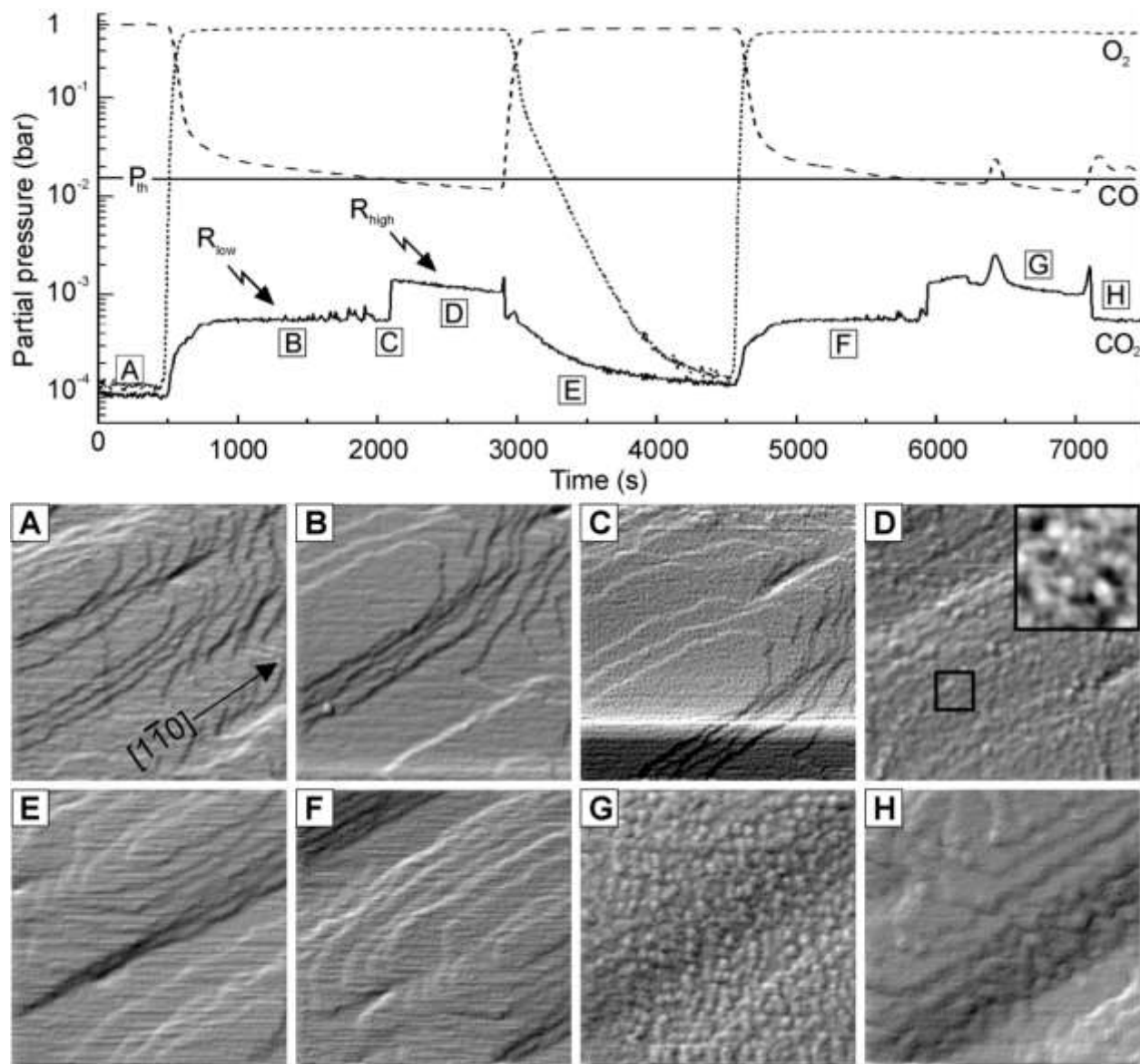


Figure 22: Top: Mass spectra of O₂, CO, and CO₂. Bottom: HPSTM images (image sizes are 210×210 nm²) of the Pt(110) surface in the presence of CO and O₂, while the surface is kept at 425 K. Mass spectra were obtained during the acquisition of the HPSTM images, by collecting the leaked gas from the reactor cell. Labels A-H indicate corresponding mass spectra and HPSTM images. There is a correlation between the roughening of the surface due to thin oxide layer formation and the higher amount of CO₂ production. Reproduced with permission from Ref.⁹⁰. Copyright 2002 American Institute of Physics.

The reaction analysis in Ref.⁹⁰ shows that it occurs in two branches, the high and the low rate branches, the former corresponding to the oxidized surface and the latter corresponding to the reduced surface, respectively. It was also argued that in both branches the reaction rates depend only on the concentration of the minority reactant, i.e. the high reaction rate depends on CO partial pressure, and the low reaction rate depends on the O₂ partial pressure. The ratio of surface coverage of CO to O is probably more relevant than the partial pressures, but there is no access to this information. According to the authors' interpretation the oxide film on the surface is the most active phase and the reaction mechanism is similar to the Mars-Van Krevelen type.

The authors argue that the roughening of the surface plays a minor role. The reactivity solely depends on the oxidation state of the surface and the concentration of each gas in the mixture. This is the dominant mechanism behind the oscillatory behavior of the reactivity to at ambient pressures, whereas changes in the surface reconstruction plays a role at low pressures.

CO oxidation on Pt(110) #2: After more than a decade the authors of Ref.⁹⁰ revisited their previous HPSTM study on the CO oxidation on the Pt(110) surface, with better resolved images.⁹¹ We will discuss these results together with the surface diffraction results of Ref.⁹² obtained under similar conditions. The HPSTM images in Figure 23 show that the surface exhibits the well-known (1×2) missing-row reconstruction (Figure 23a), which transforms into a (1×1) structure when the CO:O₂ partial pressure ratio is over 0.2 (Figure 23c). The (1×2) to (1×1) transformation initially causes slight roughening of the surface (Figure 23b). This roughness originates from the fact that the unreconstructed (1×1) surface has twice as many Pt atoms on the surface than the missing-row reconstructed surface, therefore extra atoms will either migrate to the step edges or will form clusters on the terraces. This rough surface flattens with time (Figure 23c), and the (1×1) structure becomes visible. Once the partial pressure ratio is switched to oxygen-rich conditions with CO:O₂ partial pressure ratio below 0.2, a (1×2) structure reappears on the surface (Figure 23d). This structure, however, is not the missing row reconstruction, but rather a commensurate surface oxide structure stabilized by carbonate species. This model was first suggested by surface diffraction and DFT studies in Ref.⁹². The (1×2) pattern originates from the 'lifted-row' of atoms in this commensurate oxide model. An indirect evidence that the (1×2) pattern in Figure 23d is not due to missing-rows is the lack of surface roughening during the transformation, because this would require some mass transport. Once the gas mixture is switched back to the CO-rich conditions, the surface again exhibits a slightly rough (1×1) surface (Figure 23e).

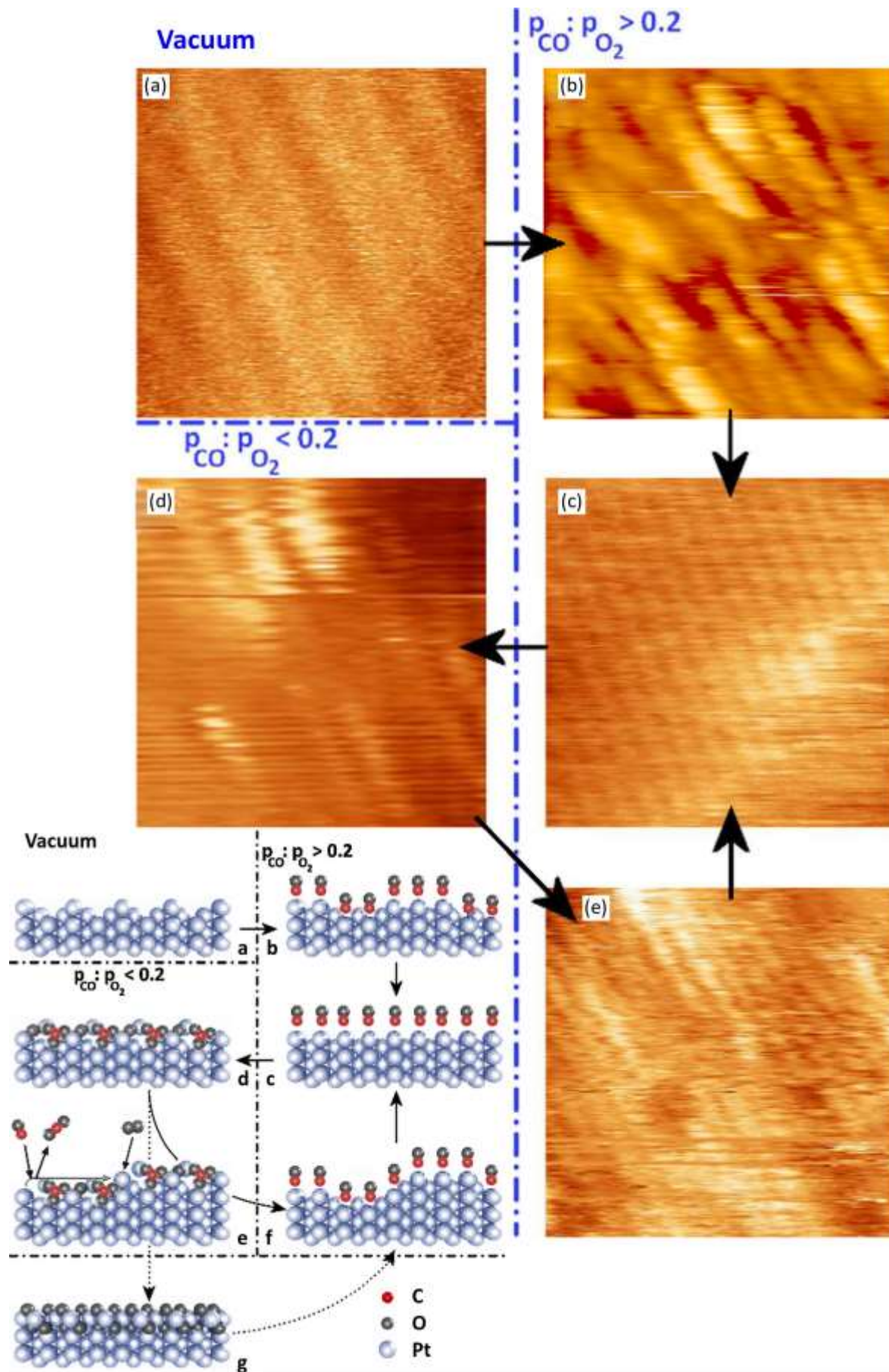


Figure 23: HPSTM images and ball-models of the CO oxidation reaction on the Pt(110) surface at 1 bar total pressure at 433 K surface temperature. The letters label corresponding images and ball-models. (a) Missing-row Pt(110)-(1×2) surface in vacuum, which transform to a CO-covered Pt(110)-(1×1) surface under CO-rich gas, as shown in (c). This transformation occurs via mass transfer on the surface, as evidenced by the rough surface in (b). (d) The lifted-row Pt(110)-(1×2) surface due to a commensurate oxide layer on the surface stabilized by carbonate species. (g) When the oxygen partial pressure is increased to higher values, a new incommensurate oxide structure forms on the surface. Both the structure in (d) or (g) can transform back to a CO-covered Pt(110)-(1×1) surface when the gas phase is switched back to CO-rich. In (a) and (c-e) image sizes are 4.5×4.5 nm², whereas in (b) image size is 15×15 nm². Reproduced with permission from Ref.⁹¹. Copyright 2015 Elsevier.

Figure 23 also shows ball-models of the each state in oxygen-rich and CO-rich conditions. An additional structure in this model is the incommensurate oxide structure (Figure 23g), which was not observed in the HPSTM study. This oxide structure requires higher oxygen partial pressures, which were not achieved in the reactor cell used in Ref.⁹¹.

6.1.2 CO Oxidation on Pd Surfaces

CO oxidation on Pd(100): One of the early HPSTM studies on CO oxidation was performed on a Pd(100) surface, and the results were similar to those observed on the Pt(110) surface discussed above.⁹⁰ Pd, like Pt, is a very active catalyst in CO oxidation; but, unlike Pt, it has 4d-valence electrons with no readily reconstructed surface. Therefore, it is not possible to attribute the activity of this surface to surface reconstructions under reaction conditions. However other changes in the surface morphology might still happen and affect reactivity. Figure 24 shows the evolution of the Pd(100) surface at 408 K in the presence of 1.25 bar of either oxygen-rich or CO-rich gas mixture, together with the mass spectra obtained simultaneously with HPSTM images. Whilst the surface is relatively flat in the presence of CO-rich gas mixture, it undergoes severe roughening in the presence of oxygen-rich gas mixtures. The flatness of the surface is recovered to a large extent once the gas mixture is changed back to CO-rich conditions (Figure 24).⁹³ Structurally, only a few differences exist between the CO oxidation studies on Pt(110) and Pd(100): Firstly, on Pd(100), the roughening of the surface is more severe under O₂-rich conditions than on Pt(110), and prolonged exposure leads to a polycrystalline surface with 4-16 nm wide grains (Figure 24c shows the early phases of this transformation). Secondly, after each cycling, the flatness of the Pd(100) surface is not fully recovered under CO-rich conditions, as small islands of vacancies and adatoms appear (Figure 24f-h), which is not observed on the Pt(110) surface. In terms of reactivity trends, both surfaces are very similar: the CO₂ production is scaled with the partial pressure of

the minority reactant, and the oxide is more active, following a Mars-Van Krevelen-like reaction mechanism, whereas in the metallic state it follows a Langmuir-Hinshelwood reaction pathway.^{90,93} In more recent surface diffraction studies, the same authors discuss the oscillatory behavior and the surface structure of the Pd(100) surface in more detail.⁹⁴⁻⁹⁵

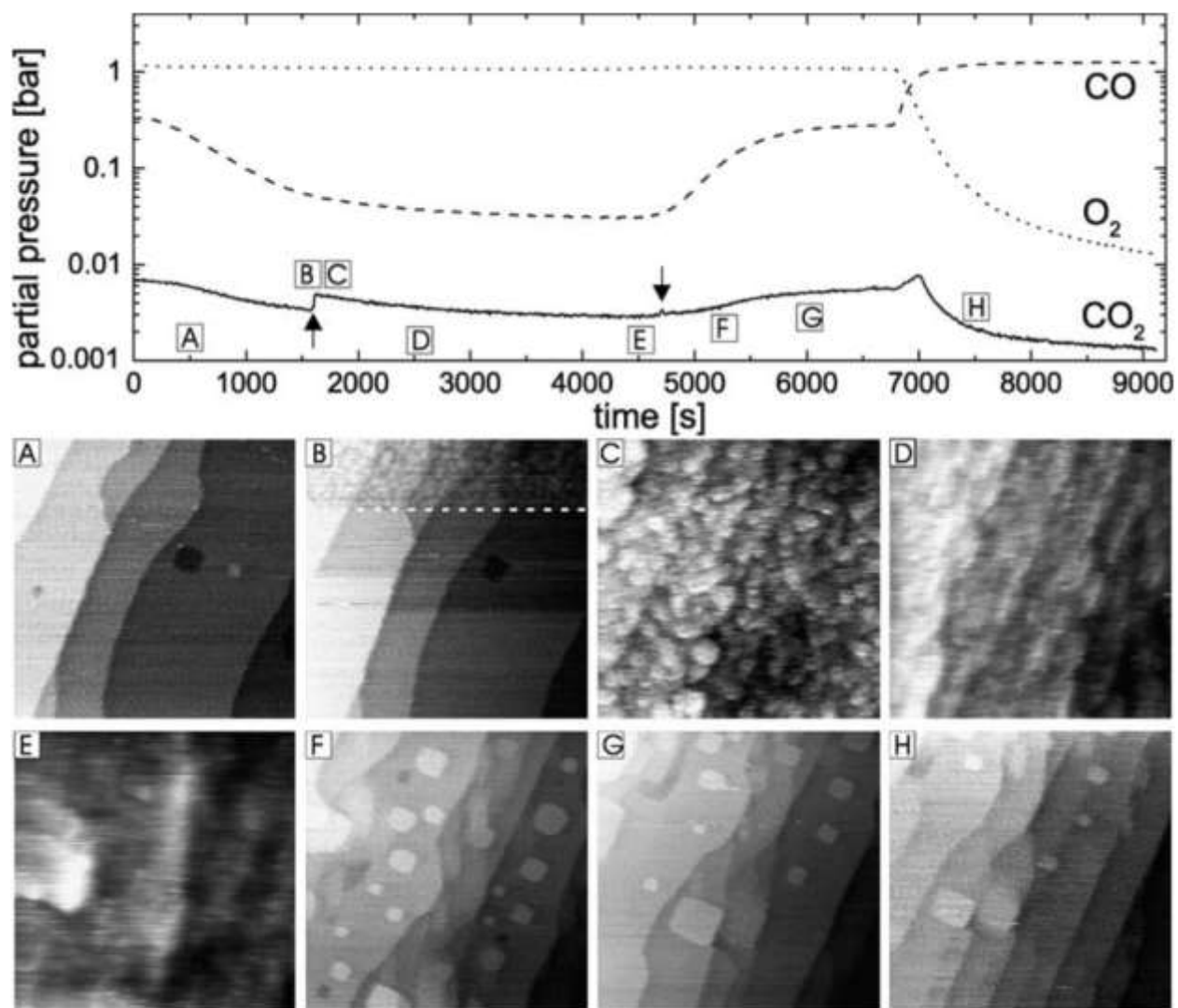


Figure 24: Top: Mass spectra of O₂, CO, and CO₂ as a function of time. Bottom: HPSTM 140×140 nm² images of the Pd(100) surface in the presence of CO and O₂, while the surface is kept at 408 K. The mass spectra were obtained during acquisition of the HPSTM images, by collecting the leaked gas from the reactor cell. Corresponding labels A-H are indicated in the mass spectra and in the HPSTM images. There is a correspondence between significant roughening of the surface due to oxide formation and the higher CO₂ production. Reproduced with permission from Ref.⁹³. Copyright 2004 Elsevier.

6.1.3 CO Oxidation on Rh Surfaces

CO oxidation on Rh(110): Many (110) surfaces of fcc metals are known to reconstruct in the form of missing rows with (1×2) structure, either in UHV or upon adsorption of molecules. One of these is Rh(110), where the oxygen atoms adsorb forming a (2×2)*p2mg* structure while changing the substrate structure from (1×1) to (1×2).⁹⁶ Interestingly, at room temperature in the presence of CO at 8×10^{-8} Torr, CO molecules replace the adsorbed oxygen atoms (observed using APXPS), likely via the CO₂ oxidation reaction, but they do not lift the missing row reconstruction of the Rh atoms.⁹⁷ Instead, the CO molecules adsorb on the remaining rows of the reconstructed surface. At ambient conditions of 0.08 Torr CO and 55 °C temperature however, (1×2) areas of the Rh(110) substrate are slowly replaced by (1×1) areas, as pure CO adsorption on bare Rh(110) at ambient pressures also exhibits a (1×1) pattern.⁹⁷ Based on these observations, a natural question arises: Would the oxygen pre-covered Rh(110) surface retain its (1×2) structure when both CO and O₂ are present in the gas phase, or would the reconstruction be lifted? Figure 25 shows three time-lapse HPSTM images at room temperature under 0.1 Torr gas mixture of 4:1 CO:O₂ mixture showing that the (1×2) reconstruction is slowly lifted. According to Ref.⁹⁷, this reconstruction does not lift in the presence of pure CO at room temperature, but it does in the presence of a 4:1 CO:O₂ gas mixture. Although this appears counterintuitive, since more CO and less O₂ should favor lifting of the oxygen-induced reconstruction, it could be explained by the exothermic nature of the CO oxidation reaction where the heat generated facilitates mass transfer on the surface, in a way similar to reconstruction lifting at 55 °C in the presence of pure CO, which is not observed at room temperature.

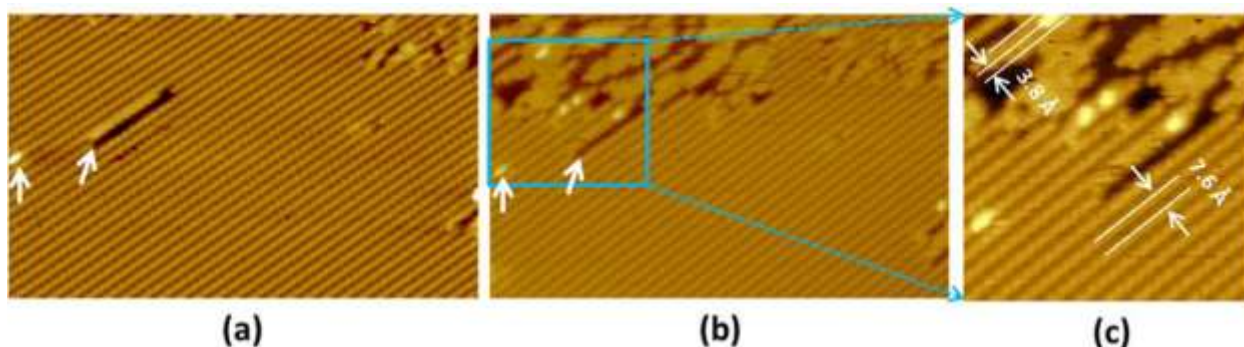


Figure 25: HPSTM images of the Rh(110)-(1×2)-O surface at room temperature in the presence of a mixture of 0.08 Torr CO and 0.02 Torr O₂. (a) Initial structure, (b-c) after 25 min, showing that some of the missing row reconstructions are lifted. Reproduced with permission from Ref.⁹⁷. Copyright 2017 American Chemical Society.

6.1.4 CO Oxidation on Cu Surfaces

Cu based catalysts are used in a variety of catalytic reactions, but they suffer from a swift deactivation during CO oxidation.⁹⁸ Solving this issue could help replacing expensive Pt catalysts in the

catalytic converters of gasoline and diesel engine vehicles. Therefore, CO oxidation on Cu surfaces has been a topic of interest both in applied catalysis and Surface Science studies. More recently HPSTM has been used to study the reaction: The first two studies were performed in the presence of CO on two oxygen pre-covered surfaces. The third study was performed in the presence of both gases.

CO oxidation on Cu(111) #1: In the first study a $\sqrt{73R5.8^\circ \times \sqrt{21R10.9^\circ}}$ overlayer structure of Cu-O was prepared on the Cu(111) surface (Figure 26-top a).⁹⁹ This overlayer structure is very similar to a layer of Cu₂O, and is often called a surface oxide. However, there is a small but significant difference: the $\sqrt{73R5.8^\circ \times \sqrt{21R10.9^\circ}}$ overlayer structure has lone oxygen atoms directly attached to the Cu(111) surface which are not present in the Cu₂O(111) surface. These atoms are easier to remove than the other oxygen atoms in the structure. In fact, it was shown with low pressure – high temperature STM studies that hexagonal and 5-7 rings containing less oxygen form after the removal of oxygen after reacting with CO.¹⁰⁰⁻¹⁰¹ Afterwards, the CO molecules adsorb on the newly formed Cu sites and remove the rest of the oxygen from the surface, thereby completely removing the overlayer from the surface.

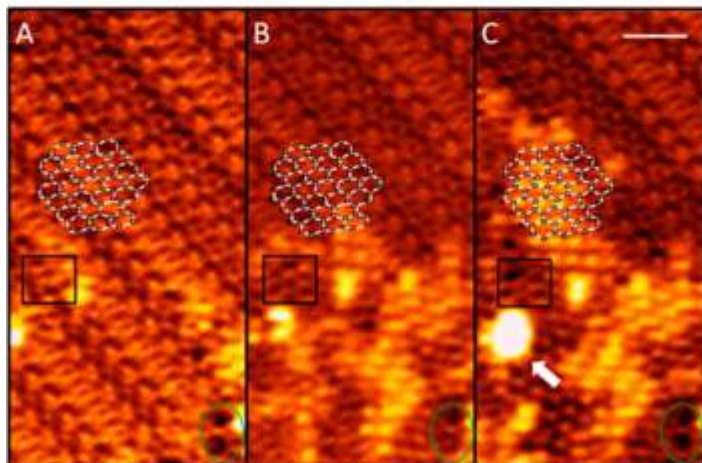
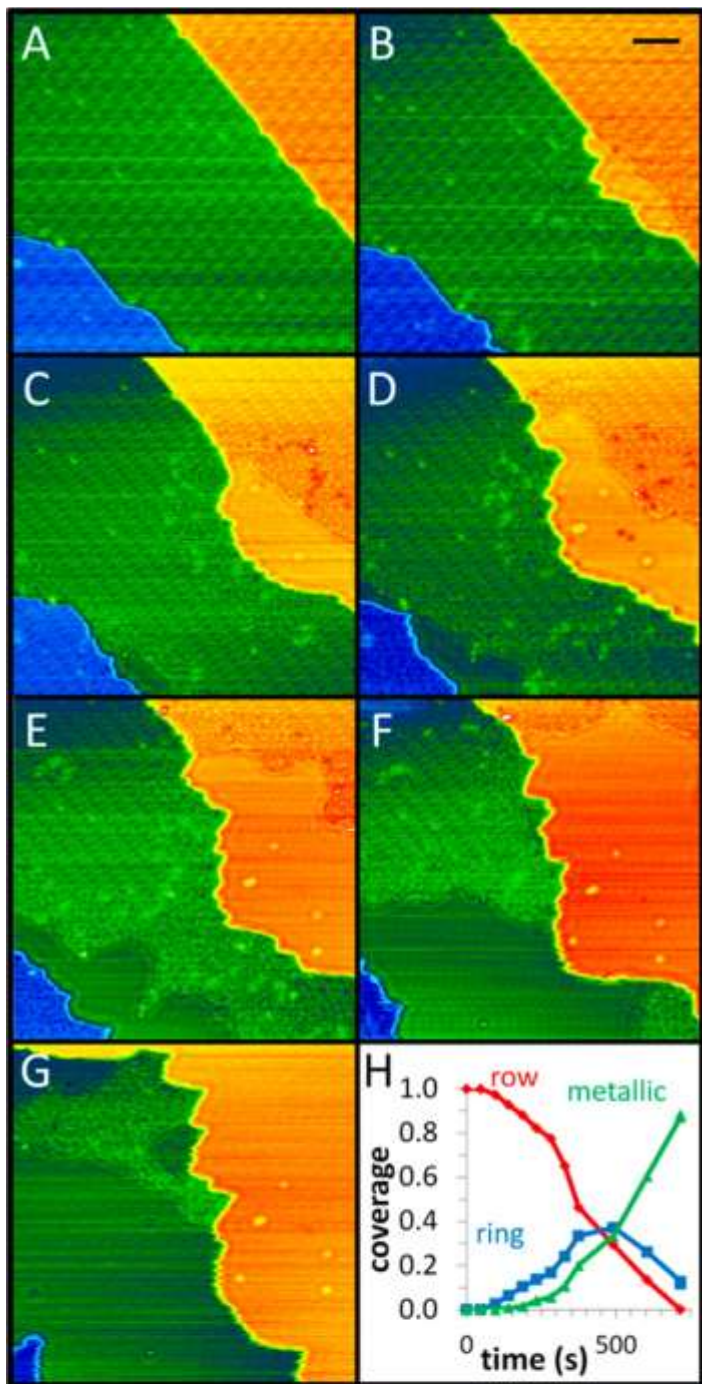


Figure 26: Time-lapse HPSTM images of the $\sqrt{73}R5.8^\circ \times \sqrt{21}R10.9^\circ$ Cu-O overlayer structure on the Cu(111) surface being removed in the presence of 10-35 mTorr CO at room temperature. Top (scale bar is 5 nm): Near step edges row-like structures due to the $\sqrt{73}R5.8^\circ \times \sqrt{21}R10.9^\circ$ overlayer, are first replaced by a hexagonal and 5-7 ring structure and then completely removed. Bottom (scale bar is 2 nm): Farther away from the step edges a removal of the $\sqrt{73}R5.8^\circ \times \sqrt{21}R10.9^\circ$ Cu-O overlayer structure is observed, first induced the formation of bright protrusions due to the newly formed hexagonal structure, buckled due to compression. The arrow shows the formation of a metallic cluster from the released Cu atoms after the reduction of the overlayer. Reproduced with permission from Ref.¹⁰². Copyright 2013 American Chemical Society.

Figure 26-top shows removal of the $\sqrt{73}R5.8^\circ \times \sqrt{21}R10.9^\circ$ overlayer structure in the presence of 10 mTorr CO at room temperature. The $\sqrt{73}R5.8^\circ \times \sqrt{21}R10.9^\circ$ overlayer structure, which appears as rows, is first replaced by a hexagonal and a 5-7 ring structure and then by a metallic surface.¹⁰¹ In this case, the reaction starts from the step edges and proceeds further into the terraces. Figure 26-bottom shows the same reaction taking place directly on terraces, initiated at defects.¹⁰¹ Different from the HPSTM images near the steps, the hexagonal structure now appears as bright protrusions due to the compressive stress on this layer in the middle of the terraces.¹⁰² The arrow on Figure 26-bottom-c indicates a metallic Cu cluster created during CO oxidation on step edges. The metallic Cu released during the process is preferentially transferred to the step edges, which appear as a growing metallic front in Figure 26-top.¹⁰²

CO oxidation on all three low-index Cu surfaces: Three oxygen-induced overlayer structures were prepared on the low Miller-index Cu surfaces following preparation recipes in the literature:^{99,103-104} Cu(111)- $\sqrt{73}R5.8^\circ \times \sqrt{21}R10.9^\circ$ -O, Cu(100)-(2 $\sqrt{2} \times \sqrt{2}R45^\circ$)-O, and Cu(110)-(2 \times 1)-O. Ball-models and STM images of these overlayer structures are shown on the left side of Figure 27. On the right side, images of each surface are shown in the presence of 0.01 Torr CO at room temperature after 0.5-1 hour since the introduction of the CO in the chamber.¹⁰⁵ The overlayer structure remains intact on the Cu(100) and Cu(110) surfaces, but is completely removed from the Cu(111) surface, in line with Ref.¹⁰². A kinetics analysis using APXPS peak intensities showed that the activation energy for removal of the surface oxygen in the overlayer structures by CO oxidation was lowest on the Cu(111) surface and highest on the Cu(110).¹⁰⁵ Although this appears counterintuitive, as the catalytic activity is usually inversely proportional to the coordination number of the surface atoms, it can be explained by the difference in adsorption energy of CO and the binding energy of oxygen in the overlayer.¹⁰⁵ In other words, following the Sabatier principle, the catalytic activity is correlated with the high oxygen binding

energy, indicating that the O chemisorption energy is a good descriptor of the CO oxidation reaction on Cu surfaces.¹⁰⁵

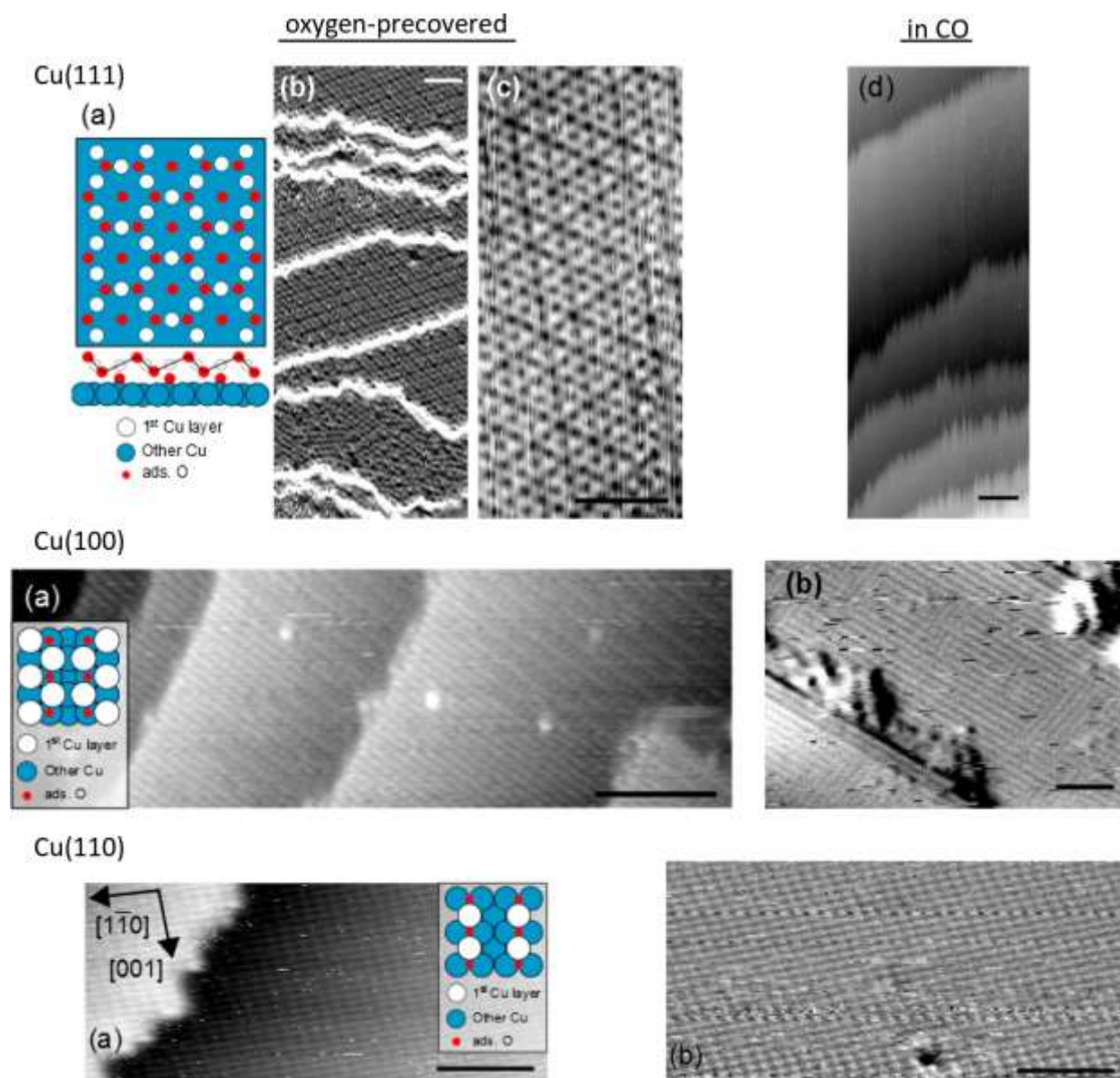


Figure 27: Left: STM images of various oxygen-induced overlayer structures on the low Miller-index Cu surfaces. Right: Same surfaces imaged in the presence of 0.01 Torr CO at room temperature, roughly 0.5-1 hours after introduction of CO into the chamber. The surface was reduced to metallic Cu only in the case of Cu(111) due to much slower kinetics on Cu(100) and Cu(110) surfaces. Scale bars are 4 nm for Cu(111) and Cu(110) images, and 5 nm for Cu(100) images. Reproduced with permission from Ref.¹⁰⁵. Copyright 2015 American Chemical Society.

CO oxidation on Cu(111) #2: Morphological changes on the Cu(111) surface in the presence of a mixture of CO and O₂ gases at room temperature was investigated in Ref.¹⁰⁶. Figure 28 shows time-lapse HPSTM images at CO:O₂ partial pressure ratios of 2:1 (top-panel), 3:1 (middle-panel), and 4:1 (bottom-panel). The first image in each case was acquired prior to gas dosing, and show the bare metallic Cu(111) surface. Under relatively oxygen-rich conditions (i.e., a CO:O₂ ratio of 2:1), the surface undergoes morphological changes, like those previously reported in the presence of pure O₂ at very low doses:¹⁰⁷ The oxidation of Cu starts at the step edges, which begin to facet as the oxide forms along the close-packed <110> directions, as shown with the green lines in the top-panel of Figure 28.¹⁰⁶ Few minutes after the gases were introduced into the chamber, the surface structure reaches equilibrium. A disordered structure forms on the surface, which does not show any additional significant changes.¹⁰⁶ When the CO partial pressure is slightly higher, a similar morphological change related to the oxidation of the Cu surface can be observed in the first ten minutes (Figure 28 middle-panel). However, after some time, metallic clusters (shown inside white circles) form on the surface, suggesting that reduction of the surface can also occur under the same conditions. This is similar to the oscillatory behavior previously mentioned on Pt surfaces: The surface is not in equilibrium, and the local chemical state of the surface oscillates between metallic and oxidic.¹⁰⁶ Such clusters disappear with time (oxidation), and other clusters form (reduction) randomly on the surface. If the CO partial pressure is even higher (Figure 28 bottom-panel), more metallic clusters are formed at the surface.¹⁰⁶

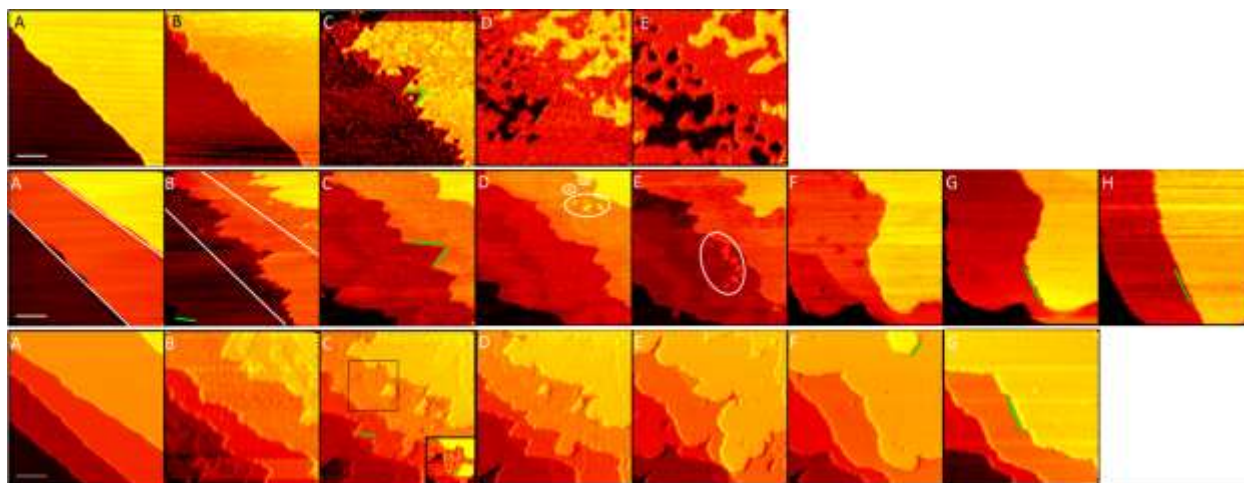


Figure 28: HPSTM images of the Cu(111) surface in the presence of a mixture of CO and O₂ at room temperature. Top row: in oxygen-rich conditions of 30 mTorr CO and 15 mTorr O₂. Bottom row: in CO-rich conditions of 32 mTorr CO and 8 mTorr O₂. Middle row: intermediate pressure ration of 30 mTorr CO and 10 mTorr O₂. Scale bar is 10 nm in each set. Whilst the top row images show roughening due to oxidation, the bottom two rows show bi-stability between the metallic and an oxidized surface. Small

clusters formed close to step edges are due to metallic Cu. Reproduced with permission from Ref.¹⁰⁶. Copyright 2014 American Chemical Society.

6.2. Ethylene Oxidation on Ag(111)

Ethylene oxidation is catalyzed by Al₂O₃-supported and promoted Ag nanoparticles in industrial practice, giving about 80% selectivity at 500 K and 10-30 bar pressure range.¹⁰⁸ The typical Ag nanoparticle size used in industry is 100-1000 nm,¹⁰⁸ which makes Surface Science studies with single-crystals good models of real catalysts for this specific case compared to other cases discussed in this Review. Two important reaction steps are involved in the oxidation of ethylene will be discussed here. One is the dissociative adsorption of O₂, and the second the reaction of ethylene with the chemisorbed O.

Oxygen on Ag(111): There is considerable amount of literature on the different structures and phases of atomic oxygen on Ag(111) and on other Ag surfaces, and many of these can found in the Refs.¹⁰⁹⁻¹¹⁰. Figure 29 shows the evolution of the Ag(111) surface at room temperature as a function of O₂ pressure.¹¹⁰ At 0.01 Torr O₂ (Fig. 29a and b), low contrast spots (dark) due to atomic oxygen are observed on the terraces in the STM images. Increasing the O₂ pressure to 0.3 Torr O₂ caused a corrugation in the STM contrast that was not present before (Figure 29c and 29d). This corrugation can be seen more clearly in the derivative images in Figure 29i and 29j. The corrugation is attributed to oxygen in subsurface layers, occupying octahedral sites according to theoretical studies.¹¹¹⁻¹¹² When the O₂ pressure was increased to 10-90 Torr the corrugation became more fine grained, which is interpreted as a result of near saturation of the subsurface with oxygen (Figure 29e and f). Upon evacuation of the chamber the oxygen on the surface remained, whilst some subsurface oxygen desorbed causing the reappearance of the corrugation in the STM contrast, as shown by the image in Fig. 29h. In Ref.¹¹⁰ it is argued that while oxide formation might be favorable at the higher pressure it is kinetically hindered on flat (111) terraces, presumably because penetration of the O and facile displacement of Ag atoms near steps and defects. Indeed regions of the surface containing many steps roughen up in the presence of O₂, due to more facile oxide formation.¹¹⁰

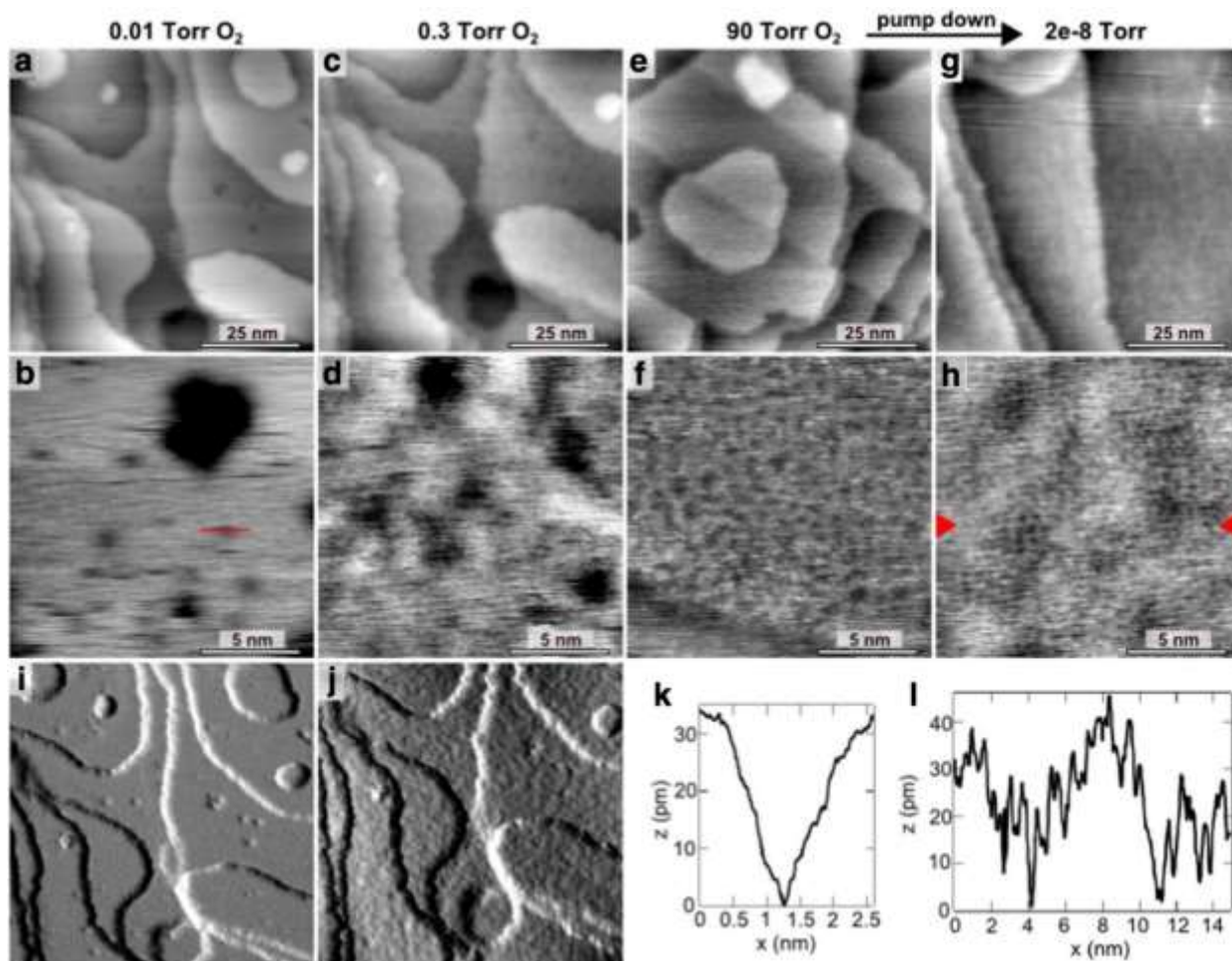


Figure 29: HPSTM images of the Ag(111) surface in presence of O₂ at various pressures at room temperature. Oxygen atoms on the surface appear as depressions, whereas subsurface oxygen appear as a corrugation in the STM contrast. (i) and (j) are derivative images of (a) and (b). Image (j) shows a corrugation not visible in (i), due to partial occupation of subsurface octahedral and tetrahedral sites. At 90 Torr O₂, no corrugation is visible again due to saturation of the subsurface sites. (k) and (l) are line profiles in (b) and (h). Reproduced with permission from Ref.¹¹⁰. Copyright 2016 Elsevier.

Ethylene oxidation on Ag(111): An XPS spectrum from the O/Ag(111) system reveals various peaks in the O 1s region due to different chemical states: One at ~530 eV, from surface or subsurface O, one at 529 eV is due to Ag₂O, and another at ~528 eV is due to ordered chemisorbed structures and is usually associated with a (4×4) Ag-O overlayer structure.^{110,113} A peak at 530 eV is the fingerprint of the desired chemical state, as Ag surfaces covered with this oxygen species heated in the presence of ethylene resulted in ethylene oxide.¹¹⁴⁻¹¹⁶ On the other hand, the same procedure results in highly undesired combustion of ethylene to CO₂ and H₂O when the surface was covered with the oxygen producing the peak at 528 eV.¹¹⁴⁻¹¹⁵ In Ref.¹¹³, it was found that under reaction conditions (0.5 mbar O₂, 0.5 bar

ethylene, 470 K surface temperature), a $(7 \times \sqrt{3})$ rect structure forms (Figure 30), which also produced the 530 eV XPS peak, and it is active in the formation of ethylene oxide.

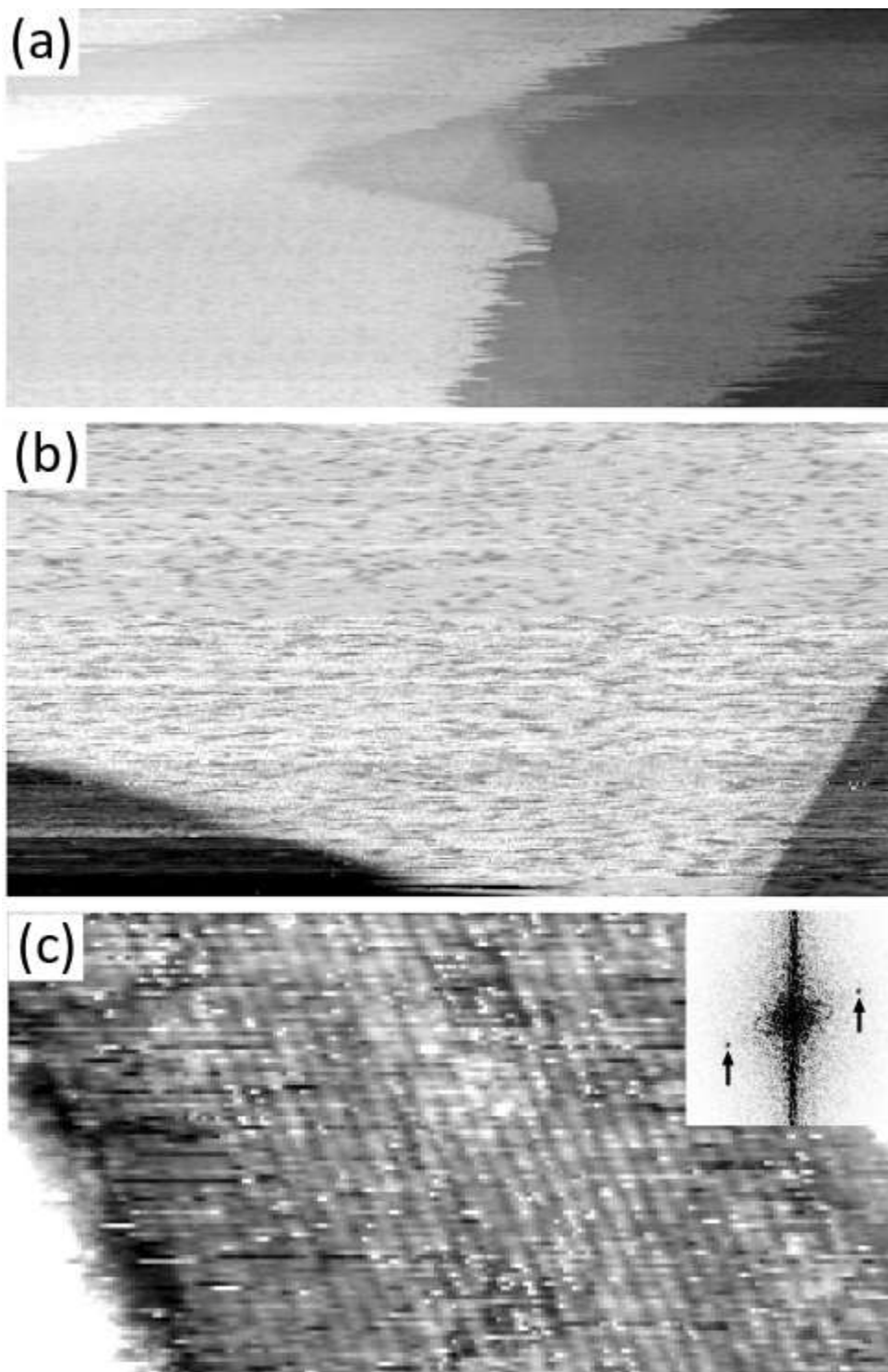


Figure 30: HPSTM images of the Ag(111) surface in the presence of 0.5 mbar of ethylene and 0.5 mbar of O₂, at a surface temperature of 470 K. Image sizes: (a) 100×45 nm², (b) 49×26 nm², (c) 25×13 nm². The atomically resolved structure in (c) corresponds to a (7×√3)rect periodicity. Reproduced with permission from Ref.¹¹³. Copyright 2013 Wiley.

6.3 NO Reduction

Both CO and NO are products found in the exhaust gases of gasoline-powered automobiles. They are toxic and cause severe air pollution. Catalysts are used therefore to convert them to inert gases via the $\text{CO} + \text{NO} \rightarrow \frac{1}{2}\text{N}_2 + \text{CO}_2$ reaction. Hydrogenation of NO is also an interesting reaction with the same idea or mitigating NO pollution.

NO reduction by CO on Pt(100): Figure 31 shows the morphology of the Pt(100) surface at around 390 K in the presence of CO and NO at various partial pressures with the total pressure fixed at 1.25 bar. As previously mentioned, the Pt(100) surface exhibits a quasi-hexagonal overlayer of Pt atoms with 6 atoms residing on top of 5 atoms in the second layers. Since no atomic resolution was obtained in the images in Figure 31, it is not possible to know if the quasi-hexagonal structure is intact or not in the presence of CO or NO. The structural analysis is based on less direct indications, like changes in morphology. Figure 31 starts with the first image that was acquired under NO-rich conditions (after cycling NO-rich and CO-rich conditions twice), where the surface exhibits vacancy islands. The authors propose that the vacancies form due to switching from the (1×1) surface structure to the quasi-hexagonal atomic structure, because the quasi-hexagonal structure has 20% more atoms and its formation should result in vacancies.¹¹⁷ Images 2-4 show time-lapse magnified images under same conditions, where the vacancy islands disappear. The authors attribute this to the tip-induced changes (tip dragging material while scanning the surface) because the larger scale image 5 shows vacancy islands outside of the scanned frame. Under CO-rich conditions (images 8-10), the process is reversed: The quasi-hexagonal reconstruction is lifted, and two-dimensional nanoclusters are formed on a (1×1) surface by the extra atoms liberated in the reconstruction,¹¹⁷ similar to observations at room temperature.³⁷ Most clusters appear near the step edges. Another evidence for these transformations is the shape of the vacancy islands and clusters, which respectively show weak hexagonal and weak rectangular geometry in higher resolution images.¹¹⁷ Final remarks should be made about oxidation of the surface in the presence of NO. When the Pt surface is oxidized, it appears rougher than under NO-rich conditions in Figure 31.¹¹⁷ Therefore, oxidation of the surface can be ruled out in this study.

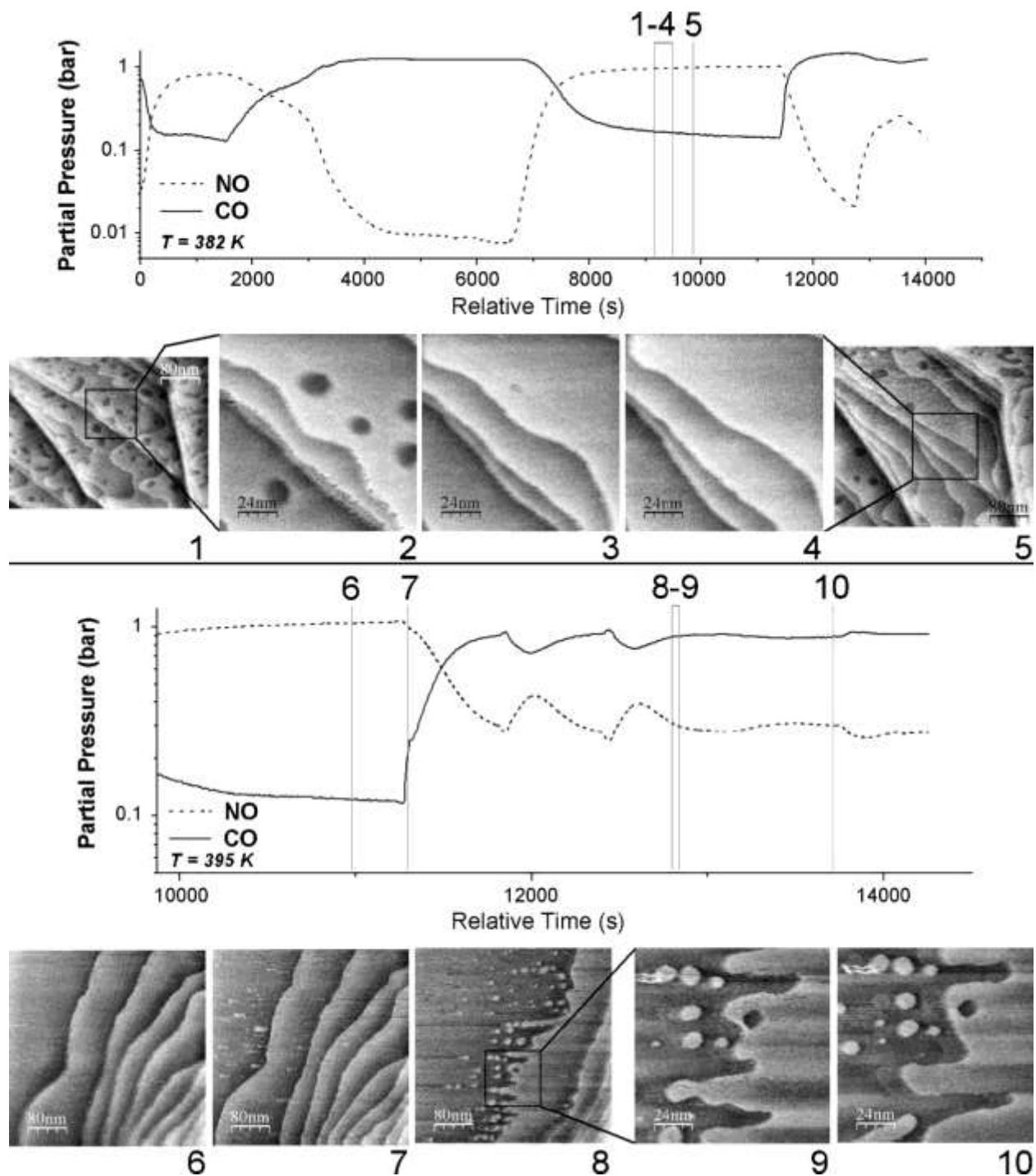


Figure 31: HPSTM images showing the surface morphology of the Pt(100) surface in the presence of CO and NO, with partial pressures indicated on the graphs above the images. Each image number corresponds to the partial pressure graphs with the same number. Surface temperature is 382 K for the upper panel images, and 395 K for the lower panel images. Because the CO-induced (1×1) surface and the NO-covered quasi-hexagonal surface have different number of surface atoms, transition between two surface

structures causes formation of two-dimensional adatom islands. Reproduced with permission from Ref.¹¹⁷. Copyright 2010 Elsevier.

NO hydrogenation on Pt(110): Figure 32 shows the evolution of the Pt(110) surface at room temperature in the presence of hydrogen and NO gas mixtures. As previously mentioned, the Pt(110) surface exhibits a missing-row (1×2) reconstruction in vacuum. The surface structure can sometimes show a few rows with (1×3) structure,²⁵ which was observed in Ref.⁹¹ in measurements prior to the acquisition of the images shown in Figure 32 due to low vacuum. In the presence of Ar, Ar+H₂ mixtures, and H₂, the Pt(110)-(1×2) structure is retained for a long period of time (Figure 32a-b).⁹¹ After 48 hours of exposure to H₂ however, the surface structure changed to a (1×4) structure (Figure 32c top). Once the NO is introduced into the chamber, either mixed with H₂ or alone, the surface restructures forming clusters with no apparent ordered structure (Figure 32c bottom and 32d).⁹¹

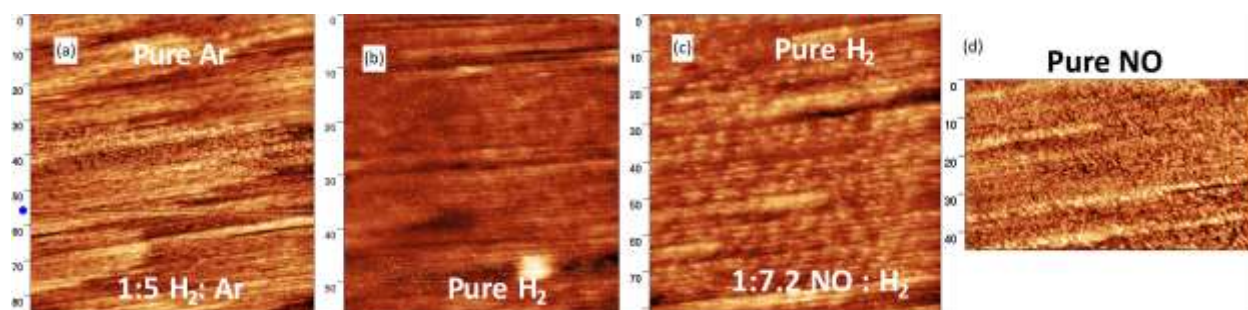


Figure 32: HPSTM images of the Pt(110) surface at room temperature at a total pressure of 1.25 bar under an evolving gas mixtures: (a) Scanning starts with pure argon (top) region, and is gradually changed to an argon-hydrogen mixture (bottom). (b) Image in pure hydrogen, which shows predominantly the missing-row Pt(110)-(1×2) structure similar that in vacuum. (c) Top part in pure H₂ after the sample was kept in H₂ for 48 hours. Bottom part of the images is in a mixture of H₂ and NO as indicated. The surface has a (1×4) structure. (d) Image in pure NO where the surface appears much rougher, with the missing row structure completely removed. Scales on each image are shown in nm units on their Y-axis. Reproduced with permission from Ref.⁹¹. Copyright 2015 Elsevier.

7. Non-reactive Co-adsorption Studies on Low Miller-Index Surfaces

CO and NO co-adsorption on Rh(111): In the previous sections, we discussed that at room temperature, ambient pressures of CO and NO on Rh(111) result in the formation of (2×2) and (3×3) adlayer structures, respectively.^{38,46} Here, we discuss the co-adsorption of these two molecules on the Rh(111) surface and the adsorbate exchange process. Figure 33 shows the HPSTM images obtained at room temperature in different partial pressures of CO and NO. When the gas mixture is CO-rich (0.5 Torr

CO and 0.15 Torr NO), the surface exhibits a (2×2) pattern similar to the CO-covered Rh(111) surface (Figure 33a), however the increase of NO partial pressure causes new bright spots to appear due to displacement of top-site CO by NO molecules.¹¹⁸ This is due to the sensitivity of the tunneling current to the electronic structure of the surface. As was shown in Ref.¹¹⁸, the tunneling current is much higher for top site adsorbed CO or NO than it is for hollow site adsorbed molecules, so that molecules at the hollow sites become “invisible” in the images. Since the NO molecules first displace CO from the hollow sites, they are not observed in the images until their population is high enough to displace the CO from the top sites, which occurs when the pressure of NO increases to 0.7 Torr (Figure 33b). The NO-CO exchange (and vice versa) on the surface can also be monitored via time-lapse STM images, as those shown with the arrows in Figure 33c under NO-rich conditions (0.5 Torr CO and 0.92 Torr NO). The model shown in Figure 33d suggests the surface to be NO-rich,¹¹⁸ as IR spectroscopy under reaction conditions suggest the hollow sites to be occupied with NO and the top sites to be occupied with CO.¹¹⁹⁻¹²⁰ At NO-richer gas mixtures (0.1 Torr CO and 0.32 Torr NO), most of the surface still exhibits a (2×2) pattern (Figure 33e and f).¹¹⁸ The (3×3) due to NO-covered areas also start appearing under these conditions in smaller areas on the surface.¹¹⁸ Some of the observations here were confirmed unambiguously by APXPS as top and hollow molecules produce XPS peaks at different binding energies that permit their identification and measurement of their coverage.¹²¹

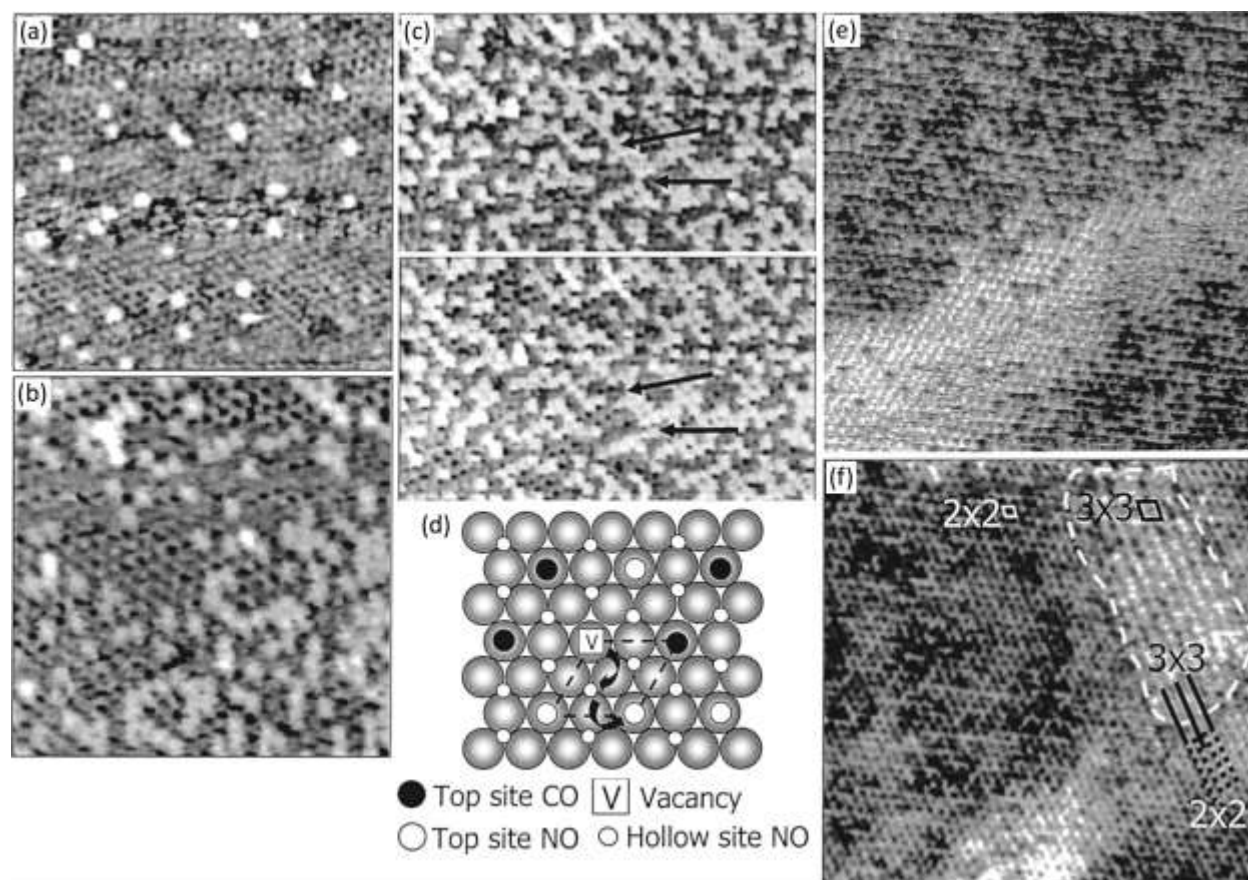


Figure 33: HPSTM of the Rh(111) surface at room temperature under different partial pressure mixtures of CO and NO: (a) 0.5 Torr CO, 0.15 Torr NO; (b) 0.5 Torr CO, 0.7 Torr NO; (c) 0.5 Torr, 0.92 Torr NO; (e-f) 0.1 Torr CO, 0.32 Torr NO. In (a-c) the bright features correspond to NO molecules on the top sites of the (2×2) pattern induced by CO. The STM contrast in such structures originates from the top-site adsorbed molecules only, so that they correspond to top-site adsorbed NO molecules only. At higher NO ratio (3×3) patterns appear, similar to those in pure NO adsorption. Reproduced with permission from Ref.¹¹⁸. Image sizes are 12×12 nm² in (a) and (b), 20×11.5 nm² in (c), and 20×20 nm² in (e) and (f). Copyright 2002 American Chemical Society.

CO and oxygen co-adsorption on Pt(111): In a previous section we showed the reaction between oxygen and CO on the Pt(111) surface slightly below room temperature. However, in that case the oxygen was pre-adsorbed on the surface forming the well-known (2×2) structure. In the presence of 1 Torr O₂ at room temperature the terraces of the Pt(111)-(1×1) surface remain unchanged (Figure 34-top a).¹²² In our opinion, this is likely due to atomic oxygen reacting away immediately with the background CO. In fact, a traditional surface science study showed that O₂ molecules, adsorbed on a Pt(111) surface at 100 K, completely dissociate as the surface is warmed to room temperature.¹²³ We should also mention here that in another study, to be discussed later, the (2×2)-O structure on the Pt(111) terraces appear only after ~2

hours of exposure to 1 Torr O₂. The more active step edges, however, are oxidized (Figure 34-top a).¹²² Once CO is added into the gas mixture, at 0.01 Torr partial pressure, a somewhat ordered structure due to adsorbed CO on the Pt(111) surface appeared (Figure 34-top b). Increasing the CO partial pressure changed the moiré pattern of the CO adlayer structure (Figure 34-top c). Although these structures appear similar to the ($\sqrt{19} \times \sqrt{19}$) R23.4°-13CO structure obtained at room temperature at 1 Torr CO and above, they are not exactly the same.¹²² This means that even weakly adsorbed O₂ molecules on the surface can affect the structure to CO. This could be related to the steric repulsion between adsorbed CO molecules and adsorbed O₂ molecules and the fragile structure of a moiré structure that is perturbed easily with changes in adsorbate density and inclusion of foreign species.

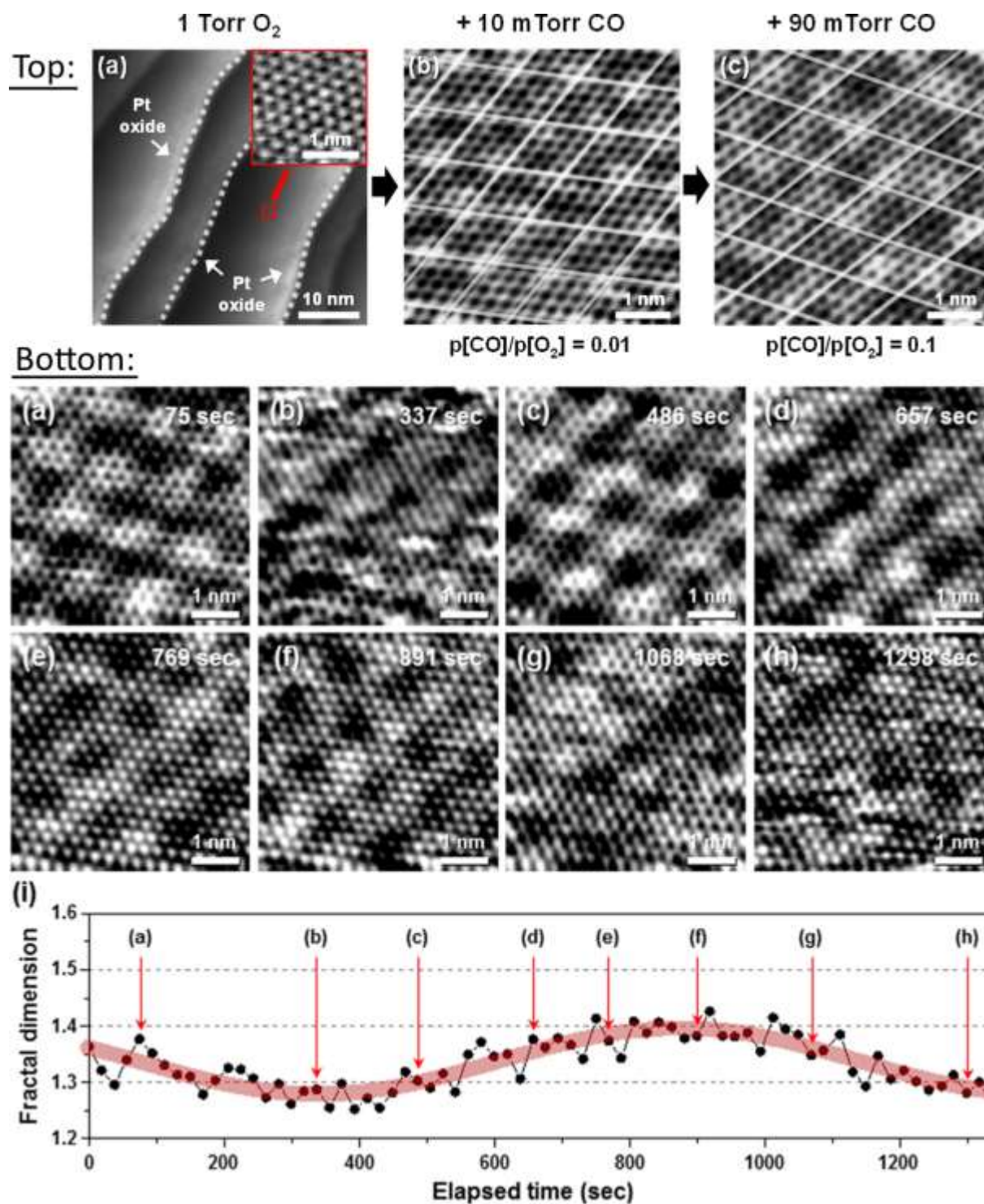


Figure 34: Top: HPSTM images of the Pt(111) surface at 1 Torr of O_2 , and after increasing the total pressure by adding CO to gas mixture. Whilst the terraces appear structureless when only O_2 is present, new structures are formed once CO is added. Bottom: HPSTM images of the Pt(111) surface under 10.5 Torr of mixed CO and O_2 gas (1:3 ratio), which show structural changes at atomic scale as a function of time. (i) Plot of the fractal dimension from each HPSTM image vs time. It can be fit with a periodic

function, which shows the oscillatory behavior between high-ordered surface structure (due to the CO adlayer) and disordered surface structure (due to O₂ adsorption perturbing the CO adlayer structure). The sample temperature was kept at room temperature during image acquisition. Reproduced with permission from Ref.¹²². Copyright 2018 American Chemical Society.

Time-lapse HPSTM images were obtained in the presence of a 10.5 Torr gas mixture with 1:3 CO:O₂ partial pressure ratio (Figure 34-bottom). Interestingly, the CO adlayer structure on the surface exhibits a bistability, as it switches between an ordered structure and a disordered structure.¹²² A fractal dimension analysis (fractal refers to the mathematical self-similarity of the geometric form¹²⁴) is shown at the bottom of Figure 34. A higher fractal dimension is indicative of a more ordered pattern. The resulting graph could be fit with a sinusoidal function with a periodicity of 1067 s.¹²² This periodicity reflects the ensemble behavior of molecules and indicates probably a metastable structure.¹²² Such analysis of the adsorption kinetics has not been applied before, and it is a clear representation of one of the new avenues that is opened up by performing HPSTM measurements at higher chemical potentials that mitigate kinetic hindrances.

CO, ethylene and hydrogen co-adsorption on Pt(111): In the previous sections, we have shown a few examples where HPSTM was used to monitor the surface morphology during catalytic reactions on surfaces. We will now show a few examples of reactions on surfaces which are deactivated due to poisoning, especially CO-poisoning. The first example is the ethylene hydrogenation reaction on Pt(111). Upon adsorption on Pt(111) at room temperature ethylene converts to ethylidyne by losing one hydrogen atom and transferring another to the other carbon to form a methyl group.¹²⁵ STM and LEED studies at low temperatures have shown that the ethylidyne adlayer on Pt(111) has a (2×2) structure, occupying the fcc threefold hollow sites.¹²⁶⁻¹²⁸ At room temperature, the (2×2) structure is still observable by LEED, but not by STM, indicating that the ethylidyne mobility on Pt(111) at room temperature is much faster than the STM scan rate. Hydrogen adsorbs dissociatively, with the hydrogen atoms occupying fcc threefold hollow sites forming a (1×1) structure at saturation.¹²⁹⁻¹³¹ Figure 35a shows the Pt(111) surface in the presence of 20 mTorr H₂, which shows no discernible features on the surface.¹³² This is due to the high mobility and small corrugation of the hydrogen atom on the Pt(111) surface, making it difficult to image by STM at room temperature. Because both atomic hydrogen and ethylidyne are mobile on the surface, the HPSTM image in presence of both hydrogen and ethylene (20 mTorr each) shows no discernible features (Figure 35b). However, once 2.5 mTorr CO is included into the gas mixture, an ordered structure appears on the surface (Figure 35c and 35d). The structure resembles the ($\sqrt{19}\times\sqrt{19}$) R23.4° structure obtained in the presence of pure CO, but IR spectroscopy indicates that both CO and ethylidyne are

present on the surface, with CO occupying top sites.¹³³⁻¹³⁴ Based on the HPSTM images and the IR spectra, the model in Figure 35d was suggested in Ref.¹³². Finally, we should note here that the surface shown in Figure 35c is inactive as no ethane can be detected with mass spectroscopy, whereas the surface shown in Figure 35b is active producing ethane. This poisoning of the surface is related to the reduction in adsorbate mobility, as immobile CO blocks sites and hinders the mobility of the atomic hydrogen and ethylidyne.¹³²

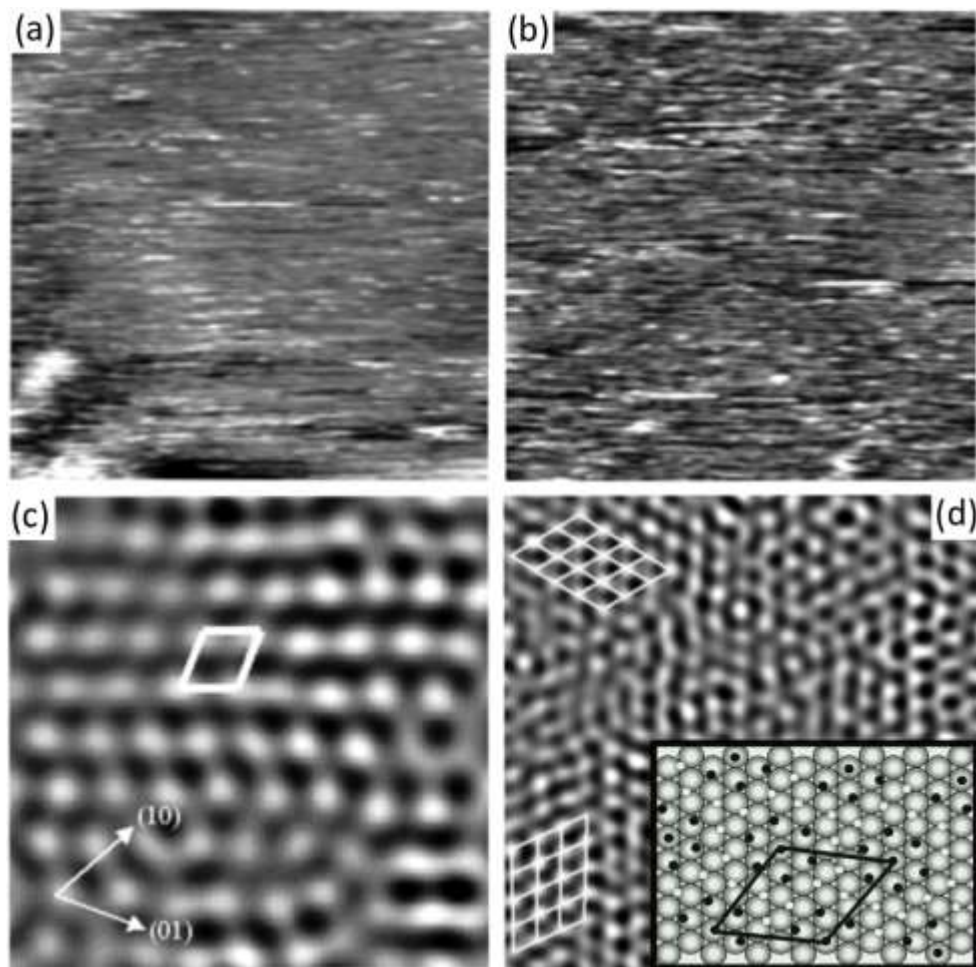


Figure 35: HPSTM images of the Pt(111) surface under different gas mixtures: (a) 20 mTorr H₂, (b) 20 mTorr H₂ and 20 mTorr ethylene, (c-d) 20 mTorr H₂, 20 mTorr ethylene and 2.5 mTorr CO. The presence of CO induced the formation of a structure on the surface similar to the ($\sqrt{19}\times\sqrt{19}$) R23.4° structure. The HPSTM image in (d) shows two rotation domains of ($\sqrt{19}\times\sqrt{19}$) R23.4°. The inset in (d) shows the proposed model for the co-adsorption of CO and ethylidyne, where the black dots represent CO and the white dots ethylidyne. Image sizes are 10×10 nm² in (a-c), and 20×20 nm² in (d). Adapted with permission from Ref.¹³². Copyright (2004) American Chemical Society.

CO, ethylene and hydrogen co-adsorption on Rh(111): The adsorption structure of hydrogen and ethylene on Rh(111) is similar to that on Pt(111),¹³⁵⁻¹³⁸ with the noted difference that both species adsorb on the hcp threefold hollow sites on Rh(111) instead of the fcc sites as in Pt(111).^{135,137} Figures 36a and 36b show the HPSTM images of the Rh(111) surface in the presence of 20 mTorr hydrogen, and a mixture of 20 mTorr hydrogen and 20 mTorr ethylene, respectively.¹³² In both cases, no ordered structure is visible in images due to the rapid diffusion of atomic hydrogen and ethylidyne on the surface. This surface is active for ethane production. Once 5.6 mTorr CO is added into the mixture of 20 mTorr hydrogen and 20 mTorr ethylene, three different ordered structures appear on the surface (Figure 36c-h). One of these structures is the (2×2) adlayer structure observed in the presence of pure CO (discussed earlier in this Review, with 3 CO molecules per unit cell) and they cover around 20% of the surface (Figure 36g and h). The other two structures originate from co-adsorption of CO and ethylidyne on the surface (Figures 36c and 36e). The suggested unit cell models of the both (4×2) and c(4×2) patterns are shown in Figures 36d and 36f. Similar to Pt(111), the presence of adsorbed CO on the surface reduced the mobility of adsorbates and poisoned the ethylene hydrogenation reaction.¹³²

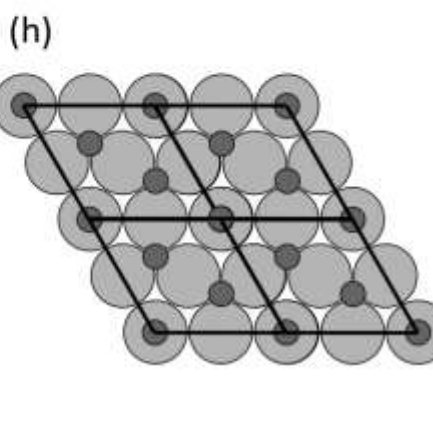
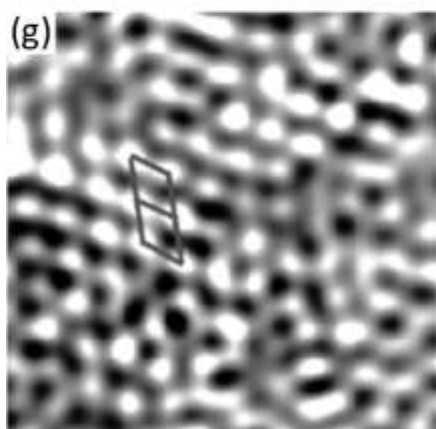
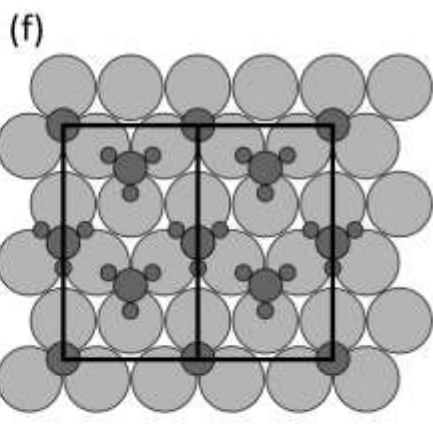
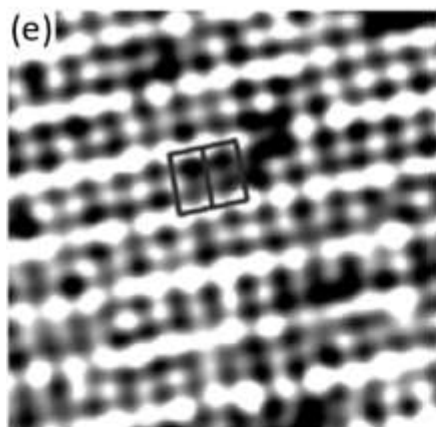
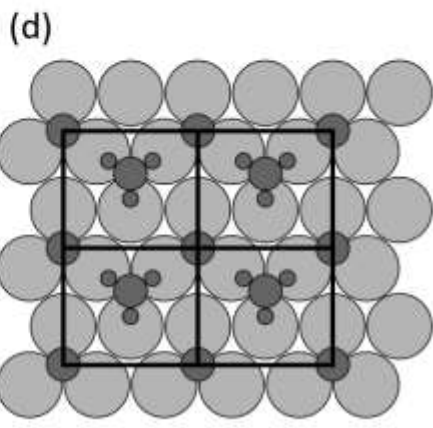
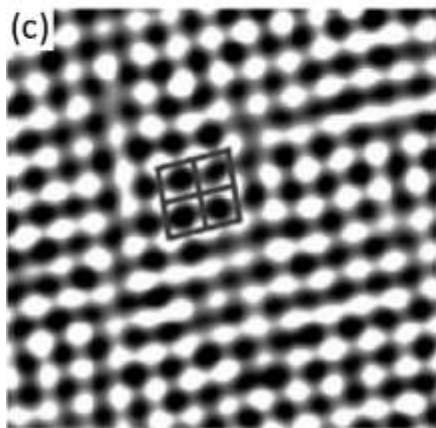
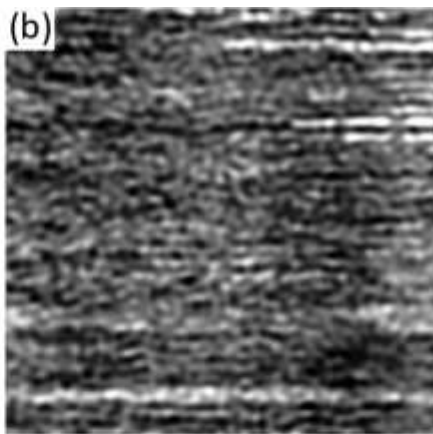
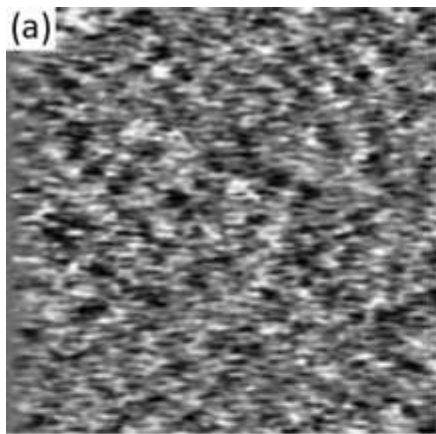


Figure 36: HPSTM images of the Rh(111) surface under different gas mixtures: (a) 20 mTorr H₂, (b) 20 mTorr H₂ and 20 mTorr ethylene, (c, e, g) 20 mTorr H₂, 20 mTorr ethylene and 5.6 mTorr CO. The addition of CO into the gas mixture resulted in three different adlayer patterns observed on the Rh(111) surface attributed to c(4×2), (4×2), and (2×2) structures shown in (d), (f), and (h), respectively. Whilst the (2×2) pattern is due to CO adsorbates only, the other two structures are due to co-adsorption of CO and ethylidyne. Image sizes are 10×10 nm² in (a-c), and 5×5 nm² in (e) and (g). Adapted with permission from Ref.¹³². Copyright (2004) American Chemical Society.

CO, ethylene and hydrogen co-adsorption on Pt(100): In previous sections we discussed the structural changes observed on the quasi-hexagonal overlayer structure of the Pt(100) surface in the presence of CO and in the presence of ethylene. Even at low pressures, CO lifts the reconstruction and results in the formation of clusters with (1×1) structure on the surface. This was also observed for ethylene, but a more recent publication attributed this to the effect of CO contamination from the background,⁵⁴ as pure ethylene did not lift the quasi-hexagonal reconstruction. Similar to hydrogen and ethylene co-adsorption HPSTM studies discussed above for Rh(111) and Pt(111) surfaces, together with online mass spectroscopy, ethane forms as a result of ethylene hydrogenation on the Pt(100) surface at room temperature, whilst addition of some CO into the gas mixture poisons the surface.¹³⁹ Figure 37a shows the HPSTM image of the Pt(100) surface at room temperature in the presence of 0.5 Torr hydrogen and 0.5 Torr ethylene, which shows no ordered structure. This is because of the rapid diffusion of atomic hydrogen and ethylene adsorbates on the surface.¹³⁹ Once the scanning speed is increased from 60 nm/s to 150 nm/s, some structure can be observed on the surface (Figure 37b), as the STM scanning speed becomes comparable with the diffusion rate of the adsorbates on the surface. After addition of 3 mTorr CO into the gas admixture, the surface breaks up into clusters, similar to those observed in the presence of pure CO (Figure 37c and d). The presence of strongly adsorbed CO, which hampers the diffusion of atomic hydrogen and ethylene-related adsorbates, is the reason of the poisoning of this model catalyst surface.¹³⁹

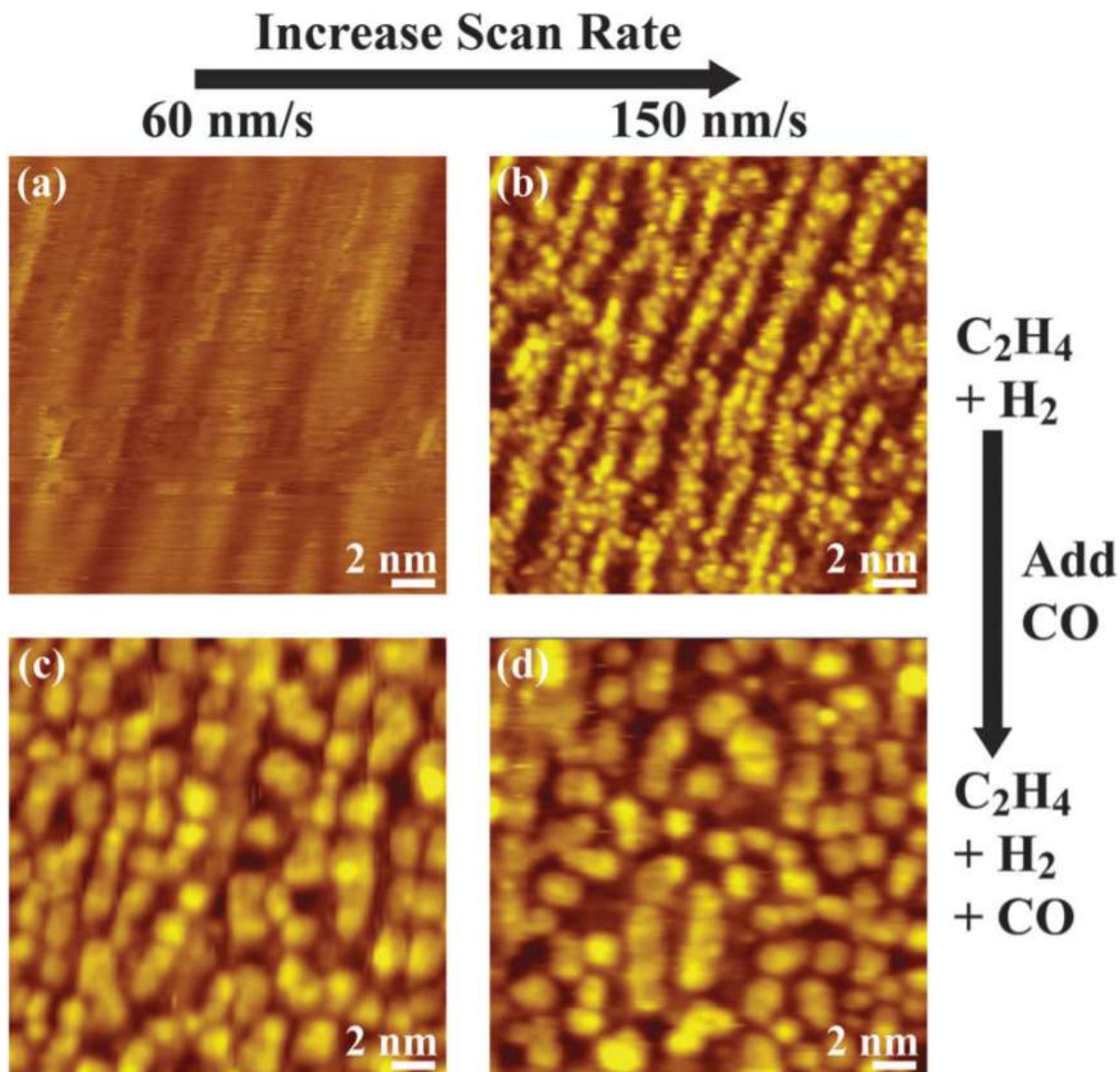


Figure 37: HPSTM images of the Pt(100) surface under different gas mixtures with different scanning speeds: (a and b) 0.5 Torr H_2 and 0.5 Torr ethylene with 60 nm/s and 150 nm/s scanning speed, (c and d) 0.5 Torr H_2 , 0.5 Torr ethylene and 3 mTorr CO with 60 nm/s and 150 nm/s scanning speed. Adsorption of CO from the higher pressure gas breaks up the surface into clusters. Adapted with permission from Ref.¹³⁹. Copyright (2013) Royal Society of Chemistry.

8. Adsorption and Reactions on Vicinal Surfaces

A particularly interesting question is what happens to vicinal surfaces in the presence of gases at room temperature and above. So far, we only investigated low Miller-index surfaces and established that the surface can undergo structural changes due to the presence of gases. Even these low Miller-index

surfaces have steps and kinks, however, vicinal surfaces have a much higher density of steps and kinks and might break up into clusters easier than low Miller-index surfaces. In addition, vicinal surfaces can also undergo other changes like step-doubling or step-bunching. Clustering, as we discussed before, is driven by the difference in adsorbate binding energies in low- and high-coordination sites, and it is expected more likely to occur on metals with low cohesive energy. The stability of regularly spaced steps of vicinal surfaces in UHV, on the other hand, is due to the repulsive electrostatic interactions of the dipoles at the step edges and from the elastic force fields arising from step atoms pushing down into the bulk. Both the electrostatic and elastic forces decay fast with distance, and can be altered by adsorbates, which is the driving force for step doubling reconstructions.

CO on Pt(557) and Pt(332): Some of the first HPSTM studies that demonstrate the effects mentioned above were performed on the stepped Pt(111) surfaces about a decade ago. We have shown previously that the Pt(111) surface does not undergo any structural changes in the presence of up to almost 1 bar CO at room temperature, and instead, a dense layer of CO forms.¹⁹ In contrast, the vicinal (regularly stepped) Pt(557) and Pt(332) surfaces, which form a $\sim 10^\circ$ angle with the (111) terraces, did reconstruct by formation of Pt clusters (e.g. Figure 38).¹⁴⁰ Interestingly, the shape and symmetry of the clusters are different in the two surfaces, despite very similar atomic structure. This is related to the different local structure of the steps in these surfaces, the Pt(557) with square (A-type or 100-type), and the Pt(332) with local triangular atomic structure arrangements (B-type or 111-type), respectively.¹⁴⁰ As illustrated in Figure 38, the Pt(557) surface can undergo two different type of structural changes in the presence of CO at room temperature: At low pressures, the terrace widths and the step heights double (Figure 38b). At ambient pressures however, the surface breaks up into triangular clusters, which occupy the doubled terraces (Figure 38c). It is also worth noting that once the measurement chamber is evacuated, the clusters disappear and the surface structure at low CO pressures is recovered.¹⁴⁰ The Pt(332) surface, on the other hand, does not undergo step-doubling at low CO pressures, and breaks up into rectangular clusters (instead of triangular clusters) at ambient CO pressures.¹⁴⁰ The clustering phenomenon was also indirectly observed via the core-level shifts during APXPS experiments.¹⁴⁰

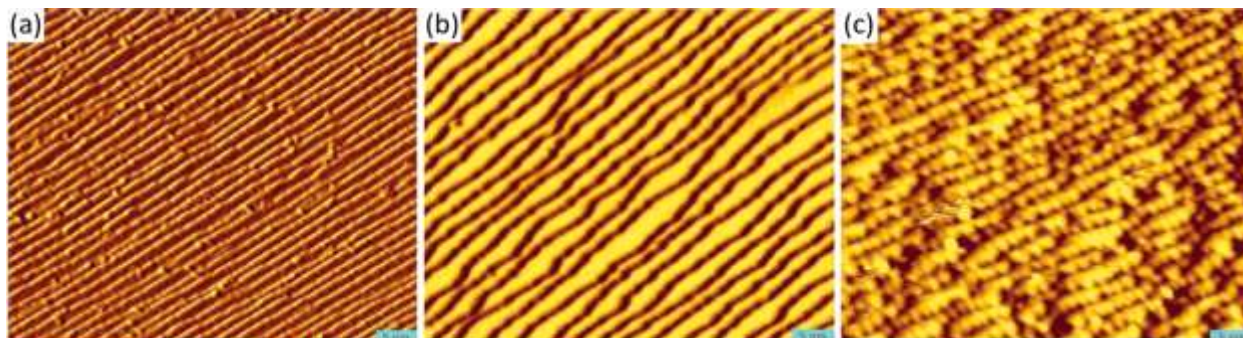


Figure 38: HPSTM images of Pt(557) (a) in UHV at 10^{-10} Torr base pressure, (b) under $\sim 5 \times 10^{-8}$ Torr CO which produces a coverage to cause step-doubling of the surface, and (c) at 1 Torr the coverage is close to 1 ML and causes restructuring and formation of clusters of Pt atoms inside the double-width terraces. Images are $40 \times 50 \text{ nm}^2$ in size. Adapted with permission from Ref.¹⁴⁰. Copyright (2010) American Association for the Advancement of Science.

Pt(997) surface, which has a terrace width approximately 1.5 times larger than those of Pt(557) and Pt(332), was shown to not break up into clusters in the presence of CO, but only reconstruct by step doubling.¹⁴¹ This different behavior exhibited by crystals with shorter and larger terraces might be a result of the repulsive interactions between the steps which, as indicated earlier decay fast with distance between steps.¹⁴²⁻¹⁴³ In the case of Pt(111), the electrostatic interaction between the steps is significantly lower than the elastic interactions between the steps.^{142,144} In a simplistic picture, CO adsorption will weaken the interaction between the first and second surface layers, so that surface atoms are pulled out and thereby repulsive interaction between the steps should be reduced. This, however, only explains how CO adsorption can affect step doubling. The temperature for clustering to occur on vicinal surfaces is likely to be lower than for flat (111) surfaces due to lower coordination number. For instance, the cohesive energy of a Pt(111) surface atom at a step is roughly 1 eV lower than that of a surface atom on a terrace. It is clear that this is an area where a theoretical study is necessary to understand the influence of the elastic and electrostatic interactions at the step edges on the clustering phenomenon better.

CO on Pt(557) at higher temperature: The clustering of the Pt(557) surface in the presence of CO at room temperature was shown also in Ref.¹⁴⁵. In addition, once the surface temperature was increased to 363 K, more of the clusters adapted the triangular shape (Figure 39). This process is reversible, as cooling the temperature back to 300 K resulted in fewer triangular clusters and more disordered clusters (Figure 39e). The triangular clusters have the most optimized shape and size to account for CO-CO repulsive interactions at step edges,¹³⁹ therefore their formation at higher temperature was expected.¹⁴⁵

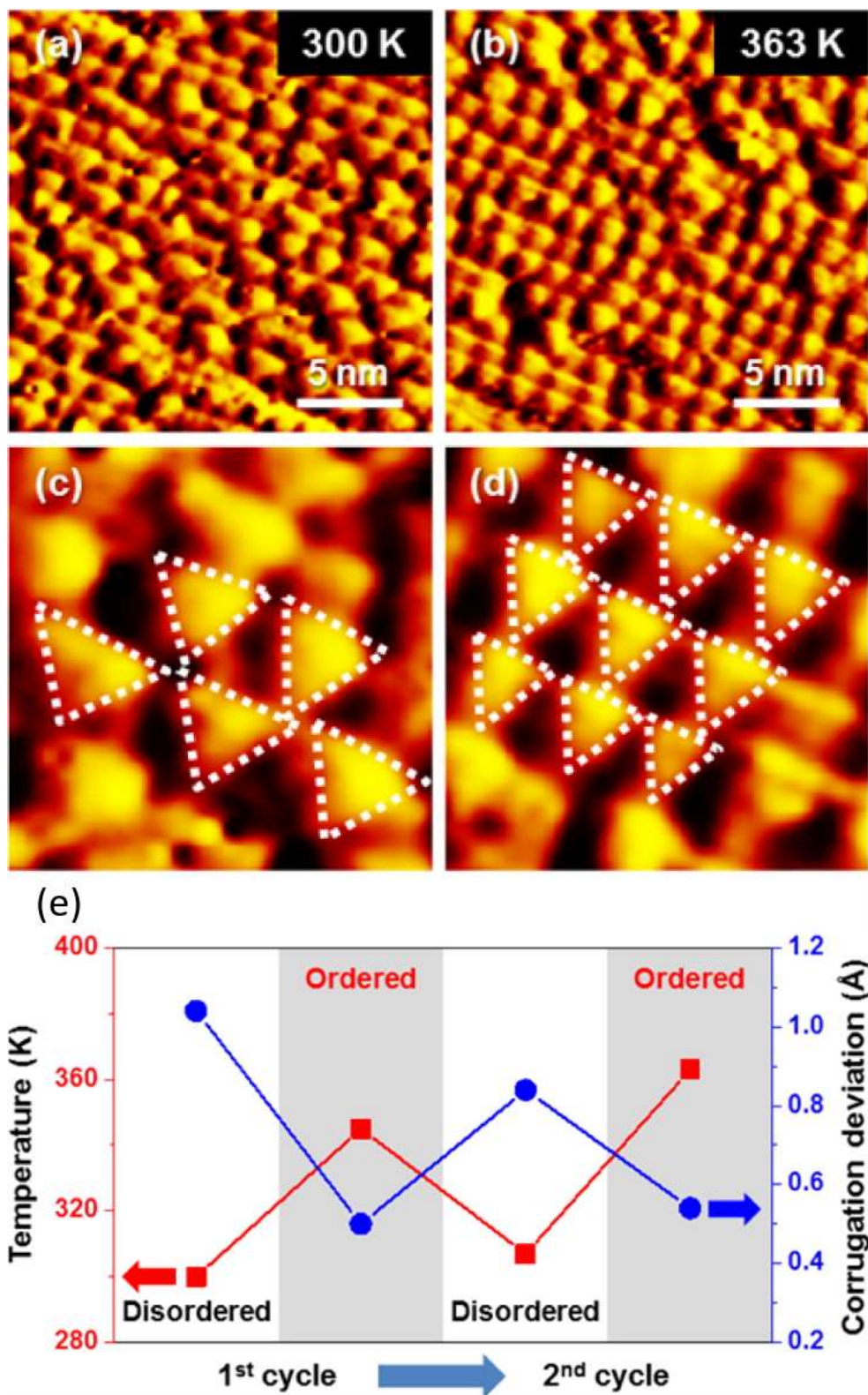


Figure 39: HPSTM images of the Pt(557) surface in the presence of 1.4 mbar CO at 300 K (images in a and c) and at 363 K (images in b and d). At 363 K, the surface is more ordered as more of the clusters

have triangular shapes. (e) shows that the disorder-order transition is reversible upon cooling the sample back to 300 K. Adapted with permission from Ref.¹⁴⁵. Copyright (2016) American Chemical Society.

CO and ethylene coadsorption on stepped Pt surfaces: Previously we discussed the break-up of the Pt(557) and Pt(332) surfaces in the presence of CO at room temperature. Figure 40a-d show these surfaces in UHV and in the presence of 0.5 Torr CO. After subsequent addition of 0.5 Torr of ethylene, the density of clusters decreased on Pt(332) (Figure 40e), but remained unchanged on Pt(557) (Figure 40f).¹⁴⁶ The difference in the clustering behaviors on Pt(557) and Pt(332) surfaces originate from the difference in step geometry and the difference in ethylene adsorption on both surfaces.¹⁴⁶

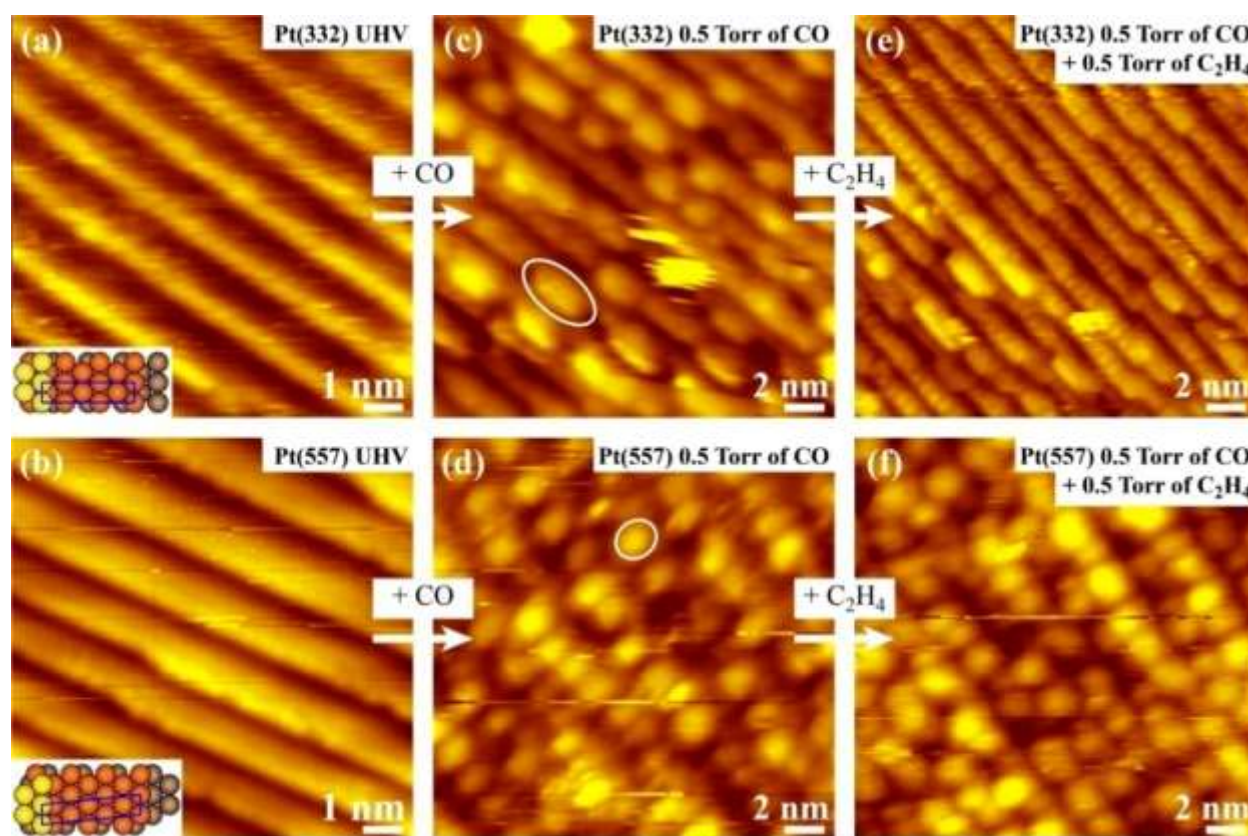


Figure 40: HPSTM images of the Pt(332) (top) and Pt(557) (bottom), from left to right: in UHV, in the presence of CO, and in the presence of CO and ethylene at room temperature. Inclusion of ethylene has no discernible effect on the structure of the Pt(557) surface, but it apparently reduces the cluster density on the Pt(332) surface. Adapted with permission from Ref.¹⁴⁶. Copyright (2014) American Chemical Society.

Pt(557) oxidation: As we discussed in the CO oxidation section, Pt-based catalysts are used in catalytic converters of most vehicles. In previous sections we have presented a few studies on the CO/Pt

system, and a few on the CO oxidation on Pt surfaces. In this Subsection we discuss the O₂/Pt system. Sufficiently high oxygen pressures produce a variety of oxygen-induced chemical states.¹⁴⁷⁻¹⁵¹ Figures 41a and 41c show the Pt(557) and Pt(111) surfaces in the presence of 1 Torr O₂, acquired approximately 30 min after introduction of the gas.¹⁵² Figures 41b and 41d show the same surface ~2 h after the gas was introduced. The line scan (in red) in Figure 41a shows a periodic array of maxima with 0.25 nm periodicity, which is close to the atomic Pt–Pt distance. Most likely, this corresponds to a one-dimensional Pt oxide chain, which was previously reported to form at the edges of stepped Pt crystals when the oxygen coverage is high^{147,149} After 2h of exposure to 1 Torr O₂, numerous clusters with ~1 nm in diameter and ~0.15 nm in height cover most of the surface (Figure 41b). These nanometer-sized clusters are roughly aligned along the original steps, suggesting that the clusters are formed from the one-dimensional oxide chain. The clusters are ascribed to a two-dimensional surface oxide phase, which was corroborated through APXPS spectra via shifts of the surface core-level peaks in the Pt 4f region.¹⁵² On Pt(111) however, only a few clusters form near the step edges and the shifted surface core-level peak was much less intense.¹⁵² Instead of a two-dimensional oxide, the terraces are covered with a hexagonal pattern corresponding to a chemisorbed oxygen (2×2) structure (Figure 41d).¹⁵² This is a precursor state of Pt oxide, but the kinetics of oxide formation on the terraces is slow. The Pt oxide is not stable upon evacuation of the chamber, as evidenced by the disappearance of the clusters in HPSTM and with the partial restoration of the Pt 4f surface peak position in APXPS.¹⁵²

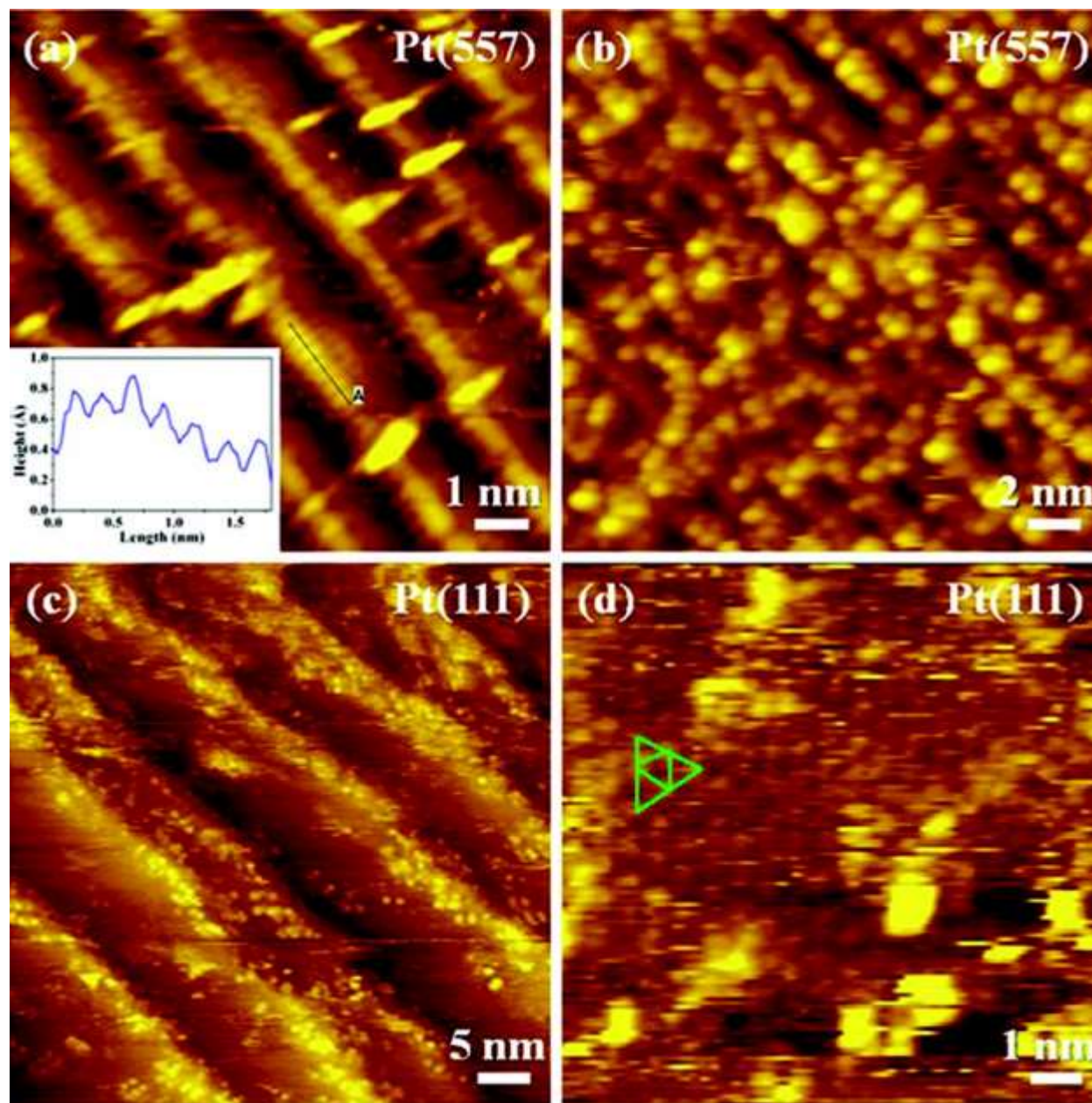


Figure 41: HPSTM images of the (a and b) Pt(557) surface and (c and d) Pt(111) surface in the presence of 1 Torr O_2 at room temperature. (a) and (c) are imaged ~ 0.5 hours, (b) and (d) are imaged ~ 2 hours after O_2 was introduced into the measurement chamber. Oxidation causes cluster formation on Pt(557) (b), whereas only a chemisorbed oxygen adlayer forms on Pt(111) with (2×2) periodicity (d). Adapted with permission from Ref.¹⁵². Copyright (2012) American Chemical Society.

H_2 oxidation on Pt(557): A prototypical reaction on Pt is hydrogen oxidation. As shown above, the Pt(557) surface breaks up into clusters in the presence of 1 Torr O_2 at room temperature due to a two-dimensional oxide formation on the surface. In comparison, hydrogen gas at 0.1 Torr pressure does not

result in changes in the morphology of the Pt(557) surface.¹⁵³ Figure 42 shows a series of images acquired in the presence of both gases, starting from ~1 Torr O₂ in Figure 42a, and progressively adding H₂, up 0.043 Torr in Figure 42d. It appears that the initial morphology of the Pt(557) surface is fully recovered at 1:22 H₂:O₂ partial pressure ratio, indicating the surface is metallic.¹⁵³ This is supported by APXPS experiments obtained under similar partial pressure ratios.¹⁵³ The APXPS experiments also suggest the surface to be covered with adsorbed species of hydroxide and molecular water when both gases are present.¹⁵³

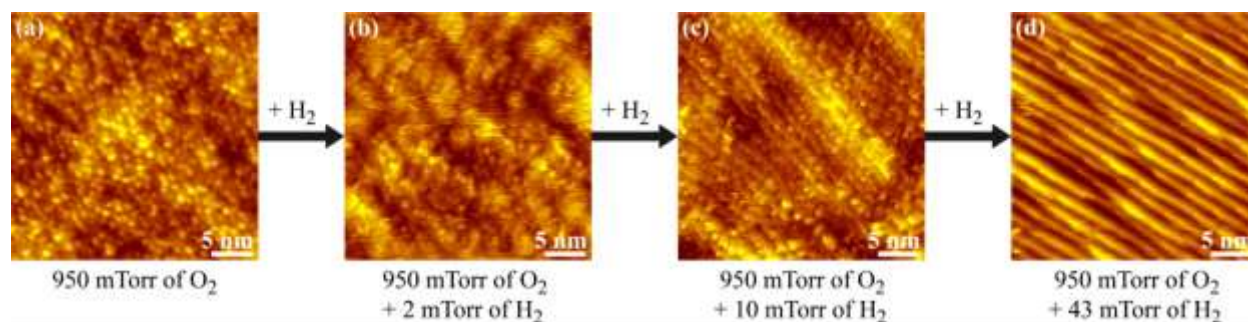


Figure 42: Evolution of the surface structure of oxidized Pt(557) surface in the presence of O₂ and H₂ gas mixture, with increasing H₂ partial pressure. A surface structure similar to the surface structure of a clean Pt(557) surface is obtained in the last stage. All images are acquired at room temperature. Adapted with permission from Ref.¹⁵³. Copyright (2013) American Chemical Society.

CO on Ni(557): It is a common practice in Ambient Pressure Surface Science experiments to use a hot-trap in the CO gas lines. This hot-trap is usually made of Cu beads heated to 240 °C in order to decompose the Ni carbonyls formed inside stainless steel pipes and gas cylinders. Interaction of CO with the Ni(110) surface was studied with surface x-ray diffraction and following important conclusions were drawn: At room temperature, CO forms a (2×1) structure with two tilted CO molecules inside the unit cell.¹⁵⁴ The same structure was observed both at low pressure and high pressure (2.3 bar) experiments. However, at ~130 °C, CO desorbs from the surface at low pressures, but at high pressures it also removes Ni atoms attached to it due to carbonyl formation.¹⁵³ As a result, (111) microfacets start forming on the Ni(110) surface.¹⁵⁴ HPSTM experiments on Ni were conducted on its (557) surface. Figure 43 illustrates the morphological changes on a stepped Ni surface at room temperature in the presence of CO gas.¹⁵⁵ It is clear that the Ni(557) surface undergoes more significant structural changes in the presence of CO than Pt(557) does. As we will mention later, Ni(111) does not break up into clusters like Ni(557). This is comparable to the earlier discussion on Pt(111) and Pt(557);¹⁴⁰ surfaces with high density of steps are more prone to cluster formation in the presence of gases. The heavy clustering observed on Ni(557) could even be associated with subcarbonyl or even a carbonyl formation.

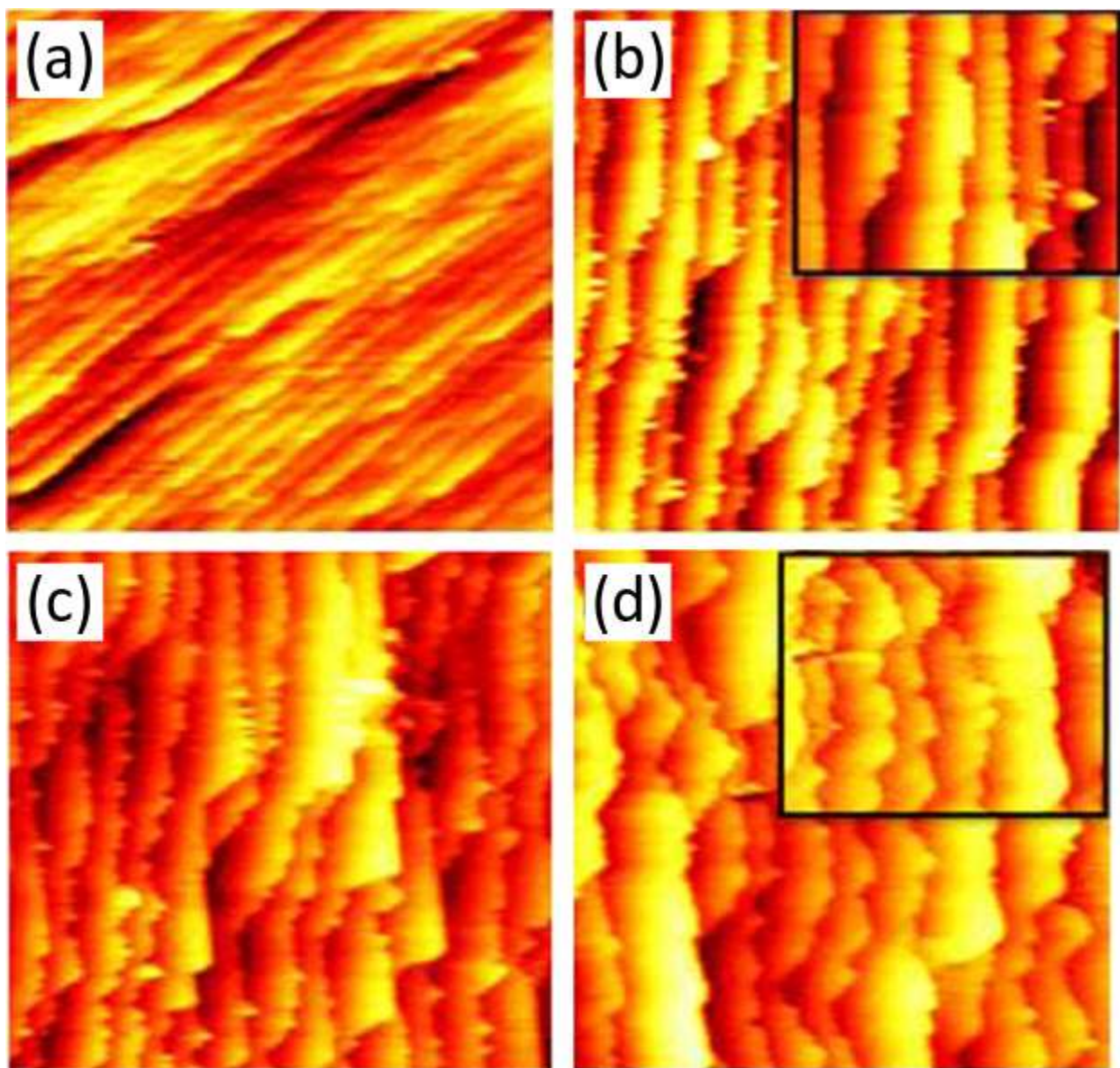


Figure 43: HPSTM images of the Ni(557) surface (a) under UHV at 3×10^{-10} Torr, (b) under UHV at 10^{-8} Torr, (c) under 10^{-6} Torr CO, and (d) in the presence of 1 Torr CO. All images have a size of 24×24 nm². Adapted with permission from Ref.¹⁵⁵. Copyright (2013) American Chemical Society.

9. Fischer-Tropsch Synthesis on Co Surfaces

Modern gas-to-liquid technology aims to produce liquid fuels and lubricants from synthesis gas (a mixture of CO, and H₂, and sometimes CO₂).¹⁵⁶⁻¹⁵⁹ The Fischer–Tropsch synthesis (FTS) consists of a series of reactions that catalytically convert synthesis gas to long-chain hydrocarbons.¹⁶⁰⁻¹⁶¹ The topic has attracted a great deal of interest in the applied catalysis research over the past few decades.¹⁶²⁻¹⁶⁵ Co is among the most often used catalyst in industrial FTS. In order to achieve an optimal catalyst design, it is

crucial to understand the fundamental processes taking place on the catalyst surface during FTS. Because of all these reasons, FTS on Co surfaces were the subject of five different HPSTM studies in the recent years.

The elemental step, and possibly the rate-limiting step, in FTS is the dissociation of the adsorbed CO molecules. Two reaction pathways have been proposed and evaluated via theoretical calculations, namely the carbide mechanism and the hydrogen-assisted mechanism. The main difference between the two is whether or not hydrogen adsorbed on the catalyst surface facilitates CO dissociation.¹⁶⁶ There is no consensus in the literature so far, as both mechanisms are suggested. Two spectroscopy studies from our group, suggest that CO does not dissociate in the absence of co-adsorbed hydrogen at room temperature, and increasing the surface temperature causes desorption of the CO molecule before it dissociates.¹⁶⁷⁻¹⁶⁸ Dissociation without hydrogen occurs only by keeping CO attached to the surface while heating the sample to above ~150 °C (i.e., in the presence of CO gas to maintain a high coverage of CO).¹⁶⁷⁻¹⁶⁸ Another important question is the nature of the 'active sites', i.e., whether the low-coordinated sites or the high-coordinated sites are the most active in the production of linear hydrocarbons, and whether more low-coordinated sites form on the surface under reaction conditions. Some of these questions are addressed in the HPSTM studies that are presented in this section.

CO hydrogenation on Co(0001) – hydrogen-rich conditions: Prior to the advent of the HPSTM, ex situ STM studies were performed on the Co(0001) surface, and it was claimed that the surface roughens under CO hydrogenation reaction conditions.¹⁶⁹ This scenario, however can only be ascertained through experiments under reaction conditions. Vibrational spectroscopy, specifically IRRAS, experiments monitoring shifts in the CO stretching frequency, supported the surface roughening under reaction conditions,¹⁷⁰ but IRRAS provides only an indirect observation and it is possible to interpret a shift in the IR frequencies with various chemical and physical effects.⁷

In contrast, no HPSTM studies on CO hydrogenation showed significant clustering of the surface. We start with the first study, which was performed under hydrogen-rich methanation conditions. The Co(0001) surface, although relatively flat, is already active and product analysis shows methane at 493-523 K and at 10 mbar total pressure ($H_2:CO$ partial pressure ratio was set to 40:1). Figure 44a shows an STM image of the Co(0001) under UHV conditions, which shows a surface with many round hillocks.¹⁷¹ Co undergoes an hcp-fcc phase transformation at 695 K, therefore the preparation of Co(0001) surfaces for HPSTM studies had to be performed below this temperature. It was found that the hillocks are due to implanted argon inside the crystal that could not be fully removed at the lower temperatures. The inset in Figure 44a shows the (1×1) lattice structure, confirming that the hillocks are indeed due to subsurface species rather than contaminations on the surface. Before examining the surface in the presence of the synthesis gas mixture, we will first examine the case with only one reactant gas species present. In the

presence of 0.25 mbar of pure CO at 493 K, the surface is covered with a $(\sqrt{7}\times\sqrt{7})R19.1^\circ$ -CO adlayer structure (Figure 44b). This is the same structure observed at low dose experiments at room temperature.¹⁷²⁻¹⁷³ In the presence of 10 mbar H₂ at 493 K, the surface structure remains unchanged compared to UHV (Figure 44c). When both gases are present, in hydrogen-rich conditions at 493 K, the surface morphology is still similar to that in UHV (Figure 44d). Higher magnification images in Figures 44e and 44f, however, show some additional features with roughly 1 Å apparent height, which might be due to chain hydrocarbons, though the main product of the reaction under such condition is methane.¹⁷¹ The step edges remain frizzled (Figure 44g) due to metals atoms detaching and reattaching to the steps thermally or induced by the STM tip. In conclusion, apart from these small features the surface does not appear to undergo significant structural changes under hydrogen-rich reaction conditions used in Ref.¹⁷¹

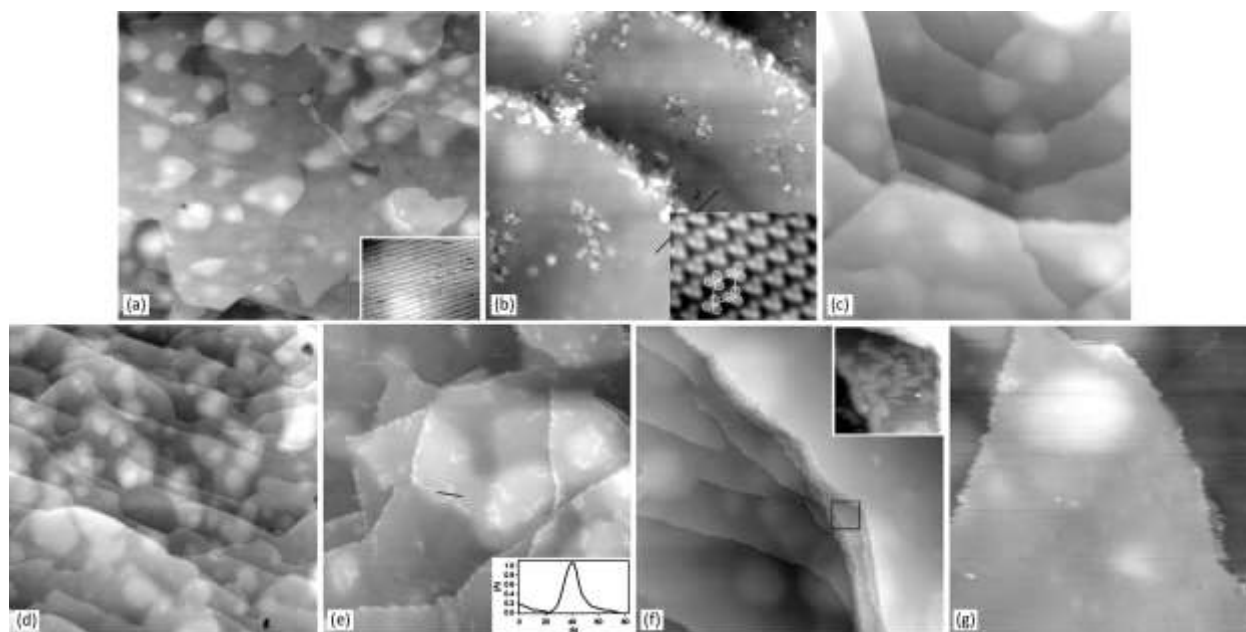


Figure 44: HPSTM images of the Co(0001) surface at 493 K (a) in UHV, (b) in the presence of 0.25 mbar CO with the $(\sqrt{7}\times\sqrt{7})R19.1^\circ$ overlayer structure shown in the inset, (c) in the presence of 10 mbar H₂, and (d-g) in the presence of 10 mbar synthesis gas mixture with 40:1 H₂:CO partial pressure ratio. Neither in the presence of H₂ nor in synthesis gas mixture, the surface undergoes significant morphological changes. Some additional features apparent in (e) and in (f), which have been attributed to linear hydrocarbons on the surface. Image sizes are $240 \times 240 \text{ nm}^2$ in (a), $45 \times 45 \text{ nm}^2$ in (b), $95 \times 95 \text{ nm}^2$ in (c), $230 \times 230 \text{ nm}^2$ in (d), $100 \times 100 \text{ nm}^2$ in (e), $90 \times 90 \text{ nm}^2$ in (f), and $50 \times 50 \text{ nm}^2$ in (g). Adapted with permission from Ref.¹⁷¹. Copyright (2014) Elsevier.

CO hydrogenation on Co(0001) – sulfur poisoning: A practical question in HPSTM experiments, and in Ambient Pressure Surface Science experiments in general, is the effect of impurities. Sulfur impurity

has severe effects on catalyst activity; for instance, adding only 13-87 ppb H₂S to synthesis gas was found to reduce the methanation rate by more than four orders of magnitude.¹⁷⁴ As noted in Ref.¹⁷⁵, even 99.999% purity hydrogen gas bottles contain some amount of sulfur impurities (as shown in the supplier datasheets), which raises the question of the effect of sulfur contamination in with such hydrogen. Indeed, it was shown that the Co(0001) surface also suffers a sulfur-induced deactivation and XPS measurements after hydrogen-rich reaction conditions show prominent peaks in the S 1s region of the XPS spectrum. It is important to note that ultra-high purity hydrogen (99.9999%) is normally used in Surface Science experiments and it does not contain sulfur impurities in traceable amounts (e.g., the images in Figure 44 were obtained using such sulfur-free hydrogen).

The HPSTM images acquired under hydrogen-rich reaction conditions with the sulfur-containing hydrogen showed striking differences with respect to the images obtained with sulfur-free hydrogen (Figure 45). The first noticeable difference is the roughness of the surface in the low-magnification image in Figure 45a: The surface still consists of atomic terraces separated by the monatomic steps, but with a high step density.¹⁷⁵ The close-up image in Figure 45b clearly shows partially ordered structures on the surface, which were not present when sulfur-free hydrogen was used. One of the ordered structures are the stripes oriented along $\langle 2\bar{1}\bar{1}0 \rangle$ directions where a local (2×2) structure can be identified. Another one is a hexagonal pattern rotated by approximately 20° with respect to the $\langle 2\bar{1}\bar{1}0 \rangle$ directions, which is probably a $(\sqrt{19}\times\sqrt{19})R23.4^\circ$ structure. A (2×2) structure is known to form by adsorbed sulfur atoms on Co(0001),¹⁷⁶⁻¹⁷⁸ whereas the $(\sqrt{19}\times\sqrt{19})R23.4^\circ$ structure had not been reported before.

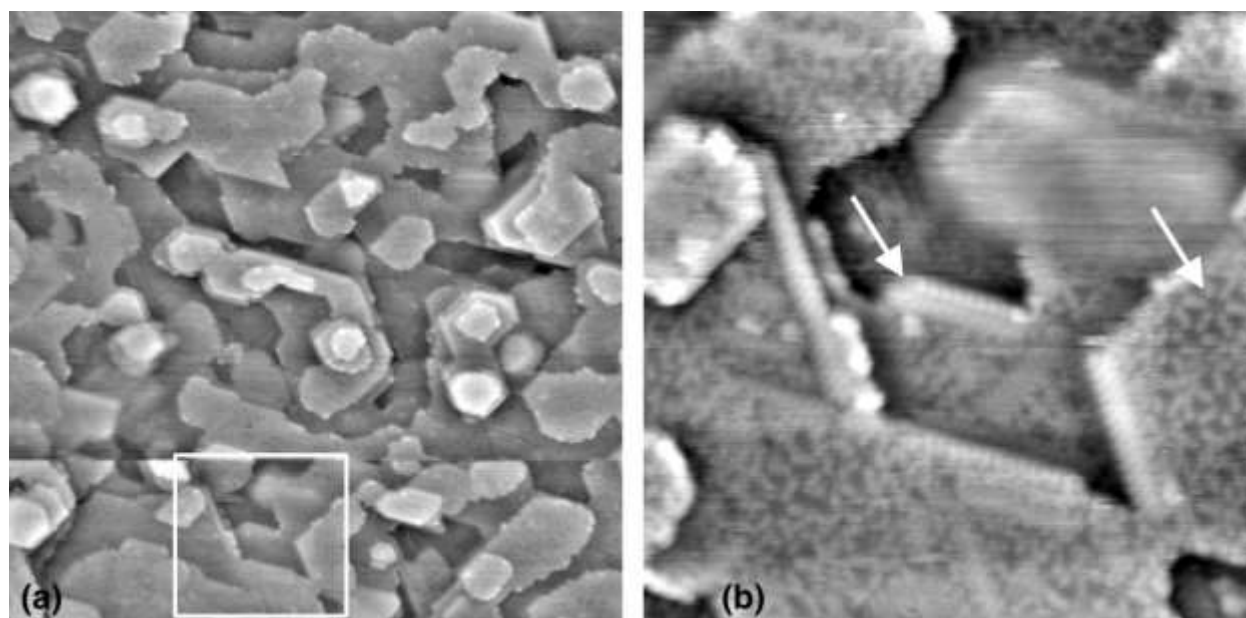


Figure 45: HPSTM images of the Co(0001) surface at 493 K in the presence of 14.5 mbar of synthesis gas mixture with 30:1 H₂:CO partial pressure ratio. Unlike in the study of Figure 44, the hydrogen gas

included traceable amounts of sulfur impurities. Image sizes are $90 \times 90 \text{ nm}^2$ in (a), and $25 \times 25 \text{ nm}^2$ in (b). Arrows mark one of the stripes with a (2×2) structure and an area with a $(\sqrt{19} \times \sqrt{19})R23.4^\circ$ structure. Adapted with permission from Ref.¹⁷⁵. Copyright (2015) Elsevier.

Several test experiments were performed in Ref.¹⁷⁵ to clarify the observations: 1- Separate H_2S dosing experiments in UHV resulted in the $(\sqrt{19} \times \sqrt{19})R23.4^\circ$ structure, with the (2×2) structure being absent. The authors believe that they were not able to prevent coadsorption of CO from the background, hence no (2×2) structure. 2- Sulfur typically adsorbs very strongly on metal surfaces, which causes the poisoning/deactivation of the surface. The Co(0001) surface was imaged after evacuating the chamber from the hydrogen-rich synthesis gas mixture, but the (2×2) and the $(\sqrt{19} \times \sqrt{19})R23.4^\circ$ patterns remained intact on the surface. This observation supports the idea that these structures originate from a strongly adsorbed sulfur. 3- When only the sulfur-containing hydrogen is present (instead of a mixture of hydrogen with CO), no ordered structures are apparent on the surface. Only after addition of CO to the gas mixture, these sulfur-induced structures stabilize on the surface. This final observation is a bit counterintuitive, but the authors believe that the $(\sqrt{19} \times \sqrt{19})R23.4^\circ$ structure on the surface originates from a mixed S/C layer instead of pure S. This is why this structure was never reported before in the literature. In other words, contrary to common assumption, the authors believe that both S and C (the latter as a product of CO hydrogenation) should be present on the surface to poison the surface.

In summary, it is evident that even small traces of impurities can play a major role in Surface Science studies at ambient pressures. Other than Ref.¹⁷⁵ there is no other HPSTM study that deals with the effects of impurities in the surface structures and chemistry. More studies focused on the role of impurities are clearly necessary in the Ambient Pressure Surface Science field.

CO on Co(0001): Here, we return to the topic of carbide-mechanism vs. hydrogen-assisted mechanism of CO dissociation. HPSTM studies were performed in the presence of pure CO in order to investigate whether the Co(0001) surface is active by direct carbide formation mechanism.¹⁷⁹ Figure 46a shows the image of the surface at 493 K, ~2 h after 0.22 mbar CO was introduced into the chamber. The most prominent structure on the surface is the hexagonal pattern from a $(\sqrt{7} \times \sqrt{7})R19.1^\circ$ adlayer structure of adsorbed CO molecules, which is also the structure observed in adsorption experiments at low temperature in UHV.¹⁸⁰⁻¹⁸¹ There is also an additional triangular structure on the surface with the edges aligned with the closed-packed directions of Co(0001). These are local stacking faults in the topmost layer, stabilized by atomic C adsorbing at the fault lines as illustrated by the model shown in inset in Figure 46b. The reconstruction of the terraces in the form of fault lines requires ejection of Co atoms from the terrace sites, which attach to the steps.¹⁷⁹ Figure 46c shows the image of the surface at 493 K, ~5.5 h after 0.22 mbar CO was introduced into the chamber. The surface evolves further, and the triangular

(N×N) superstructures now cover most of the surface. The model of the (5×5) superstructures is shown in Figure 46d. Only a small region of the surface is now covered with CO (area I in Figure 46c with a $(\sqrt{7}\times\sqrt{7})R19.1^\circ$ structure). Finally, there are also regions on the surface which are covered with Co_2C , the so-called 'clock reconstruction' (area II in Figure 46c).¹⁸² All of these results suggest that at 493 K, the Co(0001) surface is indeed active enough to dissociate the adsorbed CO molecules. However, the dissociation rate is low compared to that of methane formation discussed previously in the hydrogen-rich conditions,¹⁷⁹ suggesting that hydrogen-assisted pathway might be the desired pathway during FTS.

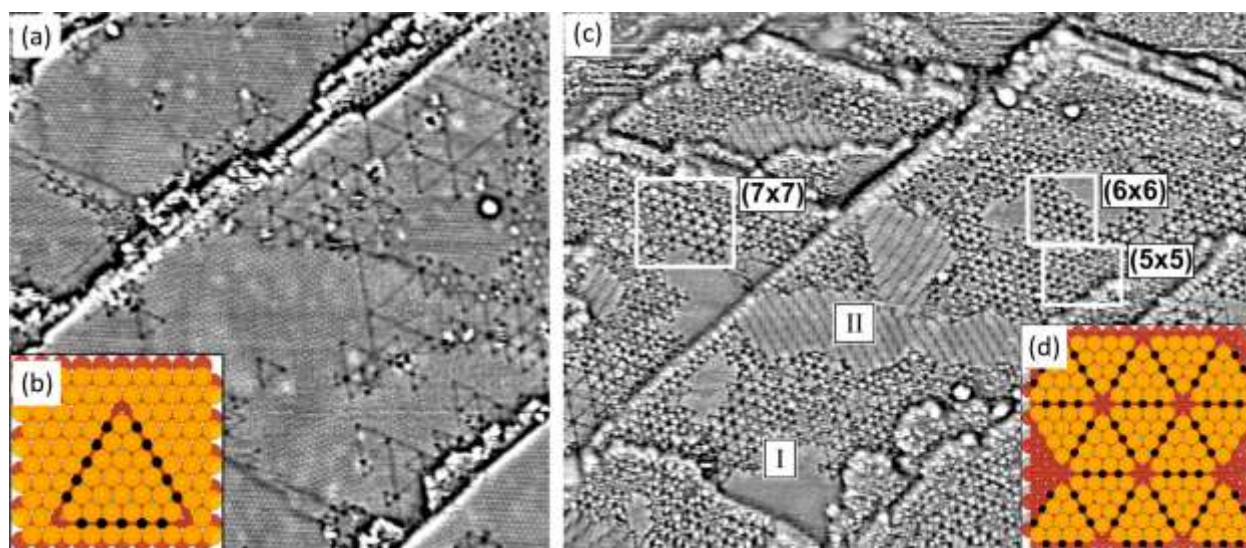


Figure 46: HPSTM images of the Co(0001) surface at 493 K in the presence of 0.22 mbar CO. (a) Image acquired ~2 h after the introduction of CO, (c) image acquired after ~5.5 h. (b) and (d) models of the local stacking faults caused by the atomic carbon and the superstructures caused by it. Most of the surface in (a) and region I in (c) have the $(\sqrt{7}\times\sqrt{7})R19.1^\circ$ structure. Area II in (c) has a structure called 'clock reconstruction', which is a surface carbide structure. Image sizes are $60\times 60\text{ nm}^2$ in (a), and $90\times 70\text{ nm}^2$ in (c). Adapted with permission from Ref.¹⁷⁹. Copyright (2015) American Chemical Society.

CO hydrogenation on Co(0001) at industrial conditions: Industrial FTS conditions typically involve pressures of up to tens of bars, 1:2 mixture of CO to H_2 , and temperatures from 200 to 350 °C.¹⁶¹ Ref.¹⁸³ marks a milestone, as these extreme conditions for Surface Science studies were reached for the first time in HPSTM studies. Figure 47a shows an HPSTM image of the Co(0001) surface at 494 K surface temperature in the presence of 4 bar of gas with CO:H₂:Ar partial pressure ratios of 1:2:2. The image was acquired 40 min after the introduction of the reactants, and shows a surface covered with a striped pattern with ~0.11 nm height, aligned with the three equivalent $\langle 10\bar{1}0 \rangle$ directions of the surface.¹⁸³ Figure 47b shows a close-up look at the stripes. FFT analysis in Figure 47b, shows an average separation of ~1.8 nm

between the stripes. The stripes have an internal structure composed of lines perpendicular to the stripes with a spacing of ~ 0.46 nm, as highlighted with blue lines in Figure 47b. These stripes formed only in the presence of both reactants but not with pure H_2 nor pure CO, and only when sufficiently high temperatures were reached.¹⁸³ Moreover, the periodicity of such structures does not correspond to cobalt carbide,¹⁸⁴ or to cobalt oxides.¹⁸⁵ The island height and the striped pattern are strongly reminiscent of patterns formed by alkane molecules on a variety of clean single-crystal metallic substrates self-assembling into regular, striped patterns.¹⁸⁶⁻¹⁸⁹ In light of all these, it was concluded in Ref.¹⁸³ that the overlayer is a two-dimensional condensate of linear hydrocarbon molecules produced during FTS lying flat on the terraces. This strong conclusion demonstrates that the HPSTM technique is not only capable of atomically imaging a single-crystal surface under industrial conditions, but also able to determine the products of this reaction. Using this model, the periodicity of the stripes can be used to estimate the average product to consist of 14 C atoms. Figure 47c shows the distribution obtained this way.

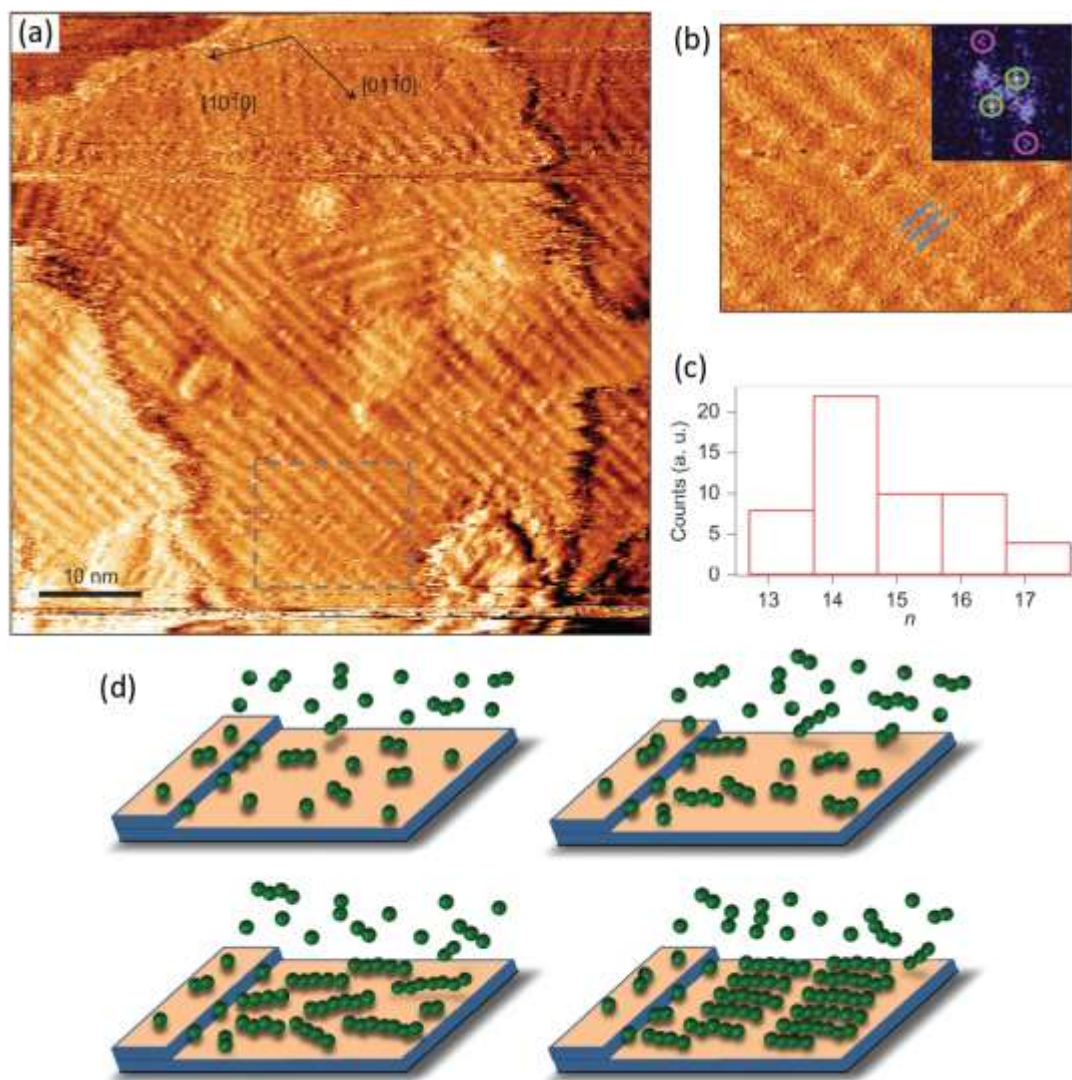


Figure 47: (a-b) Overview and the close-up HPSTM images of the Co(0001) surface during Fischer-Tropsch Synthesis (FTS) reaction. At a total pressure of 4 bar, with CO:H₂:Ar partial pressure ratios of 1:2:2, and surface temperature of 494 K. Inset in (b) FFT of the image, showing ~1.8 nm separation between the stripes and ~0.46 nm between the features inside the stripes (e.g., the blue lines in (b)), which assigned to a linear hydrocarbon on the surface. (c) distribution of the length of the hydrocarbon molecules, estimated using the separation between the stripes. (d) schematic illustration showing step edges catalyzing the growth of the linear hydrocarbons by addition of CH₂ units to the growing chain. Adapted with permission from Ref.¹⁸³. Copyright (2016) Springer Nature.

According to the Schulz–Flory–Anderson model,¹⁹⁰⁻¹⁹² the hydrocarbon chains grow via the repeated addition of CH₂ monomers to the growing chain at the active site, which results in an exponential chain length distribution, which was observed experimentally many times. In the present case, small molecules

are also produced, but they desorb swiftly to the gas phase. Longer molecules, which are produced at much lower rates, reside on the surface much longer as they have stronger interaction with the surface (since they lie flat on the surface, their interaction scales with chain length). Figure 47d is a schematic illustrating this model. The active sites where CH_2 monomer addition takes place are the step edges, and the terraces are just hosts where the long-chain can reside.¹⁸³ Terrace sites themselves are active for methanation, but this gradually slows down as the chain growth reaction proceeds since the terraces become occupied with long linear hydrocarbon molecules.¹⁸³

CO hydrogenation on a rough Co(0001): As we discussed above, the step edges are potentially the most active sites of the Co(0001) surface for long-chain hydrocarbon formation, whereas the terrace sites are only active in the production of the undesired methane as the product. A possible scenario is, however, the roughening of the flat surface by the synthesis gas mixture at ambient pressures and temperatures, which would render it highly active. Previously, we showed that this is not the case under hydrogen-rich conditions,¹⁷¹ and in this part we will show that this is also not the case when H_2 :CO partial pressure ratio is 2:1, at 950 mbar total pressure and 493 K sample temperature.¹⁹³ In fact, the contrary is true, even an initially rough surface becomes smoother under such reaction conditions.¹⁹³

Figures 48a and 48b show the as-prepared flat surface and the same surface under reaction conditions, respectively. No structural differences between these two images can be observed. Another surface was prepared by means of Ar sputtering, as shown in Figure 48c. This surface underwent structural changes and it became smoother under reaction conditions (Figures 48d and 48e). This observation indicates that the hypothesis that the origin of the activity of the Co(0001) surface is through the formation of low coordinated sites during the reaction is probably not correct. The selectivity towards the long-chain hydrocarbons is associated with the step edges present there initially, but they do not form with time. Activity studies in Ref.¹⁹³ show products with higher number of carbons to appear more on the sputtered surface (in comparison, the flat and sputtered surface a similar activity towards methane formation), however, this activity decreases with time, which can be attributed to the smoothening of the surface under reaction conditions.

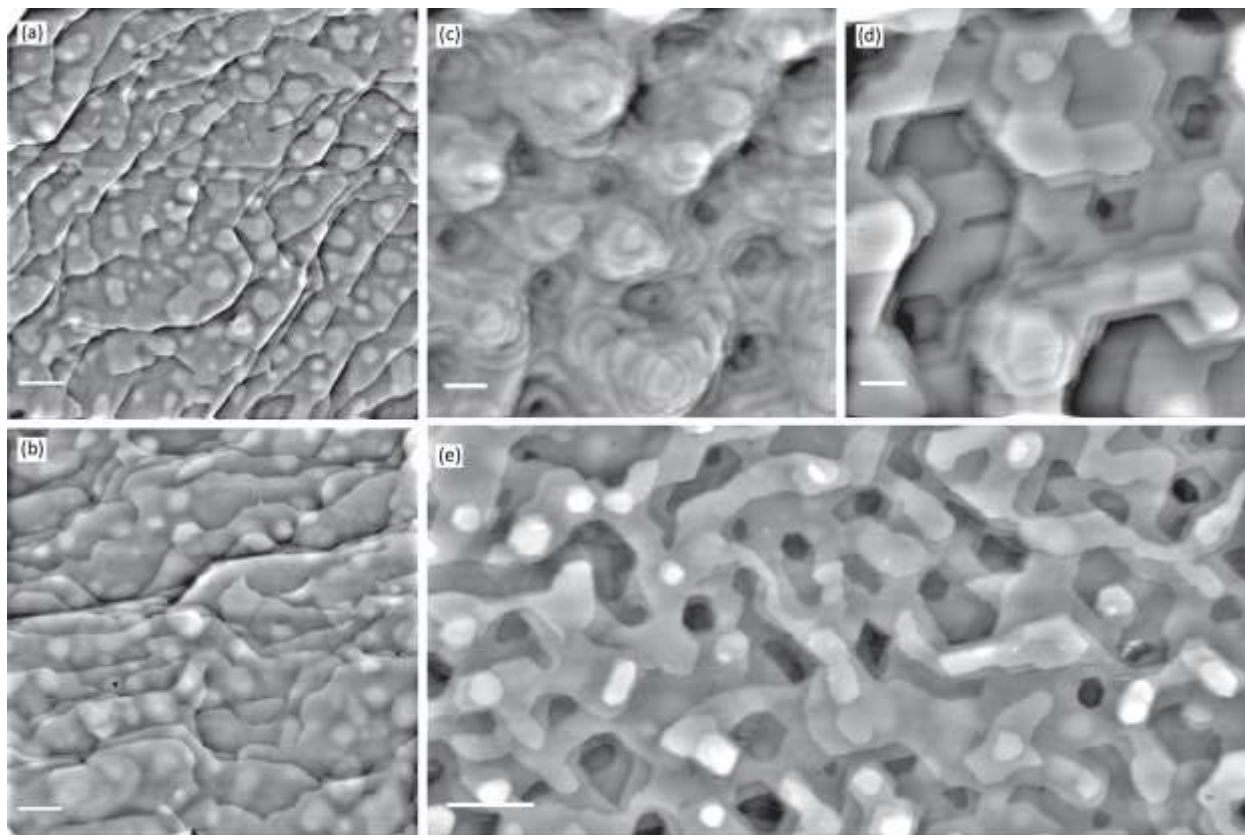


Figure 48: (a) STM image of the as-prepared Co(0001) surface and (b) when the same surface is imaged in 950 mbar total pressure with $\text{H}_2:\text{CO}$ ratio of 2:1, at 493 K, and 4.5 h after the start of the experiment. (c) shows a rough surface prepared by Ar sputtering, and (d) and (e) same surface under reaction conditions, 30 min and 5 h after the the start of the experiment, respectively. Whilst there is no change from (a) to (b), the surface becomes smoother from (c) to (e). Scale bar is 20 nm in each image. Adapted with permission from Ref.¹⁹³. Copyright (2019) Springer Nature.

10. Metal/Oxide Surfaces

Although vast majority of Surface Science studies are performed on the surfaces of pure transition metals, more than 90% of industrial-type catalysts are transition metals supported on oxides. The metal/oxide interface indeed plays a very important role in catalytic processes. The oxide support is not always inert, and often interacts strongly with the metal catalyst, particularly when the metal in the oxide has several oxidation states and is easily reducible, a phenomenon called 'strong metal support interaction' (SMSI), which is still not yet fully understood. There is only one HPSTM study performed on the metal/oxide interface. In this case, a model catalyst surface was prepared by inverse geometry; that is a thin layer of oxide was grown on the metal crystal. This geometry allows preparation of flat surfaces, which is necessary for atomic level characterization with HPSTM.

CO oxidation on CoO_x/Pt: Pt is the most widely used CO oxidation catalyst, but the cost of Pt group metals has driven efforts to replace these materials with more earth-abundant alternatives. Certain transition metal oxides, e.g. CoO_x ($1 < x < 1.33$), also has some CO oxidation activity at low temperatures,¹⁹⁴ but CoO_x catalysts suffer from deactivation under reaction conditions,^{195,196} a process attributed to water dissociation that form hydroxyls and react with CO to form bicarbonates.¹⁹⁷⁻²⁰¹ A recent work indicates that Pt nanoparticles supported on CoO_x exhibit an unusually high CO oxidation activity relative to pure Pt, and much greater than that of Pt nanoparticles supported on other metal oxides.²⁰² It is, therefore, important to understand the underlying mechanisms behind the activity of Pt/CoO_x catalysts with Surface Science techniques applicable at ambient pressures, including HPSTM.

In. Ref.²⁰³, it was shown with APXPS that the CoO_x films on the Pt(111) surface can be reduced by CO very effectively even at room temperature if it contains oxygen vacancies. An intact CoO_x film on Pt(111) is not reduced by reaction with CO, instead CO adsorbs on the oxide forming carbonates, which do not decompose until the temperature is increased to or above 260° C. A particularly interesting case is when only a submonolayer of CoO_x covers the surface, as APXPS revealed both surface carbonate and CO adsorbed on metallic Co. Structural evolution of the submonolayer oxide films was investigated with HPSTM, and the structural changes were correlated with the changes in the surface chemistry. Figure 49 shows the surface in the presence of CO and in the presence of CO and O₂ mixture at room temperature. When only CO is present, the interior of the CoO_x islands have a hexagonal structure, because they are reduced and CO adsorbs on the metallic Co (Figure 49, images at the top). The edges of the islands are higher in height, because CoO_x is not reduced here, due to strong oxygen binding following the Sabatier principle, and CO adsorbs on the oxidic site to form a surface carbonate.²⁰³ This means, contrary to the common belief that the under-coordinated sites at the periphery of the metal-oxide are the active sites in a reaction, the interior sites of the CoO_x islands are more active in the present case. When both CO and O₂ gases are present, more edges (i.e, more surface carbonate structure), appear on the surface, and the chemical state of Co remains oxidic (Figure 49, images at the bottom). This work illustrates the power of HPSTM, as the local variations in structure could be correlated directly to the two different phases observed with spatially averaging spectroscopy techniques. Combining APXPS with HPSTM and DFT calculation it was possible to obtain chemical information at the atomic level from a very complex surface.

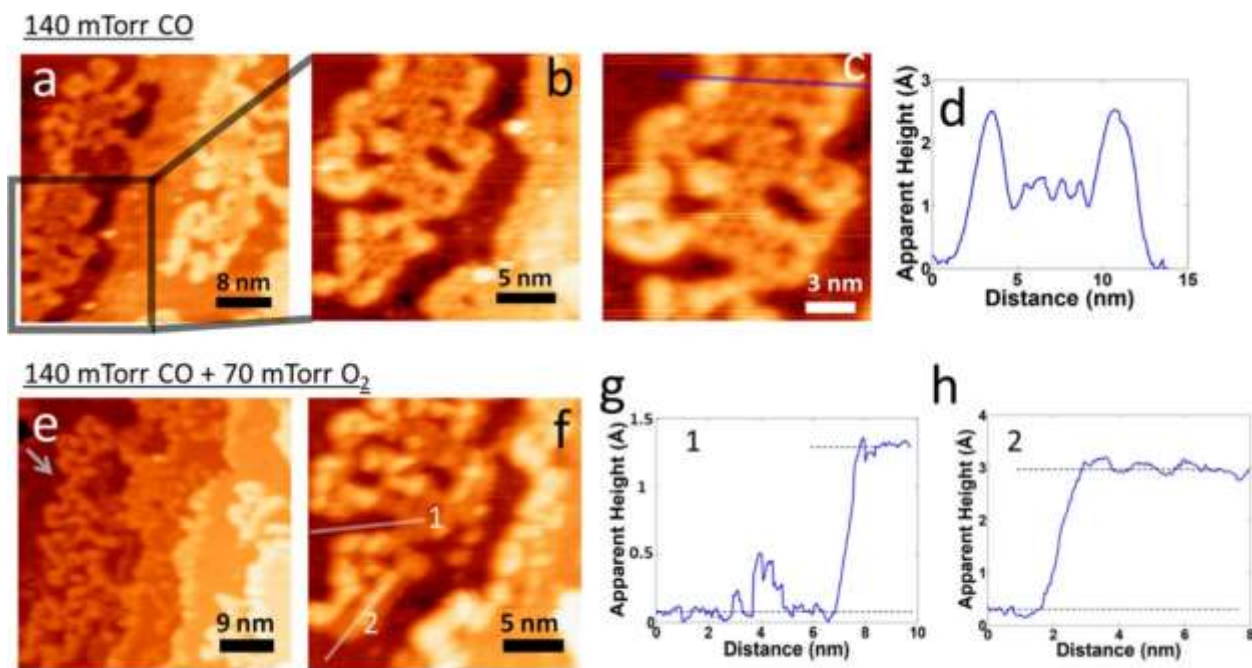


Figure 49: (a-c) HPSTM images of a submonolayer CoO_x film on Pt(111) under 140 mTorr CO. Expanded images of the film reveal a hexagonal ordered structure at the island interiors due to CO adsorbed on metallic Co, and a high contrast edge structure due to CO adsorbed on oxidic Co as a carbonate. An apparent height line profile is shown in (d) along the line in (c). Images acquired under CO + O_2 mixtures are shown in (e), and (f) for the same islands in (a)-(c). The density of oxidized step edges increases when O_2 is added to the gas mixture. Apparent height line profiles shown in (g) and (h) are along lines 1 and 2 in (f). Adapted with permission from Ref.²⁰³. Copyright (2020) American Chemical Society.

11. Bimetallic Surfaces

There is an increasing interest in bimetallic catalysts, because the flexibility in adjusting the nature of the metal components and their fractional amount. This high tunability enables the design of promising new catalysts with higher activity and selectivity compared to elemental metal catalysts.²⁰⁴⁻²⁰⁵ Some of these bimetals are called 'surface alloys', particularly for bulk immiscible metals where an alloy can still be formed on the surface. Recipes for preparing bimetallic surfaces are available in the literature thanks to decades of Surface Science studies. The main goal in bimetallic catalysis is to benefit from the desired traits of each constituent metal. Few HPSTM studies on surface alloys and on bimetallic surfaces were performed in recent years, because a thorough understanding of the single component metal systems had to first precede them. In this section we will review HPSTM studies of bulk alloys, surface alloys, and metals supported on other metals.

CO on Au-Ni(111): The earliest HPSTM study of a surface alloy was the CO adsorption and clustering of the Au-Ni(111) surface at room temperature.²⁰⁶⁻²⁰⁷ Figure 50a shows an atomically resolved STM image of the Au-Ni(111) surface alloy surface, where the Au atoms appear as depressions in the STM contrast. Such a surface alloy can be prepared by depositing submonolayers of Au on Ni(111) via evaporation, and then annealing the sample at 800 K.²⁰⁶ Under CO gas pressures between 13 and 1000 mbar clusters were formed on the surface. Time-lapse HPSTM images acquired at 13 mbar show the appearance of clusters at the step edges (Figure 50b-d), as Ni-carbonyls form at the step edges which desorb to the gas phase and leaving Au clusters behind. This process starts after an incubation time, which is due to the initial Au deposits preferentially decorating the step edges. It is important to mention that the pure Ni(111) surface does not form such clusters. The presence of Au atoms inside the Ni matrix facilitates Ni-carbonyl formation as more CO molecules can adsorb on a single Ni atom at the step edge while the neighboring Au atoms remain empty.²⁰⁶ The HPSTM observations were also supported by DFT and by Monte Carlo simulations.^{206,207} From a more practical point, these results suggest that the Ni-Au surface alloy is not stable in the presence of CO, which makes it not very useful as an alloy catalyst.

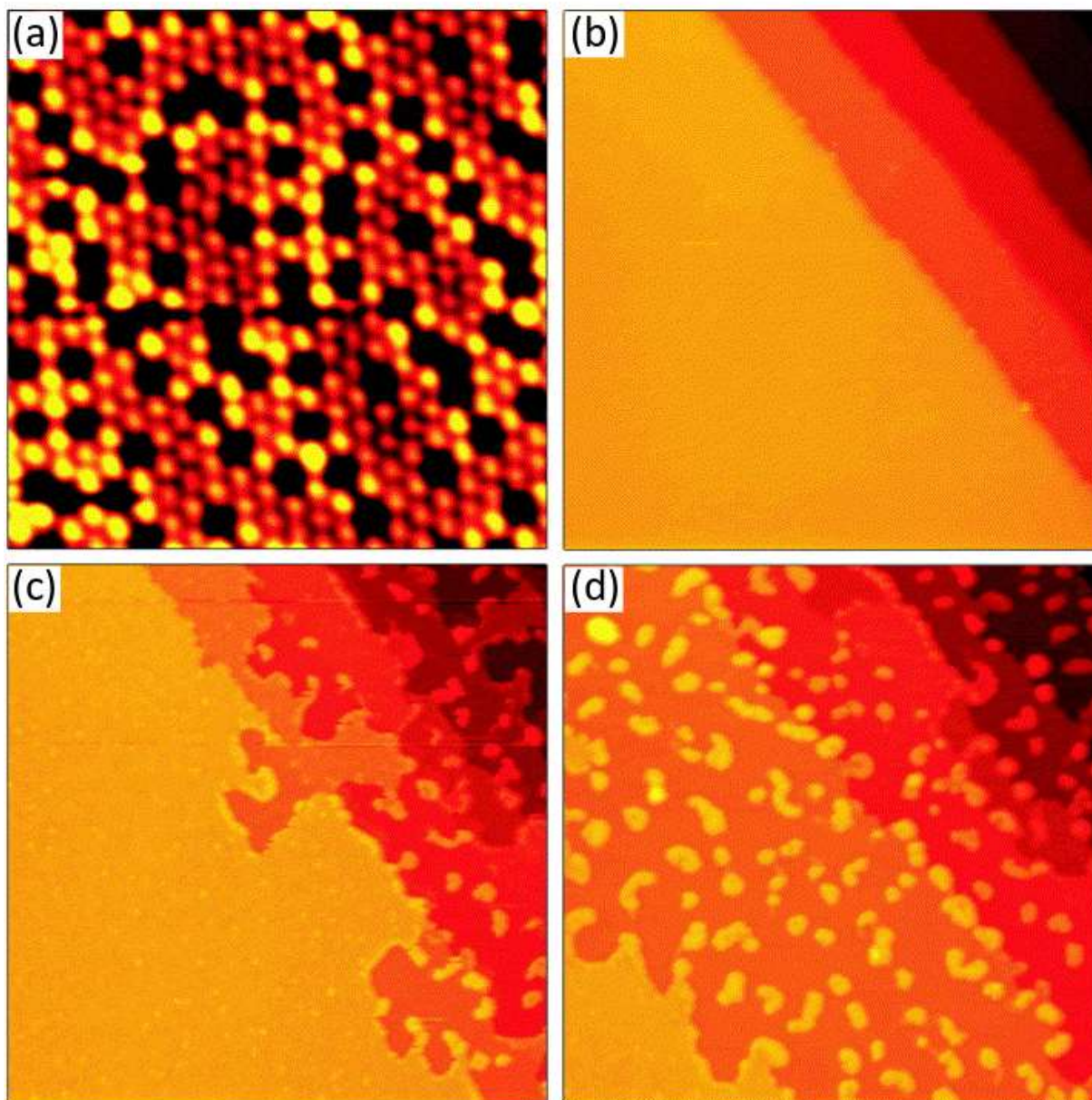


Figure 50: (a) Atomically resolved STM images of the Au-Ni(111) surface alloy, and (b-d) $100 \times 100 \text{ nm}^2$ HPSTM images in the presence of CO gas at 13 mbar pressure. All images were acquired at room temperature. (b) Image acquired immediately after addition of CO, (c) and (d) images acquired respectively 50 and 100 minutes after CO addition. The formation of Au islands is assumed to be the result of Ni-carbonyl formation and desorption to the gas phase. Adapted with permission from Ref.²⁰⁷. Copyright (2006) Elsevier.

CO on Co-Cu(110) surface: Co-Cu is another example of a surface alloy as Cu and Co are immiscible in the bulk but they can mix on the surface. Whilst pure Co is the industrially used catalyst for

the CO hydrogenation reaction for production of alkenes and alkanes,¹⁶² inclusion of Cu showed some increase in the selectivity towards valuable oxygenated products.^{208,209} More recently, bimetallic Co-Cu systems in the form of single-crystals or core-shell nanoparticles have been studied, and the effect of reactant gases in modifying their structure has been demonstrated to a certain extent.²¹⁰⁻²¹² Because of high interest in applied catalysis and in traditional Surface Science studies, ambient pressure Surface Science studies were performed using a combination of HPSTM, APXPS, IRRAS, and DFT, and the structure of a model Co-Cu surface alloy catalyst was determined at ambient CO pressures at room temperature.²¹³ Figure 51a shows an STM image of a Co-Cu(110) surface prepared according to Ref.²¹⁴. In this structure, some of the surface Cu atoms of the (2×1)-restructured 'added Cu-O rows' were replaced by the Co atoms, and the displaced Cu atoms formed islands on the surface. As Co has a higher electronic density of states close to the Fermi level, Co atoms appear brighter than the Cu atoms under STM, which allows their identification in the images. Figure 51b shows the magnified derivative image with the variations of tunneling contrast in the image reflecting this difference.

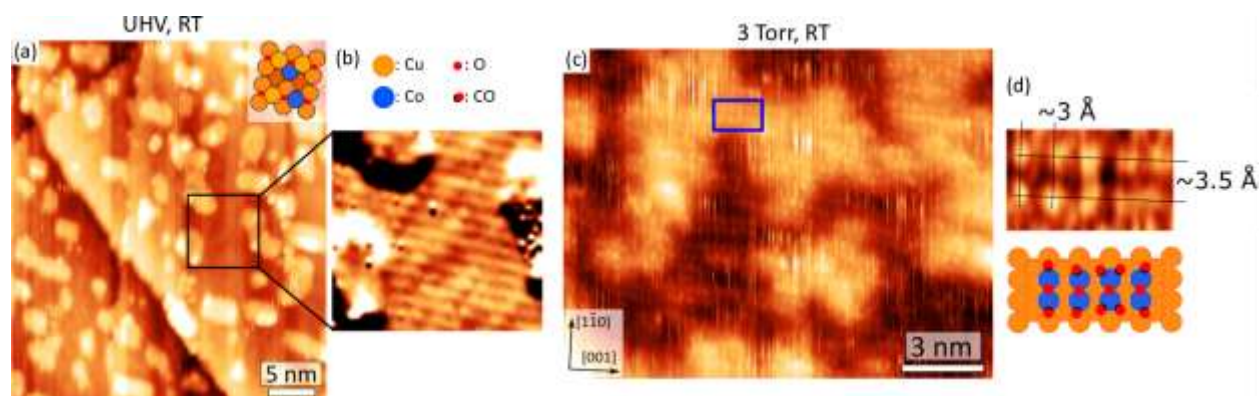


Figure 51: (a) STM image of the CuCo surface (a) prior to CO dosing in UHV, and (c) in the presence of 3 Torr CO at RT. (b, d) Expanded areas and suggested ball-models. Before dosing CO, the surface is composed of a CuCo alloy, which de-alloys in the presence of CO. In (d), the maxima are assigned to CO molecules bound to top Co sites forming dimers in short rows along the [001] direction. The expanded image in (b) is shown in derivative mode to enhance the contrast inside the linear structures which consist of both Co and Cu atoms, with Co appearing higher due to higher electron density near the Fermi level. Adapted with permission from Ref.²¹³. Copyright 2018 American Chemical Society.

Figure 51c shows an atomically resolved image of the same surface alloy in the presence of 3 Torr CO. Here the clusters appear as dimer rows in the form of pairs of bright spots along the $[1\bar{1}0]$ direction separated by 3.5 Å, substantially larger than the Cu atomic lattice spacing of 2.55 Å. This can be explained by assigning the maxima in the STM contrast to the CO molecules that are adsorbed on the top

Co-sites and tilted away from each other due to steric repulsion.²¹³ On the [001] direction the periodicity is 3 Å, which is less than the atomic periodicity 3.61 Å in that direction. This peculiar adsorption geometry can be explained by the formation of locally dense CO structures with more than one molecule per Co atom, akin to Co-carbonyls. From IRRAS spectra, it was evaluated that CO adsorbs both on top and on bridge Co sites. So the observed STM contrast originates from the CO adsorbed on the top sites, but the adsorption geometry on each dimer has combinations of 3 CO (2 top sites, 1 bridge site) and 5 CO (4 top sites, 1 bridge site) molecules.²¹³ Figure 51d shows the ball-model of a possible Cu dimer row fully covered with CO. The DFT calculations support this model by showing that isolated 2-Co atom clusters can accommodate 5 CO molecules and such clusters are energetically favored.²¹³ Independent DFT studies in Ref.²¹⁵ also found similar results, i.e., multiple CO adsorbing on single Co site. This interesting result is in line with an old result in the literature, which also suggests that multiple CO molecules can adsorb on a single Co site.²¹⁶ The authors used Co deposits on Cu(100) as their model system in that study.²¹⁶

CO oxidation on Pt₃Ni(111): The next two examples are on bulk alloys. The first is Pt-Ni, a bimetallic catalyst with an enhanced catalytic activity for the CO oxidation reaction.²¹⁷ The alloys are available commercially in many orientations. The Pt₃Ni(111) alloy was prepared by conventional sputtering and annealing cycles, which resulted in a Pt-skin on the surface, as evidenced from the 2.8 Å separation between the neighboring atoms in the STM image shown in Figure 52a.²¹⁸ Despite the same atomic structure of the pure Pt(111) surface and the topmost Pt(111)-like layer of the Pt₃Ni(111) surface, their electronic structures are significantly different.^{219,220} This difference in the electronic structure affects the structure of the CO adlayer: Whilst a moiré pattern due to high CO coverage forms on the Pt(111) surface as discussed before,¹⁹ no such structure forms on the Pt₃Ni(111) surface (Figure 52b). Instead, the (1×1) structure of the surface was observed, with CO adsorbed sites appearing brighter under HPSTM.²¹⁸ In the presence of O₂, however, more dramatic changes occur on the surface: Ni atoms from the subsurface are pulled out to the surface forming oxidized Ni clusters (Figure 52c). When both CO and O₂ are present, with a partial pressure ratio of 1 to 5, less oxidized Ni clusters are apparent on the surface (Figure 52d). Time-lapse HPSTM images show that these clusters are mobile on the surface.²¹⁸ APXPS and mass spectroscopy analysis suggest that these clusters are substoichiometric NiO_x (x<1) particles with a CO₂ production activity higher than that of both Pt(111) and Ni(111) surfaces.²¹⁸ It is well-known that during the CO oxidation reaction, a Pt surface gets poisoned at room temperature, as CO adsorbs strongly on Pt. In the case of a NiO_x-covered Pt(111), the surface is still not active enough, as reducing NiO is energetically very costly, hence a high energy barrier. In the present case, however, CO could adsorb on the Pt sites and remove the oxygen atoms at the edges of the oxide clusters that are shared between the Ni

and Pt atoms.²¹⁸ DFT calculations suggest an energy barrier as low as 0.37 eV in this case, which is why the reaction occurs even at room temperature.

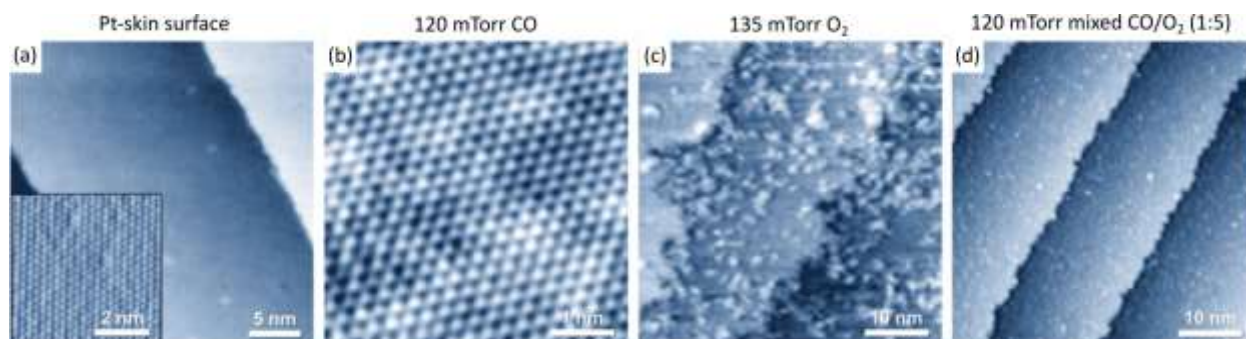


Figure 52: (a) STM image of the Pt₃Ni(111) surface in UHV, which has a layer of pure Pt atoms (called the “Pt-skin”), with the atomic periodicity of Pt(111). (b-d) HPSTM images of the Pt₃Ni(111) surface at room temperature respectively in the presence of CO, O₂, and a mixture of CO and O₂. The Pt-skin is maintained only when CO is present (b), but oxidized Ni clusters appear on the surface when O₂ alone is present (c). When both gases are present, oxidized Ni particles still appear on the surface, but in smaller size and density (d). Adapted with permission from Ref.²¹⁸. Copyright 2018 American Association for the Advancement of Science.

Water assisted oxidation of Pt₃Co: An important yet poorly studied topic in Surface Science at ambient pressures is the role of water, either as an impurity or as part of a reaction. In an attempt to establish the role of water in the oxidation of the Pt-Co alloy, combined studies using HPSTM and APXPS were performed in Ref.²²¹. The final annealing step during the preparation of Pt₃Co(111) resulted in the formation of a Pt-skin layer, as shown in the STM image in Figure 53 left-a. This surface was oxidized at 460 K surface temperature at a total gas pressure of 0.1 Torr, either in dry conditions (i.e., N₂ and O₂ mixture) or in humid conditions (i.e., H₂O and O₂ mixture). As shown in Figure 53-left b and c, two processes resulted in a different surface morphology:²²¹ Dry oxidation resulted in the formation of CoO clusters, similar to those observed on oxidized Co on Au(111).²²² Humid oxidation, on the other hand, resulted in the formation of multilayers of Co oxide. Further analysis under humid conditions was performed as a function of surface temperature. At 370 K, the surface appeared completely covered with oxidized Co clusters, due to the subsurface Co atoms segregating to the surface, similar to the previous discussion on the oxidation of the Pt₃Ni(111) crystal (Figure 53 right-a). At 440 K, however, the surface underwent a phase transition and a layer of oxidized Co covered the surface (Figure 53 right-b). The lattice mismatch between this oxide layer and the underlying surface resulted in a moiré pattern (Figure 53-right lower panel). Finally, at 480 K, multilayers of oxidized Co form on the surface and the moiré

pattern disappeared (Figure 53 right-c). APXPS spectra showed a significant amount of oxidized Co on the surface, which were strongly hydroxylated at 500 K and above.²²¹

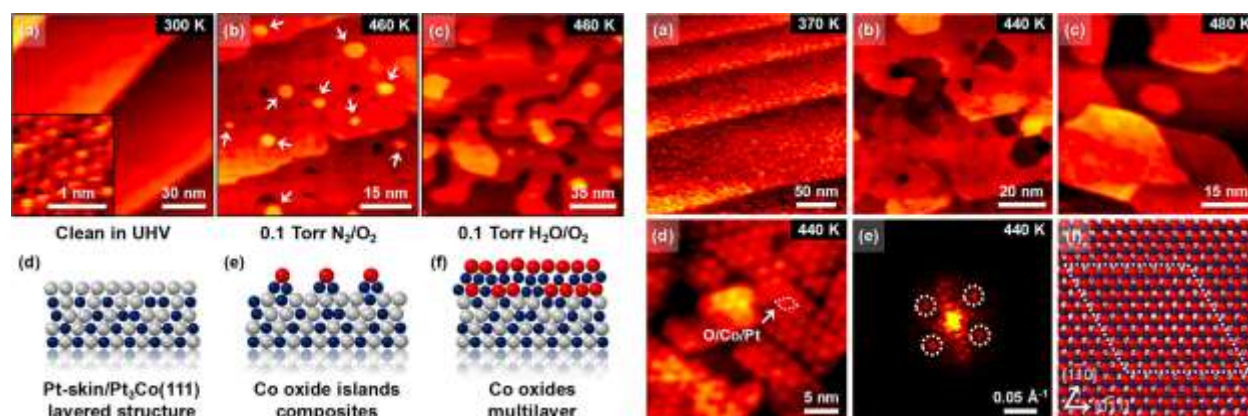


Figure 53: Left: (a) STM image of the $\text{Pt}_3\text{Co}(111)$ surface, with a Pt-skin layer and atomic periodicity similar to that of Pt(111). (b) and (c) Same surface under dry and humid oxidation conditions, respectively, showing different surface morphologies. Schematic models of the proposed structures are shown below. Right: Temperature-dependent changes in the surface structure under humid oxidizing conditions. Whilst clusters form at 370 K, a layer of O/Co/Pt forms at 440 K which results in a moiré pattern due to lattice mismatch, which becomes a multilayer and start to hydroxylate at 480 K. Adapted with permission from Ref.²²¹. Copyright 2019 American Chemical Society.

12. Conclusions and Outlook

We can separate the HPSTM studies into two main groups: Adsorption studies and reaction studies. Adsorption studies at ambient pressures on low Miller-index single-crystal surfaces revealed four different results:

- 1- The adsorbed layer has the same structure as that in the low pressure – low temperature regime. The structure of the metal remains unchanged.
- 2- A dense adsorbate layer forms on the surface, which was not previously observed. The structure of the metal remains unchanged.
- 3- The substrate surface restructures by breaking up into clusters. When this was observed on readily-reconstructed surfaces, the phenomenon was not too surprising as the initial surfaces were already prone to changes.
- 4- A more unexpected and interesting case is when unreconstructed surfaces break up into clusters, which was observed on Cu and stepped Pt surfaces.

Table 1 summarizes the adsorption studies on low Miller-index surfaces and their results that are discussed in this Review.

Table 1: Adsorption studies on Low Miller-Index surfaces in the presence of one gas species. The experiments were conducted at room temperature or slightly above. Whilst in some cases adsorption results in dense adsorbate layer structure (sometimes exactly the same as the structure observed in UHV studies) without modifying the adsorbent structure, in other cases the structure of the adsorbent evolves.

Surface	Readily reconstructed in UHV	Gas	Prominent changes in adsorbent structure once gas is added	Similar adsorbate structures in UHV and in the presence of gas	Ref.
Pt(111)	No – (1×1)	CO	No	No	19
Pt(100)	Yes	CO	Yes – reconstruction lifted	No	28
Pt(110)	Yes	CO	Yes – reconstruction lifted & mild clustering	No	37
Pt(110)	Yes	C ₂ H ₄	No	n/a	54
Cu(111)	No – (1×1)	CO	Yes – heavy clustering	No	57
Cu(100)	No – (1×1)	CO	Yes – heavy clustering	No	61
Cu(110)	No – (1×1)	CO	Yes – mild clustering	No	63
Rh(111)	No – (1×1)	CO	No	Partially	38
Rh(111)	No – (1×1)	NO	No	Partially	46
Au(111)	Yes	CO	Yes – reconstruction lifted & mild clustering	n/a – measurements after pumped	69
Au(111)	Yes	CO	Yes – reconstruction lifted & mild clustering	n/a – measurements after pumped	70
Au(110)	Yes	CO	Yes – reconstruction lifted	n/a	68
Cu(100)	No – (1×1)	CO ₂	Yes – mild clustering	n/a – low coverage	77
Cu(100)	No – (1×1)	CH ₃ OH	No	Yes – c(2×2)	79
Cu(110)	No – (1×1)	H ₂	No	Yes – (1×2)	75
Pd(111)	No – (1×1)	NO	No	Yes – (2×2)-3NO	43
Co(0001)	No – (1×1)	CO	No	Yes – ($\sqrt{7}\times\sqrt{7}$)R19.1°	179

Other adsorption studies summarized in this Review were performed on vicinal surfaces, on thin oxide films on metals, and on bimetallic surfaces. CO was found to restructure the vicinal surfaces of Pt and Ni easier than the low Miller-index surfaces. Similarly, O₂ oxidizes and thereby changes the morphology of the step edges on Pt and Ag, whereas the terraces remain metallic. On bimetallic surfaces, dealloying and surface separation phenomena were observed in the presence of gases. Both of these

phenomena were already observed numerous times with spectroscopy experiments on nanoparticle catalysts. Interestingly on bimetallic surfaces it was observed that multiple CO molecules can adsorb on Ni and Co atoms, akin to carbonyl molecules.

Some of the most common reaction studies performed in model catalysts involve CO oxidation and CO hydrogenation, the latter exclusively on Co. In the CO oxidation studies, the general trend is the bistability of the surface between a relatively smooth metallic surface and a relatively rough oxidic surface, which can explain the oscillatory behavior observed in the catalysis studies on this reaction. In the CO hydrogenation studies, the general trend is that the steps are the active sites for the formation of desired long-chain hydrocarbons, and no new steps form under reaction conditions. We can thus conclude that one of the most often asked questions related to the surface structure during FTS on Co surfaces has been addressed by Surface Science studies.

We think that the HPSTM field should in the future focus on other industrially important reactions like ethylene oxidation, methanol oxidation, methane reforming, etc.

The HPSTM field is still relatively young, with only few groups working with this technique. Within the last three decades, there are only ~50 studies with HPSTM which we covered in this Review, and only a few of them combine HPSTM with powerful ambient pressure spectroscopic techniques of APXPS, x-ray absorption spectroscopy, grazing x-ray diffraction, and of course optical techniques such as IR spectroscopy, Raman spectroscopy, etc. In the 2010-2019 decade, there was only a small increase in the number of publications compared to previous decades. The reason for this low output, in our opinion, is the difficulty of the experiments and the scarce availability of instruments. This is expected to change in the future due to the increased commercial availability of stand-alone systems (e.g., Aarhus STM and Leiden STM).

An important difficulty in HPSTM experiments is keeping the surfaces clean compared to UHV conditions. This is due to impurities in the gases used to fill the chambers, even for 99.9999% purity grade gases. For instance, in an experiment at 1 bar the partial pressure of impurities is 10^{-3} mbar, which can compete for adsorption sites in some cases. Even pure gases can displace adsorbates from walls, which can produce background impurities. These difficulties are, in some cases, surmountable, but requires stringent methodologies and refined methods of chamber cleaning and gas purification. Contamination issues in ambient pressure microscopy and spectroscopy experiments is worthy of an article of its own, therefore we will not discuss them in further detail here. We think that a good procedure to alleviate contamination issues is to periodically ignite a nitrogen plasma in the chamber to minimize the hydrocarbon contamination emanating from the chamber walls. Prior to each experiment, the measurement chamber should be baked out for 48 h over 105 °C to minimize water

impurities. It is also important to check the sample cleanliness after each experiment, i.e., after evacuation of the gases, with either XPS or AES.

Another typical issue is tip instability. In routine HPSTM operation, images of the clean surfaces are acquired in UHV prior to dosing gases with a sharp STM tip, typically made of Pt/Ir or Pt/Rh. However, once the gases are introduced into the measurement chamber, they adsorb on the tip surface and modify its chemical nature and even its physical shape so that it may become blunt. Tip-recovery procedures in ambient pressure experiments are similar to those in UHV: By electrical pulsing or by gently touching the sample surface. During imaging at ambient conditions, some gases like CO can adsorb strongly on the tip without causing tip instabilities. However most contaminated tips are unstable and produce poor quality images.

A topic we did not discuss in detail in this Review is the potential use of the STM tip to induce or catalyze reactions. Although not many recent studies are performed today, two old studies illustrate the potential utility of this procedure.^{223,224} In these studies, carbonaceous fragments were first deposited on Pt (111) by partial dehydrogenation of propylene. Then a Pt/Rh STM tip was activated by applying a voltage pulse which removed the contaminant material from the tip. The clean STM tip catalyzed the dissociation of H₂ or O₂ molecules, which respectively hydrogenated and oxygenated the carbonaceous species covering the Pt(111) surface.^{223,224} The clean metallic tip remains active until after some time it gets covered again with carbonaceous species. The procedure is more effective at smaller tip-sample distances. The tip can be deactivated by coating its apex with Au, which in return results in no hydrogenation or oxidation of the surface even after pulsing the tip.^{223,224} These results raise interesting questions. To avoid any tip-related chemistry during HPSTM experiments it may be beneficial to use inert materials, like Au-coated tips, but this comes at the expense of lower resolution due to large size of the tip apex after Au deposition. More important question is to what extent does the tip contribute to the surface structure and morphology observed on sample surfaces. Such important questions however have not received the attention that we believe they deserve.

We believe that the impact of HPSTM combined with or spectroscopy studies at high pressure (for example IRRAS, APXPS, etc.) is very high for catalysis, because there are not many options for obtaining structural information from a working catalyst. What makes such structural information very unique and important is that it can completely change the interpretation of the applied catalysis or spectroscopy studies. No other technique in our field has such an impact.

Biographies

Prof. Miquel Salmeron is a principal investigator at the Lawrence Berkeley National Laboratory and adjunct professor at UC Berkeley Materials Science and Engineering Department. Prof. Salmeron received his BA in physics from the University of Barcelona, and his PhD from the University Autònoma of Madrid, Spain, in 1975. In 1984 he moved to the Lawrence Berkeley National Laboratory as a Divisional Fellow, becoming a senior scientist in 1996. He was elected Fellow of the American Physical Society (APS) in 1996 and Fellow of the American Vacuum Society (AVS) in 2003. He received the Outstanding Scientific Accomplishment Award in Materials Chemistry in 1995, and the Outstanding Research Award in 1996 from the U.S. Department of Energy. He received the Klaus Halbach Award in 2004, and David A. Shirley Award in 2020, of the Advanced Light Source. In 2008 he received the Medard Welch Award of the AVS and the Langmuir Lectureship Award of the American Chemical Society (ACS). In 2010 he received the R&D 100 Award of R&D Magazine. In 2012 he received the Materials Research Society (MRS) Medal Award. In 2015 he received the APS Davisson-Germer Prize in Atomic or Surface Physics. Prof. Salmeron is the President of the Scientific Advisory Board of the "Institut Català de Nanotecnologia" in Barcelona, Spain.

Dr. Baran Eren is a principal investigator at the Weizmann Institute of Science. Dr. Eren received his BSc in mechanical engineering at Boğaziçi University in Istanbul, Turkey, in 2007, and his MSc in micro-nano systems at ETH in Zurich, Switzerland, in 2009. He completed his PhD with summa cum laude in experimental condensed matter physics at the University of Basel, Switzerland, in 2013. From January 2014 until joining the Weizmann Institute of Science, Israel, in September 2017, he worked as a postdoctoral fellow in the Materials Sciences Division of the Lawrence Berkeley National Laboratory in California. Dr. Eren is currently a senior scientist at the Weizmann Institute of Science, incumbent of the Alvin and Gertrude Levine career development chair, and Zuckerman STEM leadership faculty scholar.

Acknowledgements

M.S. was supported by the Office of Basic Energy Sciences of the US Department of Energy under contract no. DE-AC02-05CH11231, through the Catalysis program of the Chemical Sciences, Geosciences, and Biosciences Division. B.E. was supported by the Israel Science Foundation's (ISF) Research Grant No. 919/18. BE acknowledges the support from the Zuckerman STEM Leadership Faculty Fellowship, Ruth and Herman Albert Scholarship Program for New Scientists, and the Abramson Family Center for Young Scientists.

References:

- (1) Somorjai, G. A. *Introduction to Surface Chemistry and Catalysis*; Wiley-VCH: New York, **1999**.
- (2) Ertl, G. Reactions at Surfaces: From Atoms to Complexity. *Angew. Chem. Int. Ed.* **2008**, *47*, 3524–3535.
- (3) Langmuir, I. The Constitution and Fundamental Properties of Solids and Liquids. Part I. Solids. *J. Am. Chem. Soc.* **1916**, *38*, 1221–2295.
- (4) Binnig, G.; Rohrer, H. Scanning Tunneling Microscopy - From Birth to Adolescence. *Rev. Mod. Phys.* **1987**, *59*, 615–625.
- (5) Langmuir, I. Part II. - “Heterogeneous Reactions”. Chemical Reactions on Surfaces. *Trans. Faraday Soc.* **1922**, *17*, 607–620.
- (6) Salmeron, M.; Schlögl, R. Ambient Pressure Photoelectron Spectroscopy: A New Tool for Surface Science and Nanotechnology. *Surf. Sci. Rep.* **2008**, *63*, 169–199.
- (7) Hoffmann, F. M. Infrared Reflection-Absorption Spectroscopy of Adsorbed Molecules. *Surface Science Reports* **1983**, *3*, 107–192.
- (8) Salmeron, M. From Surfaces to Interfaces: Ambient Pressure XPS and Beyond. *Topics in Catalysis* **2018**, *61*, 2044–2051.
- (9) SPECS The Aarhus SPM Series. Online: <https://www.specs-group.com/nc/specs/products/detail/spm-aarhus-150-nap/> (accessed Oct 12, 2020).
- (10) Leiden Probe Microscopy B.V. Online: <https://leidenprobemicroscopy.com/> (accessed Oct 12, 2020).
- (11) McIntyre, B. J.; Salmeron, M.; Somorjai, G. A. A Variable Pressure/Temperature Scanning Tunneling Microscope for Surface Science and Catalysis Studies. *Rev. Sci. Instrum.* **1993**, *64*, 687–691.
- (12) Tao, F.; Tang, D.; Salmeron, M.; Somorjai, G. A. A New Scanning Tunneling Microscope Reactor Used For High-Pressure and High-Temperature Catalysis Studies. *Rev. Sci. Instrum.* **2008**, *79*, 084101.
- (13) Lægsgaard, E.; Österlund, L.; Thostrup, P.; Rasmussen, P. B.; Stensgaard, I.; Besenbacher, F. A High-Pressure Scanning Tunneling Microscope. *Rev. Sci. Instrum.* **2001**, *72*, 3537–3542.
- (14) Rasmussen, P. B.; Hendriksen, B. L. M.; Zeijlemaker, H.; Ficke, H. G.; Frenken, J. W. M. The “Reactor STM”: A Scanning Tunneling Microscope for Investigation of Catalytic Surfaces at Semi-Industrial Reaction Conditions. *Rev. Sci. Instrum.* **1998**, *69*, 3879–3884.
- (15) Herbschleb, C. T.; Van Der Tuijn, P. C.; Roobol, S. B.; Navarro, V.; Bakker, J. W.; Liu, W.; Stoltz, D.; Cañas-Ventura, M. E.; Verdoes, G.; van Spronsen, M. A.; et al. The ReactorSTM: Atomically Resolved Scanning Tunneling Microscopy under High-Pressure, High-Temperature Catalytic Reaction Conditions. *Rev. Sci. Instrum.* **2014**, *85*, 083703.

- (16) Blyholder, G. Molecular Orbital View of Chemisorbed Carbon Monoxide. *Phys. Chem.* **1964**, *68*, 2772–2777.
- (17) Gross, L.; Mohn, F.; Moll, N.; Liljeroth, P.; Meyer, G. The Chemical Structure of a Molecule Resolved by Atomic Force Microscopy. *Science* **2009**, *325*, 1110–1114.
- (18) Rupprechter, G.; Dellwig, T.; Unterhalt, H.; Freund, H.-J. High-Pressure Carbon Monoxide Adsorption on Pt(111) Revisited: A Sum Frequency Generation Study. *J. Phys. Chem. B* **2001**, *105*, 3797–3802.
- (19) Longwitz, S. R.; Schnadt, J.; Vestergaard, E. K.; Vang, R. T.; Lægsgaard, E.; Stensgaard, I.; Brune, H.; Flemming Besenbacher, F. High-coverage Structures of Carbon Monoxide Adsorbed on Pt(111) Studied by High-Pressure Scanning Tunneling Microscopy. *J. Phys. Chem. B* **2004**, *108*, 14497–14502.
- (20) Ertl, G.; Neumann, M.; Streit, K. M. Chemisorption of CO on the Pt(111) Surface. *Surf. Sci.* **1977**, *64*, 393–410.
- (21) Persson, B. N. J.; Tüshaus, M.; Bradshaw, A. M. On the Nature of Dense CO Adlayers. *J. Chem. Phys.* **1990**, *92*, 5034–4056.
- (22) Biberian, J. P.; van Hove, M. A. A New Model for CO Ordering at High Coverages on Low Index Metal Surfaces: A Correlation between LEED, HREELS and IRS: II. CO Adsorbed on fcc(111) and hcp(0001) Surfaces. *Surf. Sci.* **1984**, *138*, 361–389.
- (23) Toyoshima, R.; Yoshida, M.; Monya, Y.; Suzuki, K.; Amemiya, K.; Mase, K.; Mun, B. S.; Kondoh, H. A High-pressure-induced Dense CO Overlayer on a Pt(111) Surface: A Chemical Analysis Using In Situ Near Ambient Pressure XPS. *Phys. Chem. Chem. Phys.* **2014**, *16*, 23564–23567.
- (24) Carrasco, E.; Aumer, A.; Brown, M. A.; Dowler, R.; Palacio, I.; Song, S.; Sterrer, M. Infrared Spectra of High Coverage CO Adsorption Structures on Pt(111). *Surf. Sci.* **2010**, *604*, 1320–1325.
- (25) Fery, P.; Moritz, W.; Wolf, D. Structure Determination of the (1×2) and (1×3) Reconstructions of Pt(110) by Low-energy Electron Diffraction. *Phys. Rev. B* **1988**, *38*, 7275–7286.
- (26) Shiang, K. D.; Tsong, T. T. Energetics and Atomic Steps in the Reconstruction of the Pt(110) Plane. *Phys. Rev. B* **1995**, *51*, 5522–5525.
- (27) Thostrup, P.; Christoffersen, E.; Lorensen, H. T.; Jacobsen, K. W.; Besenbacher, F.; Nørskov, J. K. Adsorption-Induced Step Formation. *Phys. Rev. Lett.* **2001**, *126*, 102.
- (28) Thostrup, P.; Vestergaard, E. K.; An, T.; Lægsgaard, E.; Besenbacher, F. CO-induced Restructuring of Pt (110)-(1×2): Bridging the Pressure Gap with High-pressure Scanning Tunneling Microscopy. *J. Chem. Phys.* **2003**, *118*, 3724–3730.
- (29) Ahner, J.; Mocuta, D.; Ramsier, R. D.; Yates, J. T. Adsorbate–adsorbate Repulsions — The Coverage Dependence of the Adsorption Structure of CO on Cu(110) as Studied by Electron-stimulated Desorption Ion Angular Distribution. *J. Chem. Phys.* **1996**, *105*, 6553–6559.

- (30) Hagstrom, S.; Lyon, H. B.; Somorjai, G. A. Surface Structures on the Clean Platinum (100) Surface. *Phys. Rev. Lett.* **1965**, *15*, 491–494.
- (31) Ritter, E.; Behm, R. J.; Potschke, G.; Wintterlin, J. Direct Observation of a Nucleation and Growth Process on an Atomic Scale. *Surf. Sci.* **1987**, *181*, 403–411.
- (32) Thiel, P. A.; Behm, R. J.; Norton, P. R.; Ertl, G. The Interaction of CO and Pt(100). II. Energetic and Kinetic Parameters. *J. Chem. Phys.* **1983**, *78*, 7448–7458.
- (33) Borg, A.; Hilmen, A. M.; Bergene, E. STM Studies of Clean, CO- and O₂-exposed Pt(100)-hex-R0.7°. *Surf. Sci.* **1994**, *306*, 10–20.
- (34) Norton, P. R.; Davies, J. A.; Creber, D. K.; Sitter, C. W.; Jackman, T. E. The Pt(100) (5×20) ⇌ (1×1) Phase Transition: A Study by Rutherford Backscattering, Nuclear Microanalysis, LEED and Thermal Desorption Spectroscopy. *Surf. Sci.* **1981**, *108*, 205–224.
- (35) Davies, J. A.; Norton, P. R. Absolute Coverage Measurement of Adsorbed CO and D₂ on Platinum. *Nucl. Instrum. Methods* **1980**, *168*, 611–615.
- (36) Helms, C. R.; Bonzel, H. P.; Kelemen, S. The Effect of the Surface Structure of Pt on Its Electronic Properties and the Adsorption of CO, O₂, and H₂: A Comparison of Pt(100) – (5×20) and Pt(100) – (1×1). *J. Chem. Phys.* **1976**, *65*, 1773–1782.
- (37) Tao, F.; Dag, S.; Wang, L. W.; Liu, Z.; Butcher, D.R.; Salmeron, M.; Somorjai, G. A. Restructuring of hex-Pt(100) under CO Gas Environments: Formation of 2-D Nanoclusters. *Nano Lett.* **2009**, *9*, 2167–2171.
- (38) Cernota, P.; Rider, K.; Yoon, H. A.; Salmeron, M.; Somorjai, G. Dense Structures Formed by CO on Rh(111) Studied by Scanning Tunneling Microscopy. *Surf. Sci.* **2000**, *445*, 249–255.
- (39) Conrad, H.; Ertl, G.; Kuppers, J.; Latta, E. E. Interaction of NO and O₂ with Pd(111) Surfaces. I. *Surf. Sci.* **1977**, *65*, 235–244.
- (40) Chen, P. J.; Goodman, D. W. Ordered High Coverage NO Overlayers on Pd(111). *Surf. Sci.* **1993**, *297*, L93–L99.
- (41) Bertolo, M.; Jacobi, K. NO Adsorption on Pd(111) in the Temperature Range between 20 and 300 K. *Surf. Sci.* **1990**, *226*, 207–220.
- (42) Hansen, K. H.; Sljivancanin, Z.; Hammer, B.; Lægsgaard, E.; Besenbacher, F.; Stensgaard, I. An STM and DFT Study of the Ordered Structures of NO on Pd(111). *Surf. Sci.* **2002**, *496*, 1–9.
- (43) Vang, R. T.; Wang, J. G.; Knudsen, J.; Schnadt, J.; Laegsgaard, E.; Stensgaard, I.; Besenbacher, F. The Adsorption Structure of NO on Pd(111) at High Pressures Studied by STM and DFT. *J. Phys. Chem. B* **2005**, *109*, 14262–14265.

- (44) Kim, Y. J.; Thevuthasan, S.; Herman, G. S.; Peden, C. H. F.; Chambers, S. A.; Belton, D. N.; Permana, H. Chemisorption Geometry of NO on Rh(111) by X-ray Photoelectron Diffraction. *Surf. Sci.* **1996**, *359*, 269–279.
- (45) Zasada, I.; Van Hove, M. A.; Somorjai, G. A. Reanalysis of the Rh(111)+(2×2)-3NO Structure Using Automated Tensor LEED. *Surf. Sci. Lett.* **1998**, *418*, L89–L93.
- (46) Rider, K. B.; Hwang, K. S.; Salmeron, M.; Somorjai, G. A. Structure and Dynamics of Dense Monolayers of NO Adsorbed on Rh(111) in Equilibrium with the Gas Phase in the Torr Pressure Range. *Phys. Rev. Lett.* **2001**, *86*, 4330–4333.
- (47) Bond, G. C. Supported Metal Catalysts: Some Unsolved Problems. *Chem. Soc. Rev.* **1991**, *20*, 441–475.
- (48) Zaera, F.; Somorjai, G. A. Hydrogenation of Ethylene over Platinum (111) Single-Crystal Surfaces. *J. Am. Chem. Soc.* **1984**, *106*, 2288–2293.
- (49) Hatzikos, G. H.; Masel, R. I. Structure Sensitivity of Ethylene Adsorption on Pt(100): Evidence for Vinylidene Formation on (1 × 1) Pt(100). *Surf. Sci.* **1987**, *185*, 479–494.
- (50) McCrea, K. R.; Somorjai, G. A. SFG-Surface Vibrational Spectroscopy Studies of Structure Sensitivity and Insensitivity in Catalytic Reactions: Cyclohexene Dehydrogenation and Ethylene Hydrogenation on Pt(111) and Pt(100) Crystal Surfaces. *J. Mol. Catal. A: Chem.* **2000**, *163*, 43–53.
- (51) Morgan, A. E.; Somorjai, G. A. Low Energy Electron Diffraction Studies of Gas Adsorption on the Platinum (100) Single-crystal Surface. *Surf. Sci.* **1968**, *12*, 405–425.
- (52) Fischer, T. E.; Kelemen, S. R. Adsorption of Ethylene on the Pt(100) Surface. *Surf. Sci.* **1977**, *69*, 485–507.
- (53) Rønning, M.; Bergene, E.; Borg, A.; Ausen, S.; Holmen, A. Scanning Tunnelling Microscopic Studies on the Adsorption and Decomposition of Ethene on the Reconstructed Pt(100)-hex-R0.7° Surface. *Surf. Sci.* **2001**, *477*, 191–197.
- (54) Zhu, Z.; Butcher, D. R.; Mao, B.; Liu, Z.; Salmeron, M.; Somorjai, G. A. In Situ Scanning Tunneling Microscopy and X-ray Photoelectron Spectroscopy Studies of Ethylene-Induced Structural Changes on the Pt(100)-hex Surface. *J. Phys. Chem. C* **2013**, *117*, 2799–2804.
- (55) Bartels, L.; Meyer, G.; Rieder, K.-H. The Evolution of CO Adsorption on Cu(111) as Studied with Bare and CO-functionalized Scanning Tunneling Tips. *Surf. Sci.* **1999**, *432*, L621–L626.
- (56) Li, W.; Kong, L.; Feng, B.; Fu, H.; Li, H.; Zeng, X. C.; Wu, K.; Chen, L. Abnormal Phase Transition between Two-Dimensional High-Density Liquid Crystal and Low-Density Crystalline Solid Phases. *Nat. Comm.* **2018**, *9*, 198.

- (57) Eren, B.; D. Zherebetsky, D.; Patera, L. L.; Wu, C. H.; Bluhm, H.; Africh, C.; Wang, L.-W.; Somorjai, G. A.; Salmeron, M. Activation of Cu(111) Surface by Decomposition into Nanoclusters driven by CO Adsorption. *Science* **2016**, *351*, 475–478.
- (58) Lysenko, O. V.; Stepanyuk, V. S.; Hergert, W.; Kirschner, J. Mesoscopic Relaxation in Homoepitaxial Metal Growth. *Phys. Rev. Lett.* **2002**, *89*, 126102.
- (59) Lagoute, J.; Liu, X.; Fölsch, F. Link Between Adatom Resonances and the Cu(111) Shockley Surface State. *Phys. Rev. Lett.* **2005**, *95*, 13680.
- (60) Dion, M.; Rydberg, H.; Schröder, E.; Langreth, D. C.; Lundqvist, B. I. Van der Waals Density Functional for General Geometries. *Phys. Rev. Lett.* **2004**, *92*, 246401.
- (61) Eren, B.; Zherebetsky, D.; Hao, Y.; Patera, L. L.; Wang, L.-W.; Somorjai, G. A.; Salmeron, M. One-dimensional Nanoclustering of The Cu(100) Surface under CO Gas in the mbar Pressure Range. *Surf. Sci.* **2016**, *651*, 210–214.
- (62) Vollmer, S.; Witte, G.; Christof Wöll, C. Determination of Site Specific Adsorption Energies of CO on Copper. *Catal. Lett.* **2001**, *77*, 97–101.
- (63) Eren, B.; Liu, Z.; Stacchiola, D.; Somorjai, G. A.; Salmeron, M. Structural Changes of Cu(110) and Cu(110)-(2×1)-O Surfaces Under Carbon Monoxide in the Torr Pressure Range Studied With Scanning Tunneling Microscopy and Infrared Reflection Absorption Spectroscopy. *J. Phys. Chem. C* **2016**, *120*, 8227–8231.
- (64) Hollins P.; J. Pritchard, P. in: *Vibrational Spectroscopies of Adsorbates*, Vol. 15, Ed. R.F. Willis; Springer: Berlin, **1980**.
- (65) Truong, C. M.; Rodriguez, J. A.; Goodman, D. W. CO Adsorption Isotherms on Cu(100) at Elevated Pressures and Temperatures Using Infrared Reflection Absorption Spectroscopy. *Surf. Sci. Lett.* **1992**, *271*, L385–L391.
- (66) Greenler, R. G.; Hayden, B. E.; Kretzschmar, K.; Klauser, R.; Bradshaw, A. M. Proc. 9th Intern. Congress on Catalysis, 1984, Berlin IV-197, Verlag Chemie, Weinheim.
- (67) Roiaz, M.; Falivene, L.; Rameshan, C.; Cavallo, L.; Kozlov, S. M.; Rupprechter, G. Roughening of Copper (100) at Elevated CO Pressure: Cu Adatom and Cluster Formation Enable CO Dissociation. *J. Phys. Chem. C* **2019**, *123*, 13, 8112–8121.
- (68) Jugnet, W.; Cadete Santos Aires, F. J.; Deranlot, C.; Piccolo, L.; Bertolini, J. C. CO Chemisorption on Au(1 1 0) Investigated under Elevated Pressures by Polarized Reflection Absorption Infrared Spectroscopy and Scanning Tunneling Microscopy. *Surf. Sci. Lett.* **2002**, *521*, L639–L644.

- (69) Hrbek, J.; Hoffmann, F. M.; Park, J. B.; Liu, P.; Stacchiola, D.; Hoo, Y. S.; Ma, S.; Nambu, A.; Rodriguez, J. A.; White, M. G. Adsorbate-Driven Morphological Changes of a Gold Surface at Low Temperatures. *J. Am. Chem. Soc.* **2008**, *130*, 17272–17273.
- (70) Wang, J.; McEntee, M.; Tang, W.; Neurock, M.; Baddorf, A. P.; Maksymovych, P.; Yates, Jr., J. T. Formation, Migration, and Reactivity of Au–CO Complexes on Gold Surfaces. *J. Am. Chem. Soc.* **2016**, *138*, 1518–1526.
- (71) Piccolo, L.; Loffreda, D.; Cadete Santos Aires, F. J.; Deranlot, C.; Jugnet, Y.; Sautet, P.; Bertolini, J. C. The Adsorption of CO on Au(1 1 1) at Elevated Pressures Studied by STM, RAIRS and DFT Calculations. *Surf. Sci.* **2004**, *566–568*, 995–1000.
- (72) Goerge, J.; Zeppenfeld, P.; David, R.; Büchel, M.; Comsa, G. Structure of the Hydrogen Covered Cu(110) Surface Studied with Thermal Energy Helium Scattering. *Surf. Sci.* **1993**, *289*, 201–213.
- (73) Spitzl, R.; Niehus, H.; Poelsema, B.; Comsa, G. H-induced (1×2) Reconstruction of the Cu(110) Surface: Structure and Deconstruction Kinetics. *Surf. Sci.* **1990**, *239*, 243–253.
- (74) Hayden, B. E.; Lackey, D.; Schott, J. A Vibrational Study of the Hydrogen Induced Reconstructions on Cu(110). *Surf. Sci.* **1990**, *239*, 119–126.
- (75) Österlund, L.; Rasmussen, P. B.; Thostrup, P.; Lægsgaard, E.; Stensgaard, I.; Besenbacher, F. Bridging the Pressure Gap in Surface Science at the Atomic Level: H/Cu(110). *Phys. Rev. Lett.* **2001**, *86*, 460–463.
- (76) Shi, Y.; Choi, B. Y.; Salmeron, M., Water Chains Guide the Growth of Monoatomic Copper Wires on Cu(110). *J. Phys. Chem. C* **2013**, *117*, 17119–17122
- (77) Eren, B.; Weatherup, R.; Liakakos, N.; Somorjai, G. A.; Salmeron, M. Dissociative Carbon Dioxide Adsorption and Morphological Changes on Cu(100) and Cu(111) at Ambient Pressures. *J. Am. Chem. Soc.* **2016**, *138*, 8207–8211.
- (78) Hagman, B.; Posada-Borbón, A.; Schaefer, A.; Shipilin, M.; Zhang, C.; Merte, L. R.; Hellman, A.; Lundgren, E.; Grönbeck, H.; Gustafson, J. Steps Control the Dissociation of CO₂ on Cu(100). *J. Am. Chem. Soc.* **2018**, *140*, 12974–12979.
- (79) Eren, B.; Kersell, H.; Weatherup, R.; Heine, C.; Crumlin, E. J.; Friend, C. M.; Salmeron, M. Structure of the Clean and Oxygen-Covered Cu(100) Surface at Room Temperature in the Presence of Methanol Vapor in the 10 to 200 mTorr Pressure Range. *J. Phys. Chem. B* **2018**, *123*, 8112–8121.
- (80) Fang, M.; Santos, G.; Chen, Z.; Baldelli, S. Roles of Oxygen for Methanol Adsorption on Polycrystalline Copper Surface Revealed by Sum Frequency Generation Imaging Microscopy. *Surf. Sci.* **2016**, *648*, 35–41.
- (81) Greeley, J.; Mavrikakis, M. Methanol Decomposition on Cu(111): A DFT Study. *J. Catal.* **2002**, *208*, 291–300.

- (82) Hoyt, R. A.; Montemore, M. M.; Sykes, E. C. H.; Kaxiras, E. Anhydrous Methanol and Ethanol Dehydrogenation at Cu(111) Step Edges. *J. Phys. Chem. C* **2018**, *122*, 38, 21952–21962.
- (83) Chen, J.; Zhou, X.; Zhang, Y.; Jiang, B. Vibrational Control of Selective Bond Cleavage in Dissociative Chemisorption of Methanol on Cu(111). *Nature Comm.* **2018**, *9*, 4039.
- (84) Sakong, S. Methanol Oxidation on Oxygen Covered Cu Surfaces. Ph.D. Thesis, Technische Universität München, 2005.
- (85) Freund, H.-J.; Meijer, G.; Scheffler, M.; Schlögl, R.; Wolf, M. CO Oxidation as a Prototypical Reaction for Heterogeneous Processes. *Angew. Chem., Int. Ed.* **2011**, *50*, 10064–10094.
- (86) van Spronsen, M. A.; Frenken, J. W. M.; Groot, I. M. N. Surface Science under Reaction Conditions: CO Oxidation on Pt and Pd Model Catalysts. *Chem. Soc. Rev.* **2017**, *46*, 4347–4374.
- (87) Wintterlin, J.; Völkening, S.; Janssens, T. V. W.; Zambelli, T.; Ertl, G. Atomic and Macroscopic Reaction Rates of a Surface-Catalyzed Reaction. *Science* **1997**, *278*, 1931–1934.
- (88) Yeates, R. C.; Turner, J. E.; Gellman, A. J.; Somorjai, G. A. The Oscillatory Behavior of the CO Oxidation Reaction at Atmospheric Pressure over Platinum Single-crystals: Surface Analysis and Pressure Dependent Mechanisms. *Surf. Sci.* **1985**, *149*, 175–190.
- (89) Eiswirth, M.; Ertl, G. Kinetic Oscillations in the Catalytic CO Oxidation on a Pt (110) Surface. *Surf. Sci.* **1986**, *177*, 90–100.
- (90) Hendriksen, B. L. M.; Frenken, J. W. M. CO Oxidation on Pt(110): Scanning Tunneling Microscopy Inside a High-Pressure Flow Reactor. *Phys. Rev. Lett.* **2002**, *89*, 046101.
- (91) Van Spronsen, M. A.; Van Baarle, G. J. C.; Herbschleb, C. T.; Frenken, J. W. M.; Groot, I. M. N. High-pressure Operando STM Studies Giving Insight in CO Oxidation and NO Reduction over Pt(110). *Catal. Today* **2015**, *244*, 85–95.
- (92) Ackermann, M. D.; Pedersen, T. M.; Hendriksen, B. L. M.; Robach, O.; Bobaru, S. C.; Popa, I.; Quiros, C.; Kim, H.; Hammer, B.; Ferrer, S.; et al. Structure and Reactivity of Surface Oxides on Pt (110) during Catalytic CO Oxidation. *Phys. Rev. Lett.* **2005**, *95*, 255505.
- (93) Hendriksen, B. L. M.; Bobaru, S. C.; Frenken, J. W. M. Oscillatory CO Oxidation on Pd(1 0 0) Studied with in situ Scanning Tunneling Microscopy. *Surf. Sci.* **2004**, *552*, 229–242.
- (94) Van Rijn, R.; Balmes, O.; Resta, A.; Wermeille, D.; Westerström, R.; Gustafson, J.; Felici, R.; Lundgren, E.; Frenken, J. W. M. Surface Structure and Reactivity of Pd(100) During CO Oxidation Near Ambient Pressures. *Phys. Chem. Chem. Phys.* **2011**, *13*, 13167–13171.
- (95) Onderwaater, W. G.; Balmes, O.; Roobol, S. B.; Van Spronsen, M.; Drnec, J.; Carla, F. Felici, R.; Frenken, J. W. M. Oxidation of CO on Pd(100): On the Structural Evolution of the PdO Layer during the Self Sustained Oscillation Regime. *Catal. Struct. React.* **2017**, *3*, 89–94.

- (96) Africh, C.; Esch, F.; Comelli, G.; Rosei, R. Reactivity and Deconstruction of the (1×2)-Rh(110) Surface Studied by Scanning Tunneling Microscopy. *J. Chem. Phys.* **2002**, *116*, 7200–7206.
- (97) Nguyen, L.; Liu, L.; Assefa, S.; Wolverton, C.; Schneider, W. F. Tao, F. Atomic-Scale Structural Evolution of Rh(110) during Catalysis. *ACS Catal.* **2017**, *7*, 1, 664–674.
- (98) Royer, S.; Duprez, D. Catalytic Oxidation of Carbon Monoxide over Transition Metal Oxides. *ChemCatChem* **2011**, *3*, 24–65.
- (99) Matsumoto, T.; Bennett, R. A.; Stone, P.; Yamada, T.; Domen, K.; Bowker, M. Scanning Tunneling Microscopy Studies of Oxygen Adsorption on Cu(111). *Surf. Sci.* **2001**, *471*, 225–245.
- (100) Yang, F.; Choi, Y.; Liu, P.; Hrbek, J.; Rodriguez, J. A. Autocatalytic Reduction of a Cu₂O/Cu(111) Surface by CO: STM, XPS, and DFT Studies. *J. Phys. Chem. C* **2010**, *114*, 17042–17050.
- (101) Yang, F.; Choi, Y.; Liu, P.; Stacchiola, D.; Hrbek, J.; Rodriguez, J. A. Identification of 5–7 Defects in a Copper Oxide Surface. *J. Am. Chem. Soc.* **2011**, *133*, 11474–11477.
- (102) Baber, A. E.; Xu, F.; Dvorak, F.; Mudiyansele, K.; Soldemo, M.; Weissenrieder, J.; Senanayake, S. D.; Sadowski, J. T.; Rodriguez, J. A.; Matolin, V. In Situ Imaging of Cu₂O under Reducing Conditions: Formation of Metallic Fronts by Mass Transfer. *J. Am. Chem. Soc.* **2013**, *135*, 16781–16784.
- (103) Leibsle, F. M. STM Studies of Oxygen-induced Structures and Nitrogen Coadsorption on the Cu(100) Surface: Evidence for One-Dimensional Oxygen Reconstruction and Reconstructive Interactions. *Surf. Sci.* **1995**, *337*, 51–66.
- (104) Ling, W. L.; Takeuchi, O.; Ogletree, D. F.; Qiu, Z. Q.; Salmeron, M. STM Studies on the Growth of Monolayers: Co on Cu(110) with One Half Monolayer of Preadsorbed Oxygen. *Surf. Sci.* **2000**, *450*, 227–241.
- (105) Eren, B.; Lichtenstein, L.; Wu, C. H.; Bluhm, H.; Somorjai, G. A.; Salmeron, M. Reaction of CO with Preadsorbed Oxygen on Low-Index Copper Surfaces: An Ambient Pressure X-Ray Photoelectron Spectroscopy and Scanning Tunneling Microscopy Study. *J. Phys. Chem. C* **2015**, *119*, 14669–14674.
- (106) Xu, F.; Mudiyansele, K.; Baber, A. E.; Soldemo, M.; Weissenrieder, J.; White, M. G.; Stacchiola, D. J. Redox-Mediated Reconstruction of Copper during Carbon Monoxide Oxidation. *J. Phys. Chem. C* **2014**, *118*, 15902–15909.
- (107) Wiame, F.; Maurice, V.; Marcus, P. Initial Stages of Oxidation of Cu(111). *Surf. Sci.* **2007**, *601*, 1193–1204.
- (108) Mendes, G.C.C.; Brandão, T.R.S.; Silva, C.L.M. Ethylene Oxide Sterilization of Medical Devices: A Review. *Am. J. Infect. Control* **2007**, *35*, 574–581.
- (109) Montemore, M. M.; van Spronsen, M. A.; Madix, R. J.; Friend, C. M. O₂ Activation by Metal Surfaces: Implications for Bonding and Reactivity on Heterogeneous Catalysts. *Chem. Rev.* **2018**, *118*, 2816–2862.

- (110) Heine, Ch.; Eren, B.; Lechner, B. A. J.; Salmeron, M. A Study of the O/Ag(111) System with Scanning Tunneling Microscopy and X-Ray Photoelectron Spectroscopy at Ambient Pressures. *Surf. Sci.* **2016**, *652*, 51–57.
- (111) Li, W.-X.; Stampfl, C.; Scheffler, M. Subsurface Oxygen and Surface Oxide Formation At Ag(111): A Density-Functional Theory Investigation. *Phys. Rev. B* **2003**, *67*, 045408.
- (112) Todorova, M.; Li, W. X.; Ganduglia-Pirovano, M. V.; Stampfl, C.; Reuter, K.; Scheffler, M. Role of Subsurface Oxygen in Oxide Formation at Transition Metal Surfaces. *Phys. Rev. Lett.* **2002**, *89*, 096103.
- (113) Böcklein, S.; Günther, S.; Wintterlin, J. Scanning Tunneling Microscopy of a Silver Surface during Catalytic Formation Of Ethylene Oxide. *Angew. Chem. Int. Ed.* **2013**, *52*, 5518–5521.
- (114) Grant, R. B.; Lambert, R. M. A Single-crystal Study of the Silver-Catalysed Selective Oxidation and Total Oxidation of Ethylene. *J. Catal.* **1985**, *92*, 364–375;
- (115) Bukhtiyarov, V. I.; Boronin, A. I.; Savchenko, V. I. Two Oxygen States and the Role of Carbon in Partial Oxidation of Ethylene over Silver. *Surf. Sci.* **1990**, *232*, L205–L209;
- (116) Bukhtiyarov, V. I.; Prosvirin, I. P.; Kvon, R. I. Study of Reactivity of Oxygen States Adsorbed at a Silver Surface towards C₂H₄ by XPS, TPD and TPR. *Surf. Sci.* **1994**, *320*, L47–L50;
- (117) Herbschleb, C. T.; Bobaru, S. C.; Frenken, J. W. M. High-pressure STM study of NO reduction by CO on Pt(100). *Catal. Today* **2010**, *154*, 61–67.
- (118) Rider, K. B.; Hwang, K. S.; Salmeron, M.; Somorjai, G. A. High-Pressure (1 Torr) Scanning Tunneling Microscopy (STM) Study of the Coadsorption and Exchange of CO and NO on the Rh(111) Crystal Face. *J. Am. Chem. Soc.* **2002**, *124*, 5588–5593.
- (119) Permana, H.; Ng, K. Y. S.; Peden, C. H. F.; Schmieg, S. J.; Lambert, D. K.; Belton, D. N. Adsorbed Species and Reaction Rates for NO–CO over Rh(111). *J. Catal.* **1996**, *164*, 194–206.
- (120) Zhdanov, V. P.; Kasemo, B. Mechanism and Kinetics of the NO-CO Reaction on Rh. *Surf. Sci. Rep.* **1997**, *29*, 31–90.
- (121) Requejo, F.G.; Hebenstreit, E.L.D.; Ogletree, D.F.; Salmeron, M. An In Situ XPS Study of Site Competition between CO and NO on Rh(111) in Equilibrium with the Gas Phase. *J. Catal.* **2004**, *226*, 83–87.
- (122) Kim, J.; Noh, M. C.; Doh, W. H.; Park, J. Y. In Situ Observation of Competitive CO and O₂ Adsorption on the Pt(111) Surface Using Near-Ambient Pressure Scanning Tunneling Microscopy. *J. Phys. Chem. C.*, *122*, 6246–6254.
- (123) Gland, J. L.; Sexton, B. A.; Fisher, G. B. Oxygen Interactions with the Pt(111) Surface. *Surf. Sci.* **1980**, *95*, 587–602.
- (124) Zunino, L.; Garavaglia, M. Moiré by Fractal Structures. *J. Mod. Opt.* **2003**, *50*, 1477–1486.

- (125) Zaera, F.; French, C. R. Mechanistic Changes in the Conversion of Ethylene to Ethylidyne on Transition Metals Induced By Changes in Surface Coverages. *J. Am. Chem. Soc.* **1999**, *121*, 2236–2243.
- (126) Starke, U. Barbieri, A.; Materer, N.; Van Hove, M. A.; Somorjai, G. A. Ethylidyne on Pt(111): Determination of Adsorption Site, Substrate Relaxation and Coverage By Automated Tensor LEED. *Surf. Sci. Lett.* **1993**, *286*, 1–14.
- (127) Land, T. A.; Michely, T.; Behm, R. J.; Hemminger, J. C.; Comsa, G. Direct Observation of Surface Reactions by Scanning Tunneling Microscopy: Ethylene→Ethylidyne→Carbon Particles→Graphite on Pt(111). *J. Chem. Phys.* **1992**, *97*, 6774–6783.
- (128) Land, T. A.; Michely, T.; Behm, R. J.; Hemminger, J. C.; Comsa, G. STM Investigation of the Adsorption and Temperature Dependent Reactions of Ethylene on Pt(111). *Appl. Phys. A* **1991**, *53*, 414–417.
- (129) Umezawa, K.; Ito, T.; Asada, M. Nakanishia, S.; Ding, P.; Lanford, W. A.; Hjörvarsson, B. Adsorption of Hydrogen on the Pt(111) Surface from Low-energy Recoil Scattering. *Surf. Sci.* **1997**, *387*, 320–327.
- (130) Batra, I. P.; Barker, J. A.; Auerbach, D. J. Helium Scattering from (1 × 1) H-Pt(111). *J. Vac. Sci. Technol. A.* **1984**, *2*, 943–973.
- (131) Christmann, K. Interaction of Hydrogen with Solid Surfaces. *Surf. Sci. Rep.* **1988**, *9*, 1–163.
- (132) Tang, D. C. Hwang, K. S.; Salmeron, M.; Somorjai, G. A. High Pressure Scanning Tunneling Microscopy Study of CO Poisoning of Ethylene Hydrogenation on Pt(111) and Rh(111) Single-crystals. *J. Phys. Chem. B.* **2004**, *108*, 13300–13306.
- (133) Chen P, Kung KY, Shen YR, Somorjai GA. Sum Frequency Generation Spectroscopic Study of CO/Ethylene Coadsorption on the Pt(111) Surface and CO Poisoning of Catalytic Ethylene Hydrogenation. *Surf. Sci.* **2001**, *494*, 289–297.
- (134) Ainsworth, M. K.; Mccoustra, M. R. S.; Chesters, M. A.; Sheppard, N.; De La Cruz, C. An Infrared Study of Ethene and CO Coadsorption on Pt[111] and a Pt/SiO₂ Catalyst: Ambiguities in the Interpretation of Difference Spectra. *Surf. Sci.* **1999**, *437*, 9–17.
- (135) Payne, S. H.; Kreuzer, H. J.; Frie, W.; Hammer, L.; Heinz, K. Adsorption and Desorption of Hydrogen on Rh(311) and Comparison with Other Rh Surfaces. *Surf. Sci.* **1999**, *421*, 279–295.
- (136) Yanagita, H.; Fujioka, H.; Aruga, T.; Takagi, N.; Nishijima, M. Vibrational Spectra of Hydrogen on the Rh(111) Surface. *Surf. Sci.* **1999**, *441*, 507–514.
- (137) Wander, A.; Van Hove, M. A.; Somorjai, G. A. Molecule-induced Displacive Reconstruction in a Substrate Surface: Ethylidyne Adsorbed on Rh(111) Studied by Low-energy-electron Diffraction. *Phys. Rev. Lett.* **1991**, *67*, 626–628.

- (138) Bowker, M.; Gland, J. L.; Joyner, R. W.; Li, Y.; Slin'ko, M. M.; Whyman, R. Stoichiometric Hydrogenation of Ethene on Rh(111); Mechanism, Importance of Weakly Adsorbed Ethene, and Relationship to Homogeneous Catalysis. *Catal. Lett.* **1994**, *25*, 293–308.
- (139) Butcher, D. R.; Zhu, Z.; Mao, B. Wang, H.; Liu, Z.; Salmeron, M.; Somorjai, G. A Mobility on the Reconstructed Pt(100)-hex Surface in Ethylene and in its Mixture with Hydrogen and Carbon Monoxide. *Chem. Commun.* **2013**, *49*, 6903–6905.
- (140) Tao, F.; Dag, S.; Wang, L. W.; Liu, Z.; Butcher, D. R.; Bluhm, H.; Salmeron, M.; Somorjai, G. A. Break-up of Stepped Platinum Catalyst Surfaces by High CO Coverage. *Science* **2010**, *327*, 850–853.
- (141) Balmes, O.; Prevot, G.; Torrelles, X.; Lundgren, E.; Ferrer, S. Diatomic Steps in Pt(997) Surfaces Are Better Catalysts than Monatomic Steps for the CO Oxidation Reaction near Atmospheric Pressure. *ACS Catal.* **2016**, *6*, 1285–1291.
- (142) Prévot, G.; Steadman, P.; Ferrer, S. Determination of the Elastic Dipole at the Atomic Steps of Pt(977) from Surface X-ray Diffraction. *Phys. Rev. B* **2003**, *67*, 245409.
- (143) Giesen, M.; Icking-Konert, G. S. Step-step Interaction Energy on Cu(111) Vicinal Surfaces. *Surf. Rev. Lett.* **1999**, *6*, 27–34
- (144) Prévot, G.; Coati, A.; Garreau, Y. Grazing-incidence X-ray Diffraction Measurement of the Relaxations and Elastic Step Interactions on Cu(211) and Cu(322). *Phys. Rev. B* **2004**, *70*, 205406.
- (145) Kim, J.; Noh, M. C.; Doh, W. H.; Park, J. Y. Thermal Evolution and Instability of CO-induced Platinum Clusters on the Pt (557) Surface at Ambient Pressure. *J. Am. Chem. Soc.* **2016**, *138*, 1110–1113.
- (146) Zhu, Z.; Barroo, C.; Lichtenstein, L.; Eren, B.; Wu, C. H.; Mao, B.; Visart de Bocarmé, T.; Liu, Z.; Kruse, N.; Salmeron, et al. Influence of Step Geometry on the Reconstruction of Stepped Platinum Surfaces under Coadsorption of Ethylene and CO. *J. Phys. Chem. Lett.* **2014**, *5*, 2626–2631.
- (147) Wang, J. G.; Li, W. X.; Borg, M.; Gustafson, J.; Mikkelsen, A.; Pedersen, T. M.; Lundgren, E.; Weissenrieder, J.; Klikovits, J.; Schmid, M.; et al. One-Dimensional PtO₂ at Pt Steps: Formation and Reaction with CO. *Phys. Rev. Lett.* **2005**, *95*, 256102.
- (148) Held, G.; Jones, L. B.; Seddon, E. A.; King, D. A. Effect of Oxygen Adsorption on the Chiral Pt{531} Surface. *J. Phys. Chem. B* **2005**, *109*, 6159–6163.
- (149) Bandlow, J.; Kaghazchi, P.; Jacob, T.; Papp, C.; Trankenschuh, B.; Streber, R.; Lorenz, M. P. A.; Fuhrmann, T.; Denecke, R.; Steinrück, H. P. Oxidation of Stepped Pt(111) Studied by X-ray Photoelectron Spectroscopy and Density Functional Theory. *Phys. Rev. B* **2011**, *83*, 174107.
- (150) Li, W. X.; Österlund, L.; Vestergaard, E. K.; Vang, R. T.; Matthiesen, J.; Pedersen, T. M.; Lægsgaard, E.; Hammer, B.; Besenbacher, F. Oxidation of Pt(110). *Phys. Rev. Lett.* **2004**, *93*, 146104.

- (151) Butcher, D. R.; Grass, M. E.; Zeng, Z.; Aksoy, F.; Bluhm, H.; Li, W.-X.; Mun, B. S.; Somorjai, G. A.; Liu, Z. In Situ Oxidation Study of Pt(110) and Its Interaction with CO. *J. Am. Chem. Soc.* **2011**, *133*, 20319–20325.
- (152) Zhu, Z.; Tao, F.; Zheng, F.; Chang, R.; Li, Y.; Heinke, L.; Liu, Z.; Salmeron, M.; Somorjai, G. A. Formation of Nanometer-Sized Surface Platinum Oxide Clusters on a Stepped Pt(557) Single-crystal Surface Induced by Oxygen: A High Pressure STM and Ambient-Pressure XPS Study. *Nano Lett.* **2012**, *12*, 1491–1497.
- (153) Zhu, Z.; Melaet, G.; Axnanda, S.; Alayoglu, S.; Liu, Z.; Salmeron, M. Somorjai, G. A. Structure and Chemical State of the Pt(557) Surface During Hydrogen Oxidation Reaction Studied by in situ Scanning Tunneling Microscopy and X-Ray Photoelectron Spectroscopy. *J. Am. Chem. Soc.* **2013**, *135*, 12560–12563.
- (154) Peters, K. F.; Walker, C. J.; Steadman, P.; Robach, O.; Isern H.; Ferrer, S. Adsorption of Carbon Monoxide on Ni(110) above Atmospheric Pressure Investigated with Surface X-Ray Diffraction. *Phys. Rev. Lett.* **2001**, *86*, 5325.
- (155) Nguyen, L.; Cheng, F.; Zhang, S.; Tao, F. Visualization of Surfaces of Pt and Ni Model Catalysts in Reactive Environments Using Ambient Pressure High Temperature Scanning Tunneling Microscopy and Understanding the Restructurings of Surfaces of Model Metal Catalysts under Reaction Conditions at Near Ambient Pressure. *J. Phys. Chem. C* **2013**, *117*, 971–977.
- (156) Wender, I. Reactions of Synthesis Gas. *Fuel Process. Technol.* **1996**, *48*, 189–297.
- (157) Schulz, H. Short History and Present Trends of Fischer–Tropsch Synthesis. *Appl. Catal. A* **1999**, *186*, 3–12.
- (158) Geerlings, J. J. C.; Wilson, J. H.; Kramer, G. J.; Kuipers, H. P. C. E.; Hoek, A.; Huisman, H. M. Fischer–Tropsch Technology – From Active Site to Commercial Process. *Appl. Catal. A* **1999**, *186*, 27–40.
- (159) Khodakov, A. Y.; Chu, W.; Fongarland, P. Advances in the Development of Novel Cobalt Fischer–Tropsch Catalysts for Synthesis of Long-Chain Hydrocarbons and Clean Fuels. *Chem. Rev.* **2007**, *107*, 1692–1744.
- (160) Fischer, F.; Tropsch, H. Über die Herstellung Synthetischer Ölgemische (Synthol) durch Aufbau aus Kohlenoxyd und Wasserstoff. *Brennstoff-Chemie* **1923**, *4*, 276–285.
- (161) Van Der Laan, G. P.; Beenackers, A. A. C. M. Kinetics and Selectivity of the Fischer–Tropsch Synthesis: A Literature Review. *Catal. Rev.: Sci. Eng.* **1999**, *41*, 255–318.
- (162) Iglesia, E. Design, Synthesis, and Use of Cobalt-based Fischer-Tropsch Synthesis Catalysts. *Appl. Catal. A* **1997**, *161*, 59–78.
- (163) Dry, M. E. The Fischer–Tropsch process: 1950–2000. *Catal. Today* **2002**, *71*, 227–241.

- (164) Torres Galvis, H. M.; De Jong, K. P. Catalysts for Production of Lower Olefins from Synthesis Gas: A Review. *ACS Catal.* **2013**, *3*, 2130–2149.
- (165) Jiao, F.; Li, J.; Pan, X.; Xiao, J.; Li, H.; Ma, H.; Wei, M.; Pan, Y.; Zhou, Z.; Li, M.; et al. Selective Conversion of Syngas to Light Olefins. *Science* **2016**, *351*, 1065–1068.
- (166) Shetty, S.; van Santen, R. A. CO Dissociation on Ru and Co surfaces: The Initial Step in the Fischer–Tropsch Synthesis. *Catal. Today* **2011**, *171*, 168–173.
- (167) Tuxen, A.; Carenco, S.; Chintapalli, M.; Chuang, C.-H.; Escudero, C.; Pach, E.; Jiang, P.; Borondics, F.; Beberwyck, B.; Alivisatos, A. P.; et al. Size-Dependent Dissociation of Carbon Monoxide on Cobalt Nanoparticles. *J. Am. Chem. Soc.* **2013**, *135*, 2273–2278.
- (168) Wu, C.H.; Eren, B.; Bluhm, H.; Salmeron, M. B., Ambient-Pressure X-ray Photoelectron Spectroscopy Study of Cobalt Foil Model Catalyst under CO, H₂, and Their Mixtures. *ACS Catal.* **2017**, *7*, 1150–1157.
- (169) Wilson, J.; de Groot, C. Atomic-scale Restructuring in High-pressure Catalysis. *J. Phys. Chem.* **1995**, *99*, 7860–7866.
- (170) Oosterbeek, H. Bridging the Pressure and Material Gap in Heterogeneous Catalysis: Cobalt Fischer–Tropsch Catalysts from Surface Science to Industrial Application. *Phys. Chem. Chem. Phys.* **2007**, *9*, 3570–3576.
- (171) Ehrensperger, M.; Wintterlin, J. In situ High-Pressure High-Temperature Scanning Tunneling Microscopy of a Co(0001) Fischer–Tropsch Model Catalyst. *J. Catal.* **2014**, *319*, 274–282.
- (172) Bridge, M. E.; Comrie, C. M.; Lambert, R. M. Chemisorption Studies on Cobalt Single-crystal Surfaces: I. Carbon Monoxide on Co(0001). *Surf. Sci.* **1977**, *67*, 393–404.
- (173) Papp, H. The Chemisorption of Carbon Monoxide on a Co(0001) Single-crystal Surface; Studied by LEED, UPS, EELS, AES and Work Function Measurements. *Surf. Sci.* **1983**, *129*, 205–218.
- (174) Agrawal, P. K.; Katzer, J. R.; W.H. Manogue, Methanation over Transition Metal Catalysts: III. CoAl₂O₃ in Sulfur-poisoning Studies. *J. Catal.* **1981**, *69*, 327–344.
- (175) Ehrensperger, M.; Wintterlin, J. In situ Scanning Tunneling Microscopy of the Poisoning of a Co(0001) Fischer–Tropsch Model Catalyst by Sulfur. *J. Catal.* **2015**, *329*, 49–56.
- (176) Lahtinen, J.; Kantola, P.; Jaatinen, S.; Habermehl-Cwirzen, K.; Salo, P.; Vuorinen, J.; Lindroos, M.; Pussi, K.; Seitsonen, A. P. LEED and DFT Investigation on the (2×2)-S Overlayer on Co(0001). *Surf. Sci.* **2005**, *599*, 113–121.
- (177) Habermehl-Cwirzen, K. M. E.; Kauraala, K.; Lahtinen, J. Hydrogen on Cobalt: The Effects of Carbon Monoxide and Sulphur Additives on the D₂/Co(0001) System. *Phys. Scripta* **2004**, *T108*, 28–32.
- (178) Habermehl-Cwirzen, K. M. E.; Lahtinen, J. Sulfur Poisoning of the CO Adsorption on Co(0001). *Surf. Sci.* **2004**, *573*, 183–190.

- (179) Böller, B.; Ehrensperger, M.; Wintterlin, J. In Situ Scanning Tunneling Microscopy of the Dissociation of CO on Co(0001). *ACS Catal.* **2015**, *5*, 6802–6806.
- (180) Papp, H. The Chemisorption of Carbon Monoxide on a Co(0001) Single-crystal Surface; Studied by LEED, UPS, EELS, AES and Work Function Measurements. *Surf. Sci.* **1983**, *129*, 205–218.
- (181) Lahtinen, J.; Vaari, J.; Kauraala, K. Adsorption and Structure Dependent Desorption of CO on Co(0001). *Surf. Sci.* **1998**, *418*, 502–510.
- (182) Zhang, X.-Q.; van Santen, R. A.; Hensen, E. J. M. Carbon-Induced Surface Transformations of Cobalt. *ACS Catal.* **2015**, *5*, 596–601.
- (183) Navarro, V.; van Spronsen, M. A.; Frenken, J. W. M. In situ Observation of Self-assembled Hydrocarbon Fischer–Tropsch Products on a Cobalt Catalyst. *Nat. Chem.* **106**, *8*, 929–934.
- (184) Nakamura, S. Study of Metallic Carbides by Electron Diffraction Part IV. Cobalt Carbides. *J. Phys. Soc. Jpn* **1961**, *16*, 1213–1219.
- (185) Bergerhoff, G.; Brown, I. D. in International Union of Crystallography (eds Allen, F. H. et al.) 77–95 (Chester, 1987).
- (186) Yamada, R.; Uosaki, K. Two-dimensional Crystals of Alkanes Formed on Au(111) Surface in Neat Liquid: Structural Investigation by Scanning Tunneling Microscopy. *J. Phys. Chem. B* **2000**, *104*, 6021–6027.
- (187) Uosaki, K.; Yamada, R. Formation of Two-dimensional Crystals of Alkanes on the Au(111) Surface in Neat Liquid. *J. Am. Chem. Soc.* **1999**, *121*, 4090–4091.
- (188) Xie, Z. X.; Xu, X.; Tang, J.; Mao, B. W. Molecular Packing in Self-Assembled Monolayers of Normal Alkane on Au(111) Surfaces. *Chem. Phys. Lett.* **2000**, *323*, 209–216.
- (189) Marchenko, J.; Cousty, A. Substrate-induced Freezing of Alkane Monolayers Adsorbed on Au(111) Dependent on the Alkane/Gold Misfit. *Surf. Sci.* **2002**, *520*, 128–136.
- (190) Schulz, G. V. Ueber die Beziehung zwischen Reaktionsgeschwindigkeit und Zusammensetzung des Reaktionsproduktes bei Macropolymerisationsvorgängen. *Z. Phys. Chem. B* **1935**, *30*, 379.
- (191) Flory, P. J. Molecular Size Distribution in Linear Condensation Polymers. *J. Am. Chem. Soc.* **1936**, *58*, 1877–1885.
- (192) Anderson, R. B.; Seligman, B.; Shultz, J. F.; Kelly, R.; Elliott, M. A. Fischer–Tropsch Synthesis. Some Important Variables of the Synthesis on Iron Catalyst. *Ind. Eng. Chem.* **1952**, *44*, 391–397.
- (193) Böller, B.; Durner, K. M.; Wintterlin, J. The Active Sites of a Working Fischer–Tropsch Catalyst Revealed by Operando Scanning Tunnelling Microscopy. *Nature Catalysis* **2019**, *2*, 1027–1034.
- (194) Royer, S.; Duprez, D. Catalytic Oxidation of Carbon Monoxide over Transition Metal Oxides. *ChemCatChem* **2011**, *3*, 24–65.

- (195) Jansson, J.; Palmqvist, A. E. C.; Fridell, E.; Skoglundh, M.; Österlund, L.; Thormählen, P.; Langer, V. J. On the Catalytic Activity of Co_3O_4 in Low-Temperature CO Oxidation. *J. Catal.* **2002**, *211*, 387–397.
- (196) Jansson, J.; Skoglundh, M.; Fridell, E.; Thormählen, P. A. Mechanistic Study of Low Temperature CO Oxidation over Cobalt Oxide. *Top. Catal.* **2001**, *16*, 385–389.
- (197) Weilach, C.; Spiel, C.; Föttinger, K.; Rupprechter, G. Carbonate Formation on Al_2O_3 Thin Film Model Catalyst Supports. *Surf. Sci.* **2011**, *605*, 1503–1509.
- (198) Song, A.; Skibinski, E. S.; DeBenedetti, W. J. I.; Ortollo-Bloch, A. G.; Hines, M. A. Nanoscale Solvation Leads to Spontaneous Formation of a Bicarbonate Monolayer on Rutile (110) under Ambient Conditions: Implications for CO_2 Photoreduction. *J. Phys. Chem. C* **2016**, *120*, 9326–9333.
- (199) Thormählen, P.; Skoglundh, M.; Fridell, E.; Andersson, B. Low-Temperature CO Oxidation over Platinum and Cobalt Oxide Catalysts. *J. Catal.* **1999**, *188*, 300–310.
- (200) Cunningham, D.A.H.; Kobayashi, T.; Kamijo, N.; Haruta Influence of Dry Operating Conditions: Observation of Oscillations and Low Temperature CO Oxidation over Co_3O_4 and $\text{Au}/\text{Co}_3\text{O}_4$ Catalysts. *M. Catal. Lett.* **1994**, *25*, 257–264.
- (201) Vayssilov, G. N.; Mihaylov, M.; Petkov, P. St.; Hadjiivanov, K. I.; Neyman, M. Reassignment of the Vibrational Spectra of Carbonates, Formates, and Related Surface Species on Ceria: A Combined Density Functional and Infrared Spectroscopy Investigation. *J. Phys. Chem. C* **2011**, *115*, 23435–23454.
- (202) An, K.; Alayoglu, S.; Musselwhite, N.; Plamthottam, S.; Melaet, G.; Lindeman, A.; Somorjai, G. A. Enhanced CO Oxidation Rates at the Interface of Mesoporous Oxides and Pt Nanoparticles. *J. Am. Chem. Soc.* **2013**, *135*, 16689–16696.
- (203) Kersell, H.; Hooshmand, Z.; Yan, G.; Le, D.; Nguyen, H.; Eren, B.; Wu, C. H.; Waluyo, I.; Hunt, A.; Nemšák, S.; et al. CO Oxidation Mechanisms on CoO_x -Pt Thin Films. *J. Am. Chem. Soc.* **2020**, *142*, 8312–8322.
- (204) Alonso, D. M.; Wettstein, S. G.; Dumesic, J. A. Bimetallic Catalysts for Upgrading of Biomass to Fuels and Chemicals. *Chem. Soc. Rev.* **2012**, *41*, 8075–8089.
- (205) Nørskov, J. K.; Abild-Pedersen, F.; Studt, F.; Bligaard, T. Density Functional Theory in Surface Chemistry and Catalysis. *Proc. Natl. Acad. Sci.* **2011**, *108*, 937–943.
- (206) Vestergaard, E. K.; Vang, R. T.; Knudsen, J.; Pedersen, T. M.; An, T.; Lægsgaard, E.; Stensgaard, I.; Hammer, B.; Besenbacher, F. Adsorbate-Induced Alloy Phase Separation: A Direct View by High-Pressure Scanning Tunneling Microscopy. *Phys. Rev. Lett.* **2005**, *95*, 126101.
- (207) Zhdanov, V. P.; Vang, R. T.; Knudsen, J.; Vestergaard, E. K.; Besenbacher, F. Propagation of a Reaction Front Accompanied by Island Formation: $\text{CO}/\text{Au}/\text{Ni}(1\ 1\ 1)$. *Surf. Sci.* **2006**, *600*, L260–L264.

- (208) Prieto, G.; Beijer, S.; Smith, M. L.; He, M.; Au, Y.; Wang, Z.; Bruce, D. A.; de Jong, K. P.; Spivey, J. J.; de Jongh, P. E. Design and Synthesis of Copper-Cobalt Catalysts for the Selective Conversion of Synthesis Gas to Ethanol and Higher Alcohols. *Angew. Chem., Int. Ed.* **2014**, *53*, 6397–6401.
- (209) Mouaddib, N.; Perrichon, V.; Martin, G. A. Characterization of Copper-Cobalt Catalysts for Alcohol Synthesis from Syngas. *Appl. Catal. A* **1994**, *118*, 63–72.
- (210) Lewis, E. A.; Jewell, A. D.; Kyriakou, G.; Sykes, E. C. H. Rediscovering Cobalt's Surface Chemistry. *Phys. Chem. Chem. Phys.* **2012**, *14*, 7215–7224.
- (211) Lewis, E. A.; Le, D.; Jewell, A. D.; Murphy, C. J.; Rahman, T. S.; Sykes, E. C. H. Dissociative Hydrogen Adsorption on Close-Packed Cobalt Nanoparticle Surfaces. *ACS Nano* **2013**, *7*, 4384–4392.
- (212) Carenco, S.; Tuxen, A.; Chintapalli, M.; Pach, E.; Escudero, C.; Ewers, T. D.; Jiang, P.; Borondics, F.; Thornton, G.; Alivisatos, A. P.; et al. Dealloying of Cobalt from CuCo Nanoparticles under Syngas Exposure. *J. Phys. Chem. C* **2013**, *117*, 6259–6266.
- (213) Eren, B.; Torres, D.; Karshioğlu, O.; Liu, Z.; Wu, C. H.; Stacchiola, D.; Bluhm, H.; Somorjai, G. A.; Salmeron, M. The Structure of Copper-Cobalt Surface Alloys in Equilibrium with Carbon Monoxide Gas. *J. Am. Chem. Soc.* **2018**, *140*, 6575–6581.
- (214) Ling, W. L.; Takeuchi, O.; Ogletree, D. F.; Qiu, Z. Q.; Salmeron, M. STM Studies on the Growth of Monolayers: Co on Cu(110) with One Half Monolayer of Preadsorbed Oxygen. *Surf. Sci.* **2000**, *450*, 227–241.
- (215) Collinge, G.; Kruse, N.; McEwen, J.-S. Dissolution of CoCu Catalyst Step Defects by Co Subcarbonyl Formation. *J. Catalysis* **2018**, *368*, 31–37.
- (216) Faló, F.; Cano, I.; Salmeron, M. CO Chemisorption on Two-dimensional Cobalt Clusters: A Surface Science Approach to Cluster Chemistry. *Surf. Sci.* **1984**, *143*, 303–313.
- (217) Mu, R.; Fu, Q.; Xu, H.; Zhang, H.; Huang, Y.; Jiang, Z.; Zhang, S.; Tan, D.; Bao, X. Synergetic Effect of Surface and Subsurface Ni Species at Pt–Ni Bimetallic Catalysts For CO Oxidation. *J. Am. Chem. Soc.* **2011**, *133*, 1978–1986.
- (218) Kim, J.; Park, W. H.; Doh, W. H.; Lee, S. W.; Noh, M. C.; Gallet, J.-J.; Bournel, F.; Kondoh, H.; Mase, K.; Jung, Y.; et al. Adsorbate-driven Reactive Interfacial Pt-NiO_{1-x} Nanostructure Formation on the Pt₃Ni(111) Alloy Surface. *Sci. Adv.* **2018**, *4*, eaat3151.
- (219) Kim, Y. S.; Jeon, S. H.; Bostwick, A.; Rotenberg, E.; Ross, P. N.; Stamenkovic, V. R.; Markovic, N. M.; Noh, T. W.; Han, S.; Mun, B. S. Role of Transition Metal in Fast Oxidation Reaction on the Pt₃TM (111) (TM = Ni, Co) Surfaces. *Adv. Energy Mater.* **2013**, *3*, 1257–1261.
- (220) Su, H.-Y.; Bao, X.-H.; Li, W.-X. Modulating the Reactivity of Ni-containing Pt(111)-skin Catalysts by Density Functional Theory Calculations. *J. Chem. Phys.* **2008**, *128*, 194707.

(221) Kim, J. Doh, W. H.; Kim, Y.; Kim, K. J.; Park, J. Y. Water-Assisted Growth of Cobalt Oxide and Cobalt Hydroxide Overlayers on the Pt₃Co(111) Surface. *ACS Appl. Energy Mater.* **2019**, 2, 8580-8586.

(222) Walton, A. S.; Fester, J.; Bajdich, M.; Arman, M. A.; Osiecki, J.; Knudsen, J.; Vojvodic, A.; Lauritsen, J. V. Interface Controlled Oxidation States in Layered Cobalt Oxide Nanoislands on Gold. *ACS Nano* **2015**, 9, 2445–2453.

(223) McIntyre, B. J.; Salmeron, M.; Somorjai, G. A. Nanocatalysis by the Tip of a Scanning Tunneling Microscope Operating Inside a Reactor Cell. *Science* **1994**, 265, 1415-1418.

(224) Schröder, U.; McIntyre, B. J.; Salmeron, M.; Somorjai, G. A. Spatially Controlled Oxidation by the Tip of a Scanning Tunneling Microscope Operating Inside a Reactor. *Surf. Sci.* **1995**, 331–333, 337–342.

TOC:

